LBL-11829
SAC-34
UC-70

SWEDISH-AMERICAN COOPERATIVE PROGRAM ON RADIOACTIVE WASTE STORAGE IN MINED CAVERNS IN CRYSTALLINE ROCK

Technical Information Report No. 34

A FIELD ASSESSMENT OF THE USE OF BOREHOLE PRESSURE TRANSIENTS TO MEASURE THE PERMEABILITY OF FRACTURED ROCK MASSES

C. B. Forster and J. E. Gale
Department of Earth Sciences
University of Waterloo
Waterloo, Ontario, Canada

June 1981

A Joint Project of

Swedish Nuclear Fuel Supply Co.
Fack 10240 Stockholm, Sweden

Operated for the Swedish
Nuclear Power Utility Industry

Lawrence Berkeley Laboratory
Earth Sciences Division
University of California
Berkeley, California 94720, USA

Operated for the U.S. Department of
Energy under Contract DE-AC03-76SF00098

This report was prepared as an account of work sponsored by the United States Government and/or the Swedish Nuclear Fuel Supply Company. Neither the United States nor the U.S. Department of Energy, nor the Swedish Nuclear Fuel Supply Company, nor any of their employees, nor any of their contractors, subcontractors, or their employees, makes any warranty, express or implied or assumes any legal liability or responsibility for the accuracy, completeness or usefulness of any information, apparatus, product or process disclosed, or represents that its use would not infringe privately owned rights.

Printed in the United States of America
Available from
National Technical Information Service
U.S. Department of Commerce
5285 Port Royal Road
Springfield, VA 22161
Price Code: A07

Lawrence Berkeley Laboratory is an equal opportunity employer.

LBL-11829
SAC-34
UC-70

A FIELD ASSESSMENT OF THE USE OF BOREHOLE PRESSURE TRANSIENTS TO MEASURE THE PERMEABILITY OF FRACTURED ROCK MASSES

C. B. Forster
J. E. Gale

Department of Earth Sciences
University of Waterloo
Waterloo, Ontario, Canada

June 1981

This work was supported by the Assistant Secretary for Nuclear Energy, Office of Waste Isolation of the U.S. Department of Energy under Contract DE-AC03-76SF00098. Funding for this project is administered by the Office of Nuclear Waste Isolation at Battelle Memorial Institute.

PREFACE

This report is one of a series documenting the results of the Swedish-American cooperative research program in which the cooperating scientists explore the geological, geophysical, hydrological, geochemical, and structural effects anticipated from the use of a large crystalline rock mass as a geologic repository for nuclear waste. This program has been sponsored by the Swedish Nuclear Power Utilities through the Swedish Nuclear Fuel Supply Company (SKBF), and the U.S. Department of Energy (DOE) through the Lawrence Berkeley Laboratory.

The principal investigators are L.B. Nilsson and O. Degerman for SKBF, and N.G.W. Cook, P.A. Witherspoon, and J.E. Gale for LBL. Other participants will appear as authors of the individual reports.

Previous technical reports in this series are listed below.

1. Swedish-American Cooperative Program on Radioactive Waste Storage in Mined Caverns by P.A. Witherspoon and O. Degerman. (LBL-7049, SAC-01).

2. Large Scale Permeability Test of the Granite in the Stripa Mine and Thermal Conductivity Test by Lars Lundstrom and Haken Stille. (LBL-7052, SAC-02).

3. The Mechanical Properties of the Stripa Granite by Graham Swan. (LBL-7074, SAC-03).

4. Stress Measurements in the Stripa Granite by Hans Carlsson. (LBL-7078, SAC-04).

5. Borehole Drilling and Related Activities at the Stripa Mine by P.J. Kurfurst, T. Hugo-Persson, and G. Rudolph. (LBL-7080, SAC-05).

6. A Pilot Heater Test in the Stripa Granite by Hans Carlsson. (LBL-7086, SAC-06).

7. An Analysis of Measured Values for the State of Stress in the Earth's Crust by Dennis B. Jamison and Neville G.W. Cook. (LBL-7071, SAC-07).

8. Mining Methods Used in the Underground Tunnels and Test Rooms at Stripa by B. Andersson and P.A. Halen. (LBL-7081, SAC-08).

9. Theoretical Temperature Fields for the Stripa Heater Project by T. Chan, Neville G.W. Cook, and C.F. Tsang. (LBL-7082, SAC-09).

10. Mechanical and Thermal Design Considerations for Radioactive Waste Repositories in Hard Rock. Part I: An Appraisal of Hard Rock for Potential Underground Repositories of Radioactive Waste by N.G.W. Cook; Part II: In Situ Heating Experiments in Hard Rock: Their Objectives and Design by N.G.W. Cook and P.A. Witherspoon. (LBL-7073, SAC-10).

11. Full-Scale and Time-Scale Heating Experiments at Stripa: Preliminary Results by N.G.W. Cook and M. Hood. (LBL-7072, SAC-11).

12. Geochemistry and Isotope Hydrology of Groundwaters in the Stripa Granite: Results and Preliminary Interpretation by P. Fritz, J.F. Barker, and J.E. Gale. (LBL-8285, SAC-12).

13. Electrical Heaters for Thermo-Mechanical Tests at the Stripa Mine by R.H. Burleigh, E.P. Binnall, A.O. DuBois, D.O. Norgren, and A.R. Ortiz. (LBL-7063, SAC-13).

14. Data Acquisition, Handling, and Display for the Heater Experiments at Stripa by Maurice B. McEvoy. (LBL-7063, SAC-14).

15. An Approach to the Fracture Hydrology at Stripa: Preliminary Results by J.E. Gale and P.A. Witherspoon. (LBL-7079, SAC-15).

16. Preliminary Report on Geophysical and Mechanical Borehole Measurements at Stripa by P. Nelson, B. Paulsson, R. Rachiele, L. Andersson, T. Schrauf, W. Hustrulid, O. Duran, and K.A. Magnussen. (LBL-8280, SAC-16).

17. Observations of a Potential Size-Effect in Experimental Determination of the Hydraulic Properties of Fractures by P.A. Witherspoon, C.H. Amick, J.E. Gale, and K. Iwai. (LBL-8571, SAC-17).

18. Rock Mass Characterization for Storage in Nucler Waste in Granite by P.A. Witherspoon, P. Nelson, T. Doe, R. Thorpe, B. Paulsson, J.E. Gale, and C. Forster. (LBL-8570, SAC-18).

19. Fracture Detection in Crystalline Rock Using Ultrasonic Shear Waves by K.H. Waters, S.P. Palmer, and W.F. Farrell. (LBL-7051, SAC-19).

20. Characterization of Discontinuities in the Stripa Granite--Time Scale Heater Experiment by R. Thorpe. (LBL-7083, SAC-20).

21. Geology and Fracture System at Stripa by A. Okliewicz, J.E. Gale, R. Thorpe, and B. Paulsson. (LBL-8907, SAC-21).

22. Calculated Thermally Induced Displacements and Stresses for Heater Experiements at Stripa by T. Chan and N.G.W. Cook. (LBL-7061, SAC-22).

23. Validity of Cubic Law for Fluid Flow in a Deformable Rock Fracture by P.A. Witherspoon, J. Wang, K. Iwai, and J.E. Gale. (LBL-9557, SAC-23).

24. Determination of In-Situ Thermal Properties of Stripa Granite from Temperature Measurements in the Full-Scale Heater Experiments: Methods and Primary Results by J. Jeffry, T. Chan, N.G.W. Cook and P.A. Witherspoon. (LBL-8424, SAC-24).

25. Instrumentation Evaluation, Calibration, and Installation for Heater Tests Simulating Nuclear Waste in Crystalline Rock, Sweden by T. Schrauf, H. Pratt, E. Simonson, W. Hustrulid, P. Nelson, A. DuBois, E. Binnall, and R. Haught. (LBL-8313, SAC-25)

26. Part I: Some Results From a Field Investigation of Thermo-Mechanical Loading of a Rock Mass When Heater Canisters are Emplaced in the Rock by M. Hood. Part II: The Application of Field Data from Heater Experiments Conducted at Stripa, Sweden for Repository Design by M. Hood, H. Carlsson, and P.H. Nelson. (LBL-9392, SAC-26).

27. Progress with Field Investigations at Stripa by P.A. Witherspoon, N.G.W. Cook, and J.E. Gale (LBL-10559, SAC-27).

28. A Laboratory Assessment of the Use of Borehole Pressure Transients to Measure the Permeability of Fractured Rock Masses by C.B. Forster and J.E. Gale. (LBL-8674, SAC-28).

29. Thermal and Thermomechanical Data for In Situ Heater Experiments at Stripa, Sweden by T. Chan, E. Binnall, P. Nelson, O. Wan, C. Weaver, K. Ang, J. Braley, and M. McEvoy. (LBL-11477, SAC-29).

30. The Effect of Radon Transport in Groundwater Upon Gamma Ray Borehole Logs by P.H. Nelson, R. Rachiele, and A. Smith. (LBL-11180, SAC-30).

31. Strength and Permeability Tests on Ultra-Large Stripa Granite Core by R. Thorpe, D.J. Watkins, W.E. Ralph, R. Hsu, and S. Flexser. (LBL-11203, SAC-31).

32. Ultrasonic and Acoustic Emission Results from the Stripa Heater Experiments. Part I: A Cross-Hole Investigation of a Rock Mass Subjected to Heating by B.N.P. Paulsson and M.S. King. Part II: Acoustic Emission Monitoring During Cool-Down of the Stripa Heater Experiment by R. Rachiele. (LBL-10975, SAC-32).

33. Numerical Modeling to Assess Possible Influence of the Mine Openings on Far-Field In Situ Stress Measurements at Stripa by T. Chan, V. Guvanasen, and N. Littlestone (LBL-12469, SAC-33).

TABLE OF CONTENTS

	Page
LIST OF FIGURES	vii
LIST OF TABLES	ix
ABSTRACT	xi
1. INTRODUCTION	1
1.1 Background and Location	1
1.2 Objectives and Scope	7
1.3 Previous Work	11
2. FRACTURE CHARACTERIZATION IN THE VENTILATION DRIFT	17
3. BOREHOLE TESTING	24
3.1 Equipment Preparation	24
3.2 Down-Hole Installation	27
3.3 Test Procedures	29
3.3.1 Injection Tests	29
3.3.2 Pressure Pulse Tests	29
4. TEST RESULTS	31
4.1 Shut-in History	31
4.2 Injection Test Results	37
4.2.1 Short-Term Tests	37
4.2.2 Long-Term Tests	40
4.3 Pressure Pulse Tests	48
4.3.1 Pressure Pulse Test Results	48
4.3.2 Comparison of Pressure Pulse Decay and Steady-State Tests	50
5. CONCLUSIONS	63
6. RECOMMENDATIONS	67
ACKNOWLEDGMENTS	69
REFERENCES	71
APPENDIX I STEREONET PLOTS OF FRACTURE ORIENTATIONS	73
APPENDIX II EQUIPMENT CALIBRATION	85
APPENDIX III BOREHOLE INSTALLATION DIAGRAMS	89
APPENDIX IV X, Y, Z COORDINATES OF TEST CAVITIES	97
APPENDIX V TEST LOG	107

Page

APPENDIX VI SELECTED PRESSURE PULSE TEST DATA 119

APPENDIX VII TEST CONDITIONS FOR ALL PRESSURE PULSE TEST DATA 133

LIST OF FIGURES

Page

1.1 Schematic of a straddle-packer system installed in a borehole . . 2

1.2 Plot of pressure vs time for a hypothetical pressure pulse test . 3

1.3 Location map of Stripa mine, Sweden 5

1.4 Plan view of underground test site 6

1.5 Location of (a) radial (R) boreholes, and (b) hydrology-geophysical (HG) boreholes in the north end of ventilation drift 8

1.6 Schematic perspective of boreholes north of the ventilation drift 9

1.7 Schematic of the test configuration used by Brace et al. (1968) . 12

2.1 Stereonet plot of fractures logged in boreholes R1 through R10 and HG1 through HG5 18

2.2 Map of fractures exposed on floor and east wall of ventilation drift 19

2.3 Stereonet plot of fractures containing chlorite logged in boreholes R6 through R10 21

2.4 Stereonet plot of fractures containing calcite logged in boreholes R6 through R10 22

2.5 Stereonet plot of fractures containing epidote logged in boreholes R6 through R10 23

3.1 Schematic of downhole equipment 25

3.2 Schematic of surface equipment with downhole connections 26

3.3 Schematic perspective of borehole installation pattern 28

4.1 Plots of pressure against time for complete test history 32

4.2 Variation in shut-in pressure as a function of distance from end of the ventilation drift in horizontal boreholes HG1 and DBH2 . . 36

4.3 Plots of pressure against time during long-term injection tests . 41

4.4 Plots of pressure against time during "Moebus" experiment 42

4.5 Pressure responses to long-Term injection tests in HG1-3 44

Page

4.6 Pressure responses to long term injection tests in HG5-2 45

4.7 Plots of normalized pressure against log time for pressure pulse tests in intervals HG5-2, HG1-3b and HG3-4 51

4.8 Plot of normalized pressure against log time for pressure pulse tests in intervals HG5-1, HG5-3 and HG2-1b 52

4.9 Summary plot of normalized pressure against log time. Curves from Figs. 4.5 and 4.6 53

4.10 Plot of normalized pressure against log time for selected pulse tests with extended decay characteristics 54

4.11 Normalized pressure decay at a wellbore intersected by a 10 μm fracture with finite volume $V_F/V_W = 1$ in series (a), or in parallel (b) with an aperture 2b fracture with infinite volume . . 56

4.12 Pulse pressure (ΔP) resulting From imposed displacement volume (ΔV) 57

4.13 Schematic diagram of typical field pressure against time decay curves 60

I.1 Stereonet plot of fracture logged in boreholes HG1 through HG5 . . 74

I.2 Stereonet plot of fractures containing calcite logged in boreholes HG1 through HG5 75

I.3 Stereonet plot of fractures containing chlorite logged in boreholes HG1 through HG5 76

I.4 Stereonet plot of fractures containing epidote logged in boreholes HG1 through HG5 77

I.5 Stereonet plot of fractures logged in boreholes R1 through R5 . . 78

I.6 Stereonet plot of fractures containing chlorite logged in boreholes R1 through R5 79

I.7 Stereonet plot of fractures containing calcite logged in boreholes R1 through R5 80

I.8 Stereonet plot of fractures containing epidote logged in boreholes R1 through R5 81

I.9 Stereonet plot of fractures logged in boreholes R6 through R10 . . 82

III.1 HG1 installation diagram 86

Page

III.2 HG3 installation diagram 87

III.3 HG4 installation diagram 88

III.4 HG5 installation diagram 89

III.5 DBH-2 installation diagram 90

LIST OF TABLES

4.1 Cavity shut-in pressures 34

4.2 Results of short-term injection tests 38

4.3 Results of long-term injection tests 43

4.4 Response to long-term injection tests 47

4.5 Pressure increase during "Moebus" experiment 49

4.6 Test displacement volumes 62

II.1 Pressure-measuring equipment 81

VII.1 Pressure pulse test data 123

ABSTRACT

A field experiment to evaluate the transient pressure pulse technique of Brace et al. (1968) as a method of determining the in-situ hydraulic conductivity of low permeability fractured rock was made. This report outlines its background, set-up, execution, and results. The experiment attempted to define: (i) the radius of influence of a pressure pulse-test in fractured rock and (ii) the correlation between pressure-pulse tests and steady-state flow tests performed in five boreholes drilled in fractured granite. Twenty-five test intervals, 2 to 3 m in length, were isolated in the boreholes, using air-inflated packers. During pressure pulse and steady-state tests, pressures were monitored in both the test and observation cavities. Rock-mass conductivities were calculated from steady-state test results and were found to range from less than 10^{-11} to 10^{-7} cm/sec. However, there was no consistent correlation between the steady-state conductivity and the pressure pulse decay characteristics of individual intervals. These conflicting test results can be attributed to the following factors:

(i) differences in volumes of rock affected by the test techniques,

(ii) effects of equipment configuration and compliance, and

(iii) complexity of the fracture network.

Although the steady-state flow tests indicate that hydraulic connections exist between most of the test cavities, no pressure responses were noted in the observation cavities (located at least 0.3 m from the test cavities) during the pulse tests. This does not mean, however, that the pressure-pulse radius of influence is less than 0.3 m, because the observation cavities were too large (about 7 liters). The lack of correlation between steady-state conductivities and the corresponding pressure pulse decay times does

not permit use of existing single-fracture type curves to analyze pulse tests performed in multiple-fracture intervals. Subsequent work should focus on the detailed interpretation of field results with particular reference to the effects of the fracture system at the test site.

1.0 INTRODUCTION

1.1 Background and Location

Brace et al. (1968) outlined a transient permeability laboratory test, which they called the pressure pulse test. They chose this technique to determine the matrix permeability of small samples of intact granite because standard steady-state tests would be inadequate in a low rock conductivity range of 10^{-8} to 10^{-12} cm/sec. Various workers have proposed that this technique could be adapted for field determination of the conductivity of fractured granitic masses, using only a single well. The steps that might be followed in such a field pressure pulse test are:

(1) To select the desired borehole intervals, data from core logs, borehole television logs, geophysical logs, and, possibly, injection tests (performed over long intervals) are used.

(2) A straddle-packer system (Fig. 1.1) is used to isolate the specified borehole interval.

(3) A pressure pulse is generated within the cavity and the resulting pressure decay is monitored with a sensitive electronic pressure transducer.

(4) Pressure-time field results may be analyzed by comparing these with those generated by numerical or analytical solutions of the diffusivity equation, using appropriate boundary conditions. The character of the resulting pressure-time decay curve (Fig. 1.2) should correspond to a unique rockmass conductivity for the particular borehole configuration and water and rock properties.

The pressure pulse technique should allow accurate measurement of small induced pressure transients, of only a few percent of in-situ water

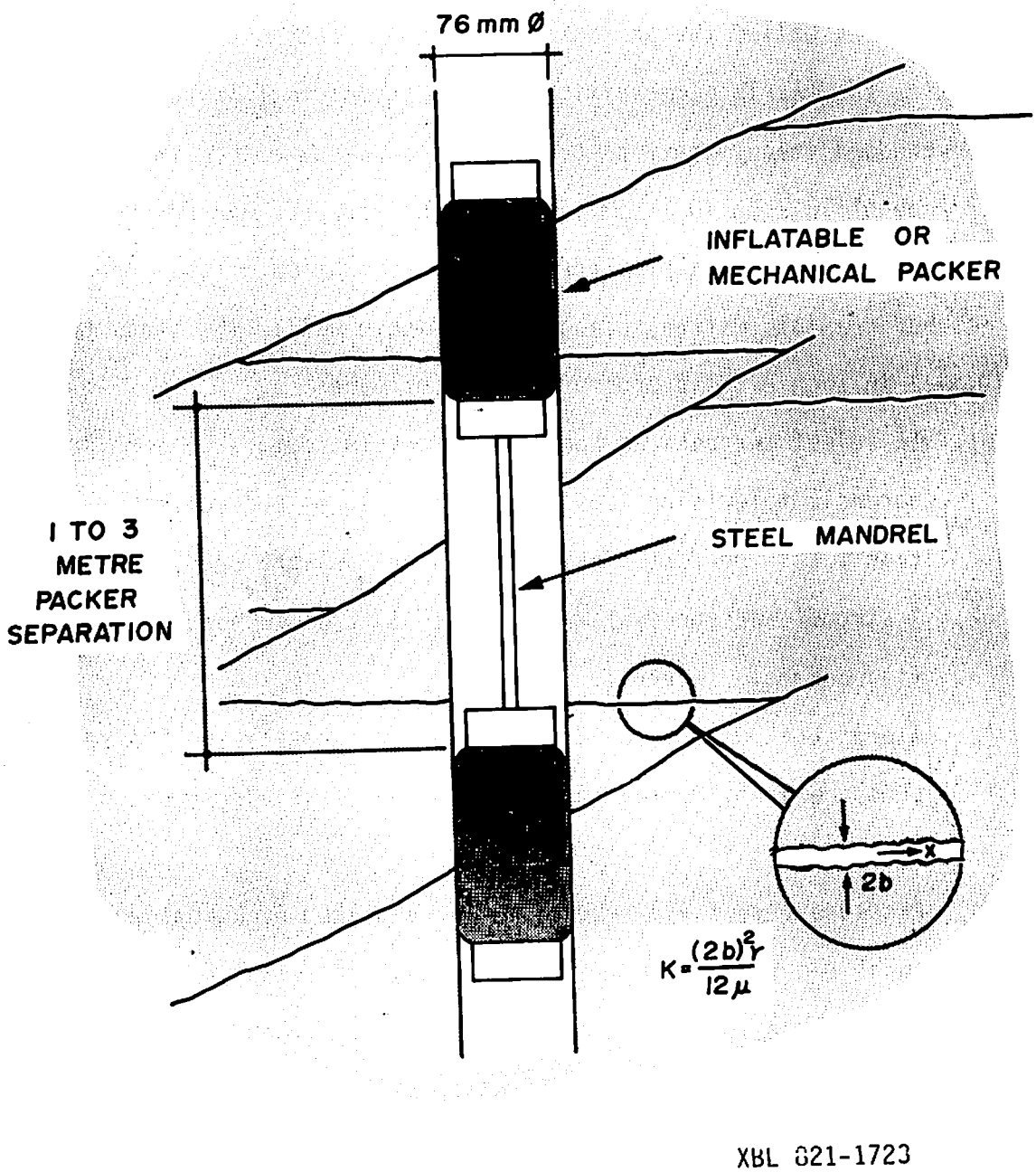

Fig. 1.1. Schematic of a straddle-packer installed in a borehole.

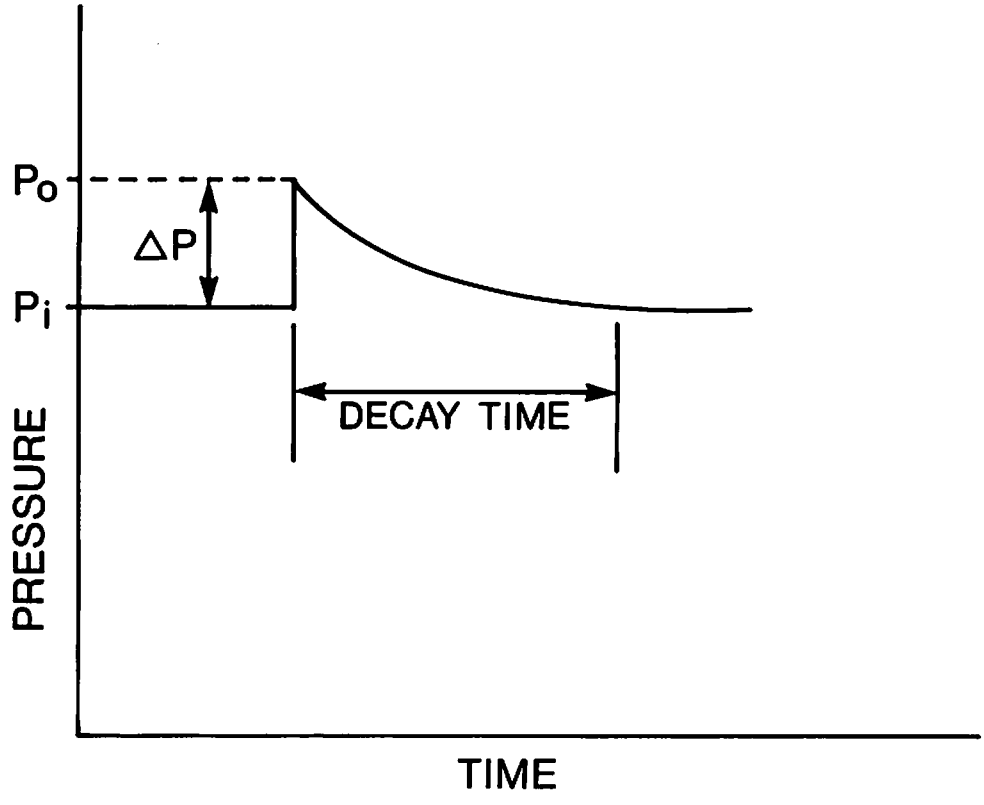

XBL 821-1722

Fig. 1.2. Plot of pressure vs. time for a hypothetical pressure pulse test.

pressures, over relatively short periods of minutes to days. This should permit one to measure low permeabilities over short borehole intervals. In fractured media, where even the simplest fracture system is difficult to understand, single fractures may be tested and overall rock mass permeabilities estimated from individual fracture characteristics (Gale and Witherspoon, 1979).

Laboratory studies have been conducted (Forster and Gale, 1980, and Gale and Raven, 1979) to assess the viability of this technique with regard to borehole equipment compliance. However, detailed in-situ testing is required before the practicality of the pressure pulse test in the field can be fully proved. In particular, the following factors must be investigated in the field environment:

1. The radius of influence, in fractured rock, of a pressure pulse test, compared with the effective radius of influence during steady state injection tests.
2. The correspondence of conductivity values between steady-state injection tests and transient pressure pulse tests performed in a fractured rock mass.
3. The effects of equipment configuration on the test results.

As a first attempt at such in situ assessment, a field testing program was designed and carried out by the authors at the U.S.- Swedish cooperative underground test facility at the Stripa mine in Sweden (Fig. 1.3). This test site (Fig. 1.4) was considered advantageous for the following reasons:

(1) The arrangement of boreholes previously drilled in the fractured granitic rock mass was thought to be conducive to assessing the

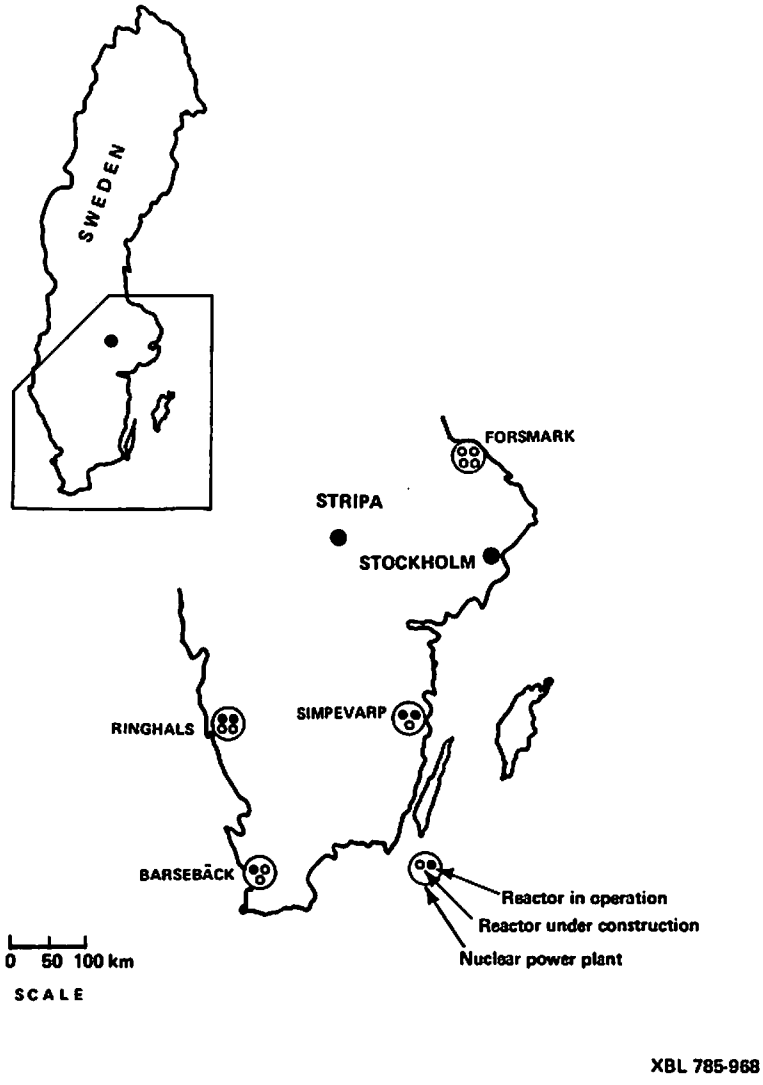

Fig. 1.3. Location map of Stripa mine, Sweden.

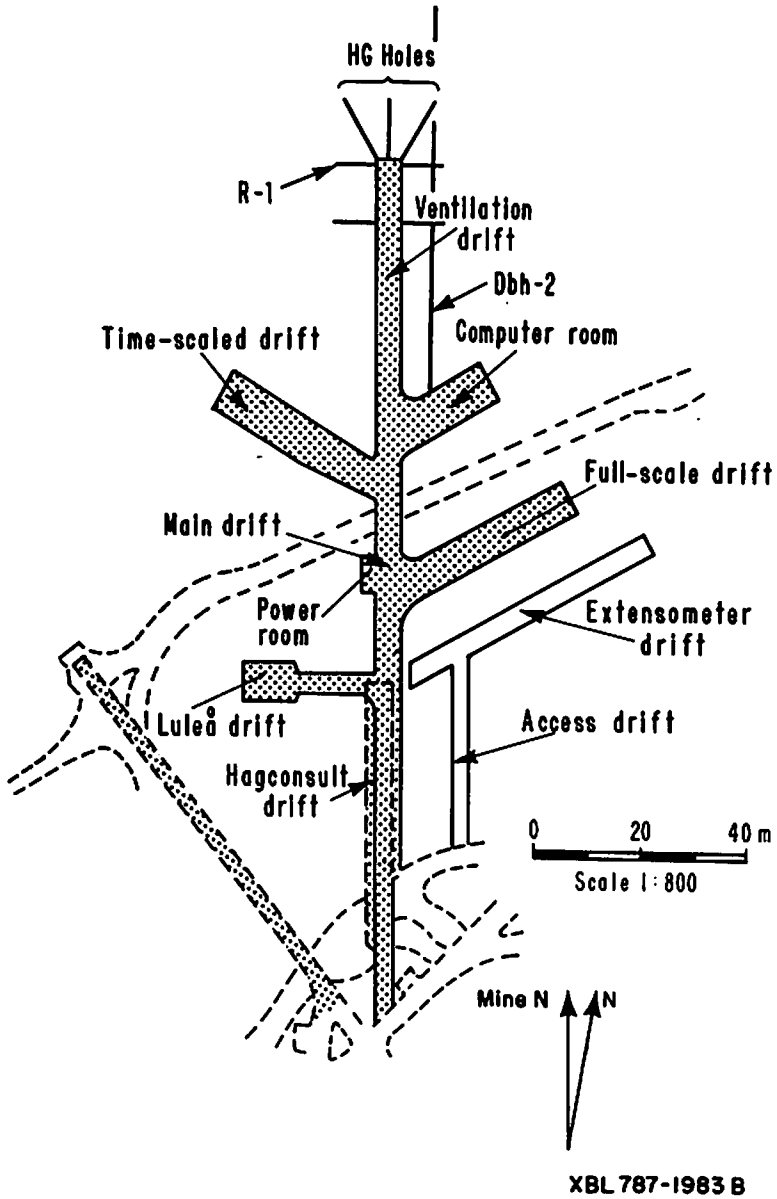

Fig. 1.4. Plan view of underground test site.

radius of influence of pressure pulse tests.

(2) All boreholes were approximately 330 meters underground. This provided essentially isothermal conditions and significant ground-water pressures throughout the pattern of relatively short (30 m) holes.

(3) Nearly all of the detailed fracture information necessary to interpret the test results was available from core logs, borehole television logs, and drift mapping.

(4) Background hydrology information was available from previous steady-state injection tests performed in the same boreholes.

The test program was carried out on the 336-m level of the mine in boreholes HG1, HG3, HG4, HG5, and DBH2, drilled in the vicinity of the ventilation drift (Fig. 1.5). A schematic 3-D perspective of the borehole layout is shown in Fig 1.6. The HG holes are all 30 m in length and 76 mm in diameter. DBH2 is 100 m in length and 56 mm in diameter, but only a 30 m section, from 48.0 m to 78.0 m, was used in this study. During the summer of 1979, hydrology testing was carried out in these holes, and additional fracture mapping was conducted in the adjacent ventilation drift.

1.2 Objectives and Scope

The purpose of this study is three-fold: (1) to compare the results of injection tests and pressure pulse tests performed in fractured granitic rock; (2) to define the radius of influence of pressure pulse tests and steady state injection tests performed in a low permeability environment; and (3) to determine the effects of the equipment configuration on the results of pressure pulse tests.

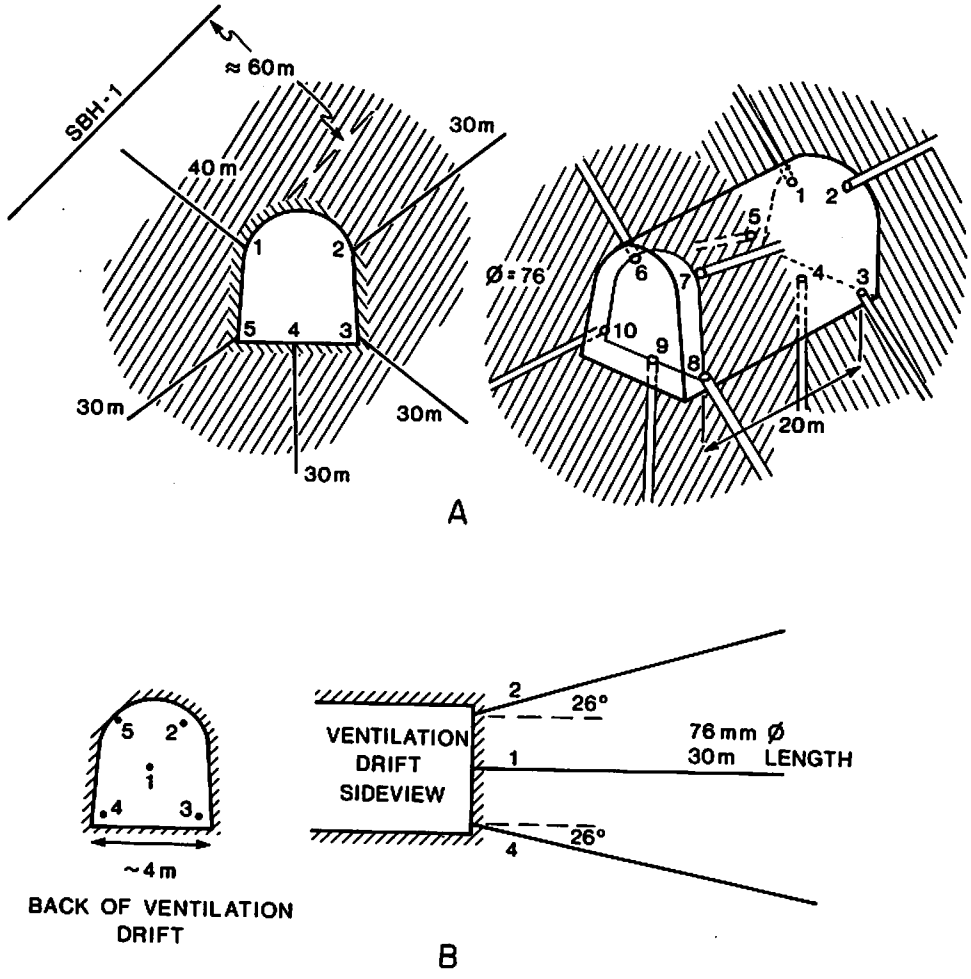

Fig. 1.5. Location of (a) radial (R) boreholes, and (b) hydrology-geophysical (HG) boreholes in the north end of ventilation drift.

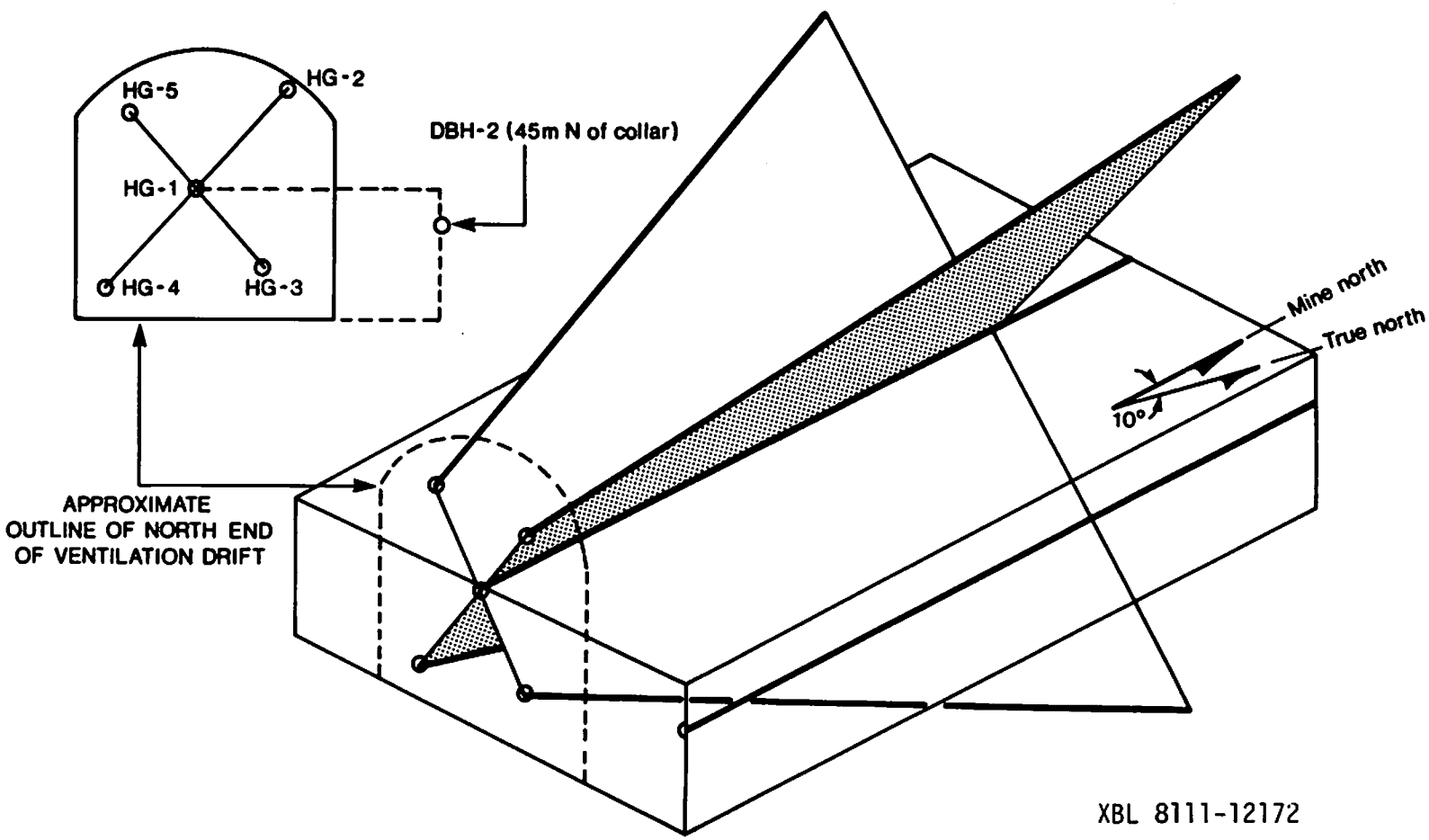

Fig. 1.6. Schematic perspective of boreholes north of the ventilation drift.

The work performed to date includes: (1) a review and preliminary interpretation of the three-dimensional fracture system as determined from core logs, fracture maps and borehole television logs; (2) a description of the borehole testing program; and (3) presentation of test results.

During the winter of 1979, pertinent fracture maps, core logs, borehole television logs, and hydrology testing results were reviewed in preparation for the field program. Dominant fracture trends were determined from the fracture data and compared to the hydrology data to assist in choosing borehole intervals to be instrumented the following summer. During the summer field program, 25 borehole intervals were isolated in HG1, HG3, HG4, HG5 and DBH2 (Fig. 1.6), using rubber packers inflated with compressed nitrogen.

In situ groundwater pressures were monitored in each cavity throughout the field program. After these pressures began to stabilize, pressure pulse tests and injection tests were performed in many of the test cavities, providing a direct comparison of each technique. During these tests, various distances around each test interval were monitored for pressure response. A variety of packer types and downhole equipment configurations were used; their effects on pulse test results should be assessed in future work. At the conclusion of the testing program, two pumping-in tests, of 19.5 and 27 hours duration, were performed in two different borehole intervals in an attempt to further define the interconnection of various cavities.

Subsequent work could focus on the detailed interpretation of the field results with particular reference to the fracture system encountered at the test site.

1.3 Previous Work

Previous researchers (Brace et al., 1968; and Lin, 1977, 1978) have concentrated on performance and analysis of pressure pulse tests in the laboratory. Numerical studies by Wang et al. (1977) and recent laboratory studies by Gale and Raven (1979) and Forster and Gale (1980) have investigated the potential of the test for field use.

Brace et al. first proposed a method for analysis of pressure pulse tests performed in the laboratory on unfractured rock samples. Tests were conducted on small samples (length of 1.61 cm and area of 5.0 cm^2) of unfractured Westerly granite, subjected to confining pressures of 125 to 144 MPa, in the configuration shown in Fig. 1.7. In their analysis, Brace and coworkers assumed that the samples were homogeneous and isotropic and that Darcy's law was valid. In addition, water properties (compressibility and viscosity) were assumed to be constant. This assumption required that pressure pulses be small and temperature variations minimal. Permeability values were calculated by assuming a constant pressure gradient, which decays exponentially to zero, along the sample. This assumption is based on a rock porosity approximately equal to zero and on a rock compressibility much less than the compressibility of water.

Using the configuration and basic assumptions of Brace et al., Lin (1977) applied analytical and numerical techniques to investigate the effects of variations in fluid reservoir volumes to optimize test times for a particular sample size. However, because of a 660-fold increase in sample size, the assumption of a constant gradient was considered incorrect. Thus, Lin used the complete differential equation in his analysis to compute a series

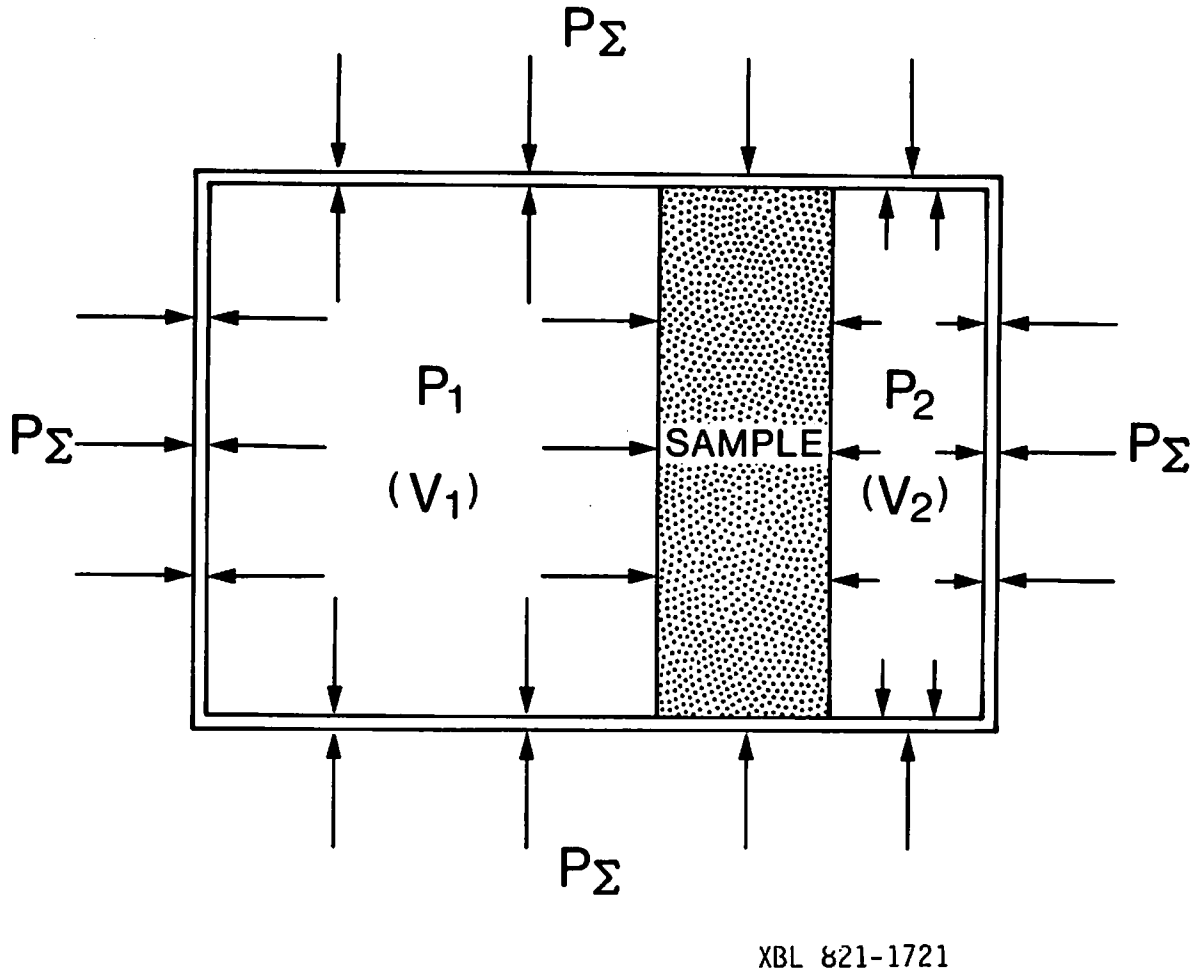

Fig. 1.7. Schematic of the test configuration used by Brace et al. (1968).

of pressure-time decay curves for a variety of combinations of rock permeabilities and reservoir volumes. Pore pressure of 28 MPa and pressure pulses (ΔP) of 2 MPa were used. The resulting data were interpreted to determine the optimum reservoir volumes for a two-reservoir test configuration. An experimental apparatus was constructed (Lin, 1978), and permeabilities of specimens of Eleana argillite were determined. These permeabilities ranged from 10^{-16} to 10^{-19} cm^2 (unfractured sample) and from 10^{-12} to 10^{-17} cm^2 (fractured sample).

Wang et al. (1977) used a numerical model to compute type curve solutions for tests performed in borehole intervals that intersected single or multiple fractures. Type curves were computed for fractures of finite or infinite extent and of variable aperture. The analyses of Wang et al. assumed that: (1) there is a continuity of flow velocities at the wellbore/fracture interface, and (2) at some distance from the well, the fractures are either closed (zero pressure gradient) or open (zero pressure). The initial conditions used by Wang required that the fluid pressure throughout the fracture equal the ambient pressure and that the fluid pressure in the wellbore be elevated above ambient by the magnitude of the pressure pulse at zero time. Other assumptions were: (1) the rock matrix is impermeable, therefore there is only fracture flow; (2) the laminar parallel-plate flow law is valid; (3) water properties (compressibility and viscosity) are independent of small variations in pressure and temperature; (4) fracture aperture and test cavity dimensions are also independent of small variations in pressure; and (5) pressure increase is instantaneous at zero time. Wang et al. concluded that since there were no variations in early-time data, despite variations in fracture volumes and boundary conditions, fracture

apertures could be estimated from the decay time. Conversely, the later time data provides information on the character of fracture boundaries and permeability. However, as Wang et al. point out, the resulting type curves are somewhat insensitive to the number and orientation of fractures. This renders data analysis potentially difficult unless a detailed knowledge of the fracture system is obtained, or only a single fracture is tested.

In these papers, the authors assume that there are no volume change effects in the test cavity (upstream reservoir in the laboratory configuration). Packer expansion or contraction during a field pressure pulse test would cause variation in the cavity volume. Laboratory studies of packer compliance were conducted by Gale and Raven (1979) and Forster and Gale (1980) to assess the effects of such volume changes on determinations of pressure pulse permeability. Full-scale borehole intervals (3 m long and 76 mm in diameter) were isolated in a steel pipe, using standard field packers (inflated with air or water) or steel plugs. Thus, different packer compliances were simulated, from the stiffness of steel plugs to the softness of air-inflated packers. Pulse tests performed on cylindrical samples (11 cm long and 5.4 cm diameter) indicated that compliance effects do exist, but their extent has not yet been fully evaluated. The air-inflated packers produced smaller compliance effects than the water-filled packers.

In addition, it was found that temperature variations of as little as $\pm$ 0.01°C, or minor air leaks in the test assembly, occurring during a test, can have a significant effect on the resulting pressure-time decay curve. Temperature variations are expected to be greater than this in surface equipment in the field, but much less at testing depths within the rock mass.

To eliminate temperature effects, therefore, the test assembly should not extend above ground surface. For tests conducted from the surface, this could be accomplished by generating the pressure pulse within the test cavity. Tests could also be conducted entirely underground. To prevent and check for air leaks, and to force air out of the borehole and pressure lines, the packers should be repeatedly inflated and deflated.

2.0 FRACTURE CHARACTERIZATION IN THE VENTILATION DRIFT

The geology of the Stripa mine and surrounding region has been described by Olkiewicz et al. (1979). Olkiewicz et al. have also documented borehole core, television, and geophysical logs, hydrology data, and fracture mapping in the vicinity of the HG holes.

During the winter of 1979, borehole core logs for the R and HG holes were reviewed and plotted on stereonet. Stereonet plots present a statistical interpretation of the distribution of fracture orientations. In this report, the stereonet plots are corrected for sample bias introduced by borehole orientation. Figure 2.1 shows a summary plot of poles to all fractures logged in the R and HG holes. The dominant fracture orientation strikes approximately 175° with a dip of 80° to the east. A secondary pole concentration indicates a fracture orientation striking approximately 10° and dipping 60° to the west. A relatively minor pole concentration indicates a fracture orientation of 120° with dip of 80° north. It appears to have been contributed by fractures logged in the HG holes. The total length of all HG holes is 150 m in the general north-south direction, while the total length of all R holes is 320 m in the general east-west direction. If Fig. 2.1 were corrected to compensate for this difference in overall hole length and orientation, the minor pole concentration would increase in importance when compared to the R hole data. Figure 2.2 shows a map (Olkiewicz et al., 1979) of the fractures exposed on the floor and east wall of the ventilation drift. The general impression given by this map suggests that the dominant fracture set strikes about 120° with a secondary set striking 10° and third set striking 170°. Thus both stereonet plots and fracture mapping indicate three

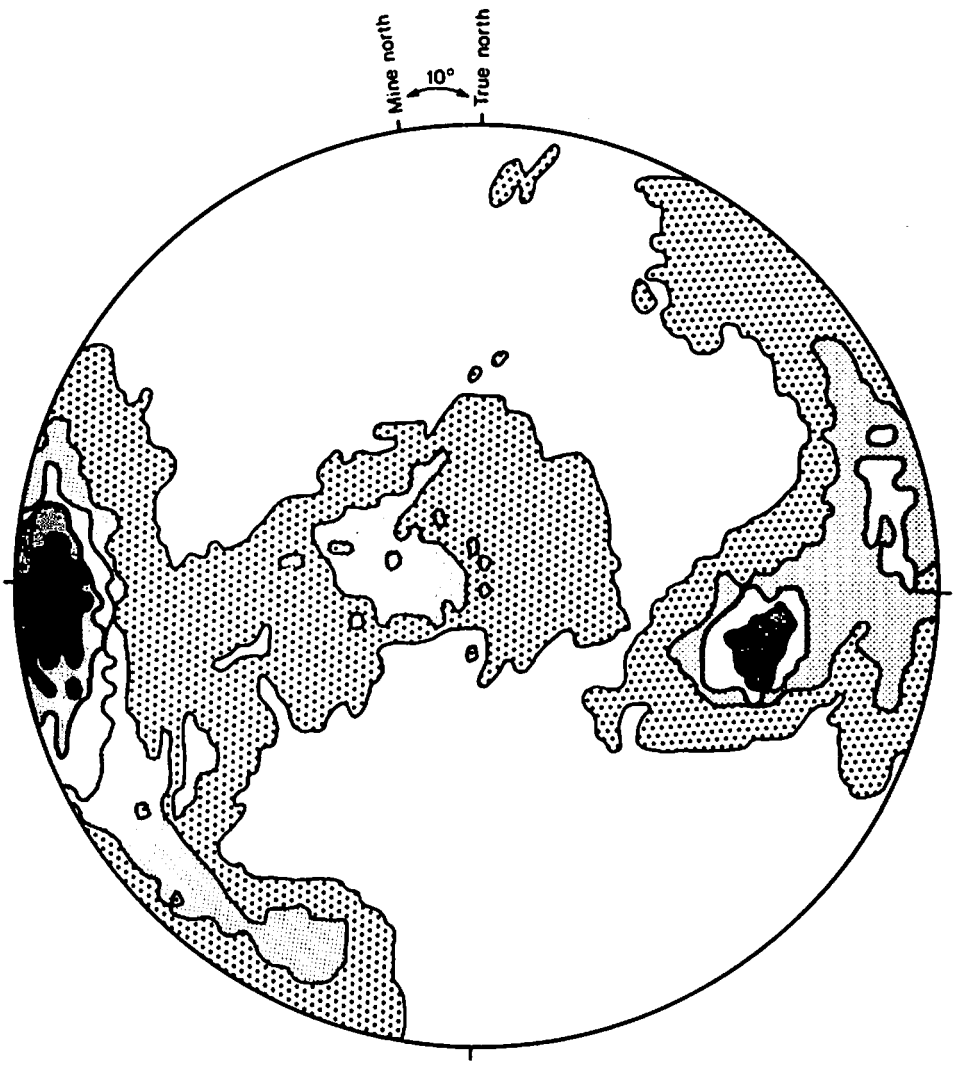

POLES TO PLANES PROJECTED ON LOWER HEMISPHERE OF EQUAL AREA PROJECTION USING SCHMIDT METHOD

Contours of Pole Density (% of total poles)	
0-1	
1-2	
2-3	
3-4	
4-5	
5-6.8	
Total Poles = 1648	
Maximum Density = 6.8	

XBL 8111-12173

Fig. 2.1. Stereonet plot of fractures logged in boreholes R1 through R10 and HG1 through HG5.

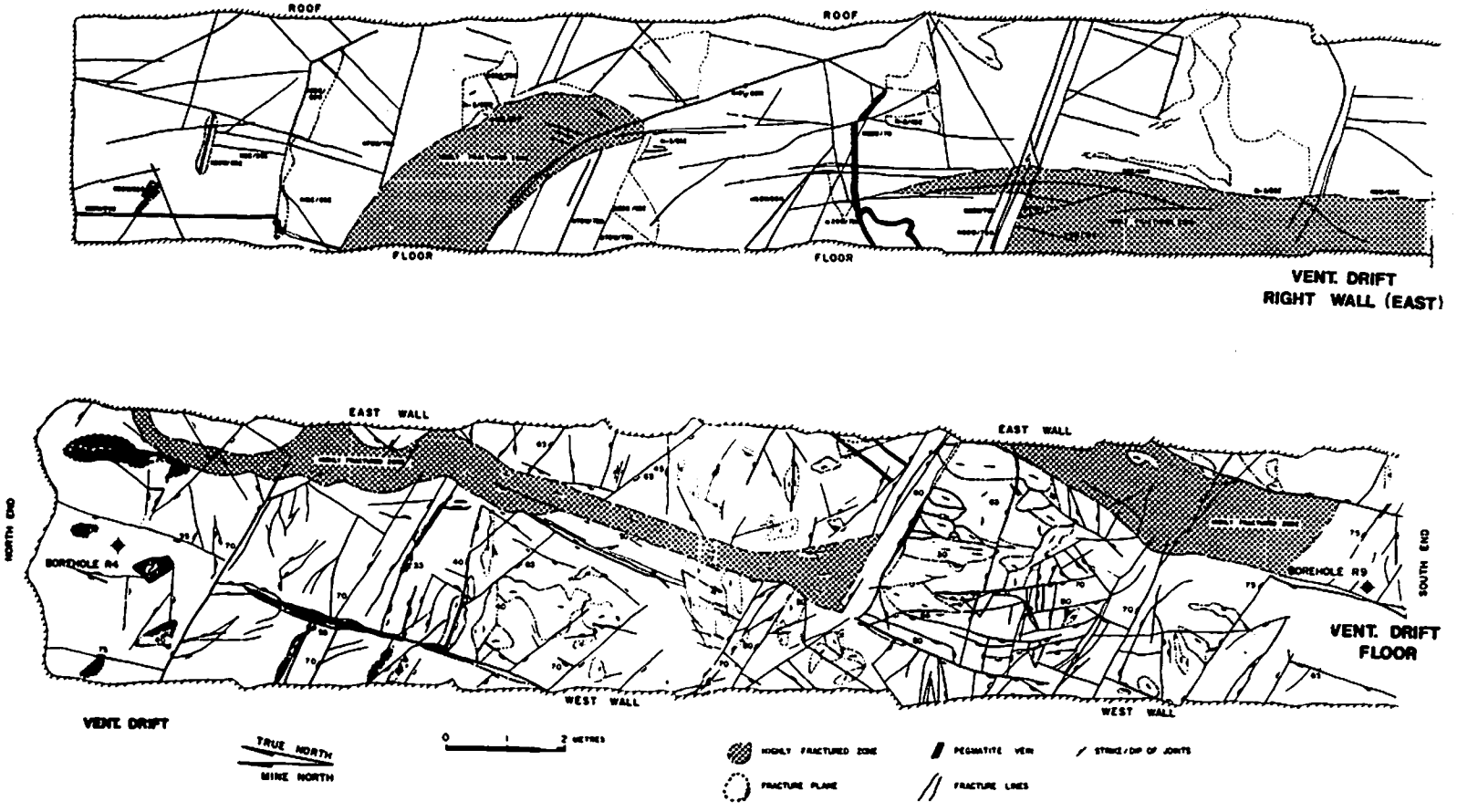

XBL 8111-12174

Fig. 2.2. Map of fractures exposed on floor and east wall of ventilation drift. (After Olkiewicz et al., 1979).

primary fracture sets but with different degrees of importance, depending upon the mapping or logging technique.

To further define the different fracture sets, three gouge types--chlorite, calcite and epidote--were noted during core logging. Stereonet plots of fractures containing each gouge type were plotted for each group of holes (R1-R5, R6-R10 and HG1-HG5) and are contained in Appendix I. However, only the group R6-R10 showed any significant difference between gouge types. Figures 2.3, 2.4, and 2.5 show that calcite-coated fractures tend to be oriented with a strike of approximately 140°; epidote - and chlorite-filled fractures, with a strike of 10°.

During the 1979 summer field program at Stripa, additional fracture mapping and borehole logging was carried out in the ventilation drift. Previous maps of the walls and floor of this drift (Fig. 2.2) served as the basis for a more detailed determination of fracture orientation and spacing. This additional mapping can be used for a more detailed interpretation of the fracture system.

From the limited data shown here, it can be seen that the fracture geometry forms a complex pattern. This pattern must be fully understood before results of hydrology testing can be properly analyzed. Three-dimensional physical models are being constructed to compare fracture geometry and hydrology data. This 3-D fracture pattern will then be combined with the hydrology data to gain an understanding of fracture interconnection and to interpret the results of interborehole tests.

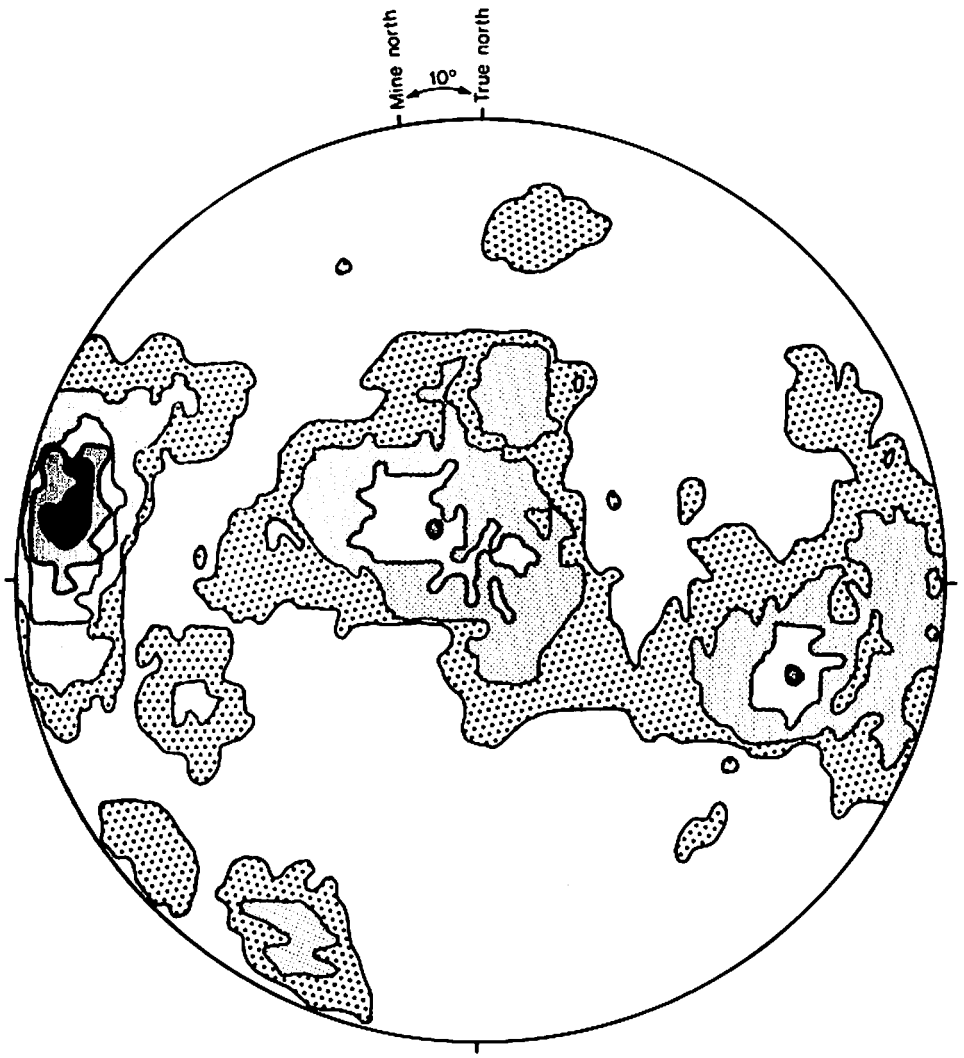

POLES TO PLANES PROJECTED ON LOWER HEMISPHERE OF EQUAL AREA PROJECTION USING SCHMIDT METHOD

Contours of Pole Density (% of total poles)	
0-1	
1-2	
2-4	
4-6	
6-8	
8-9.8	
Total Poles = 458	
Maximum Density = 9.8	

XBL 8111-12175

Fig. 2.3. Stereonet plot of fractures containing chlorite logged in boreholes R6 through R10.

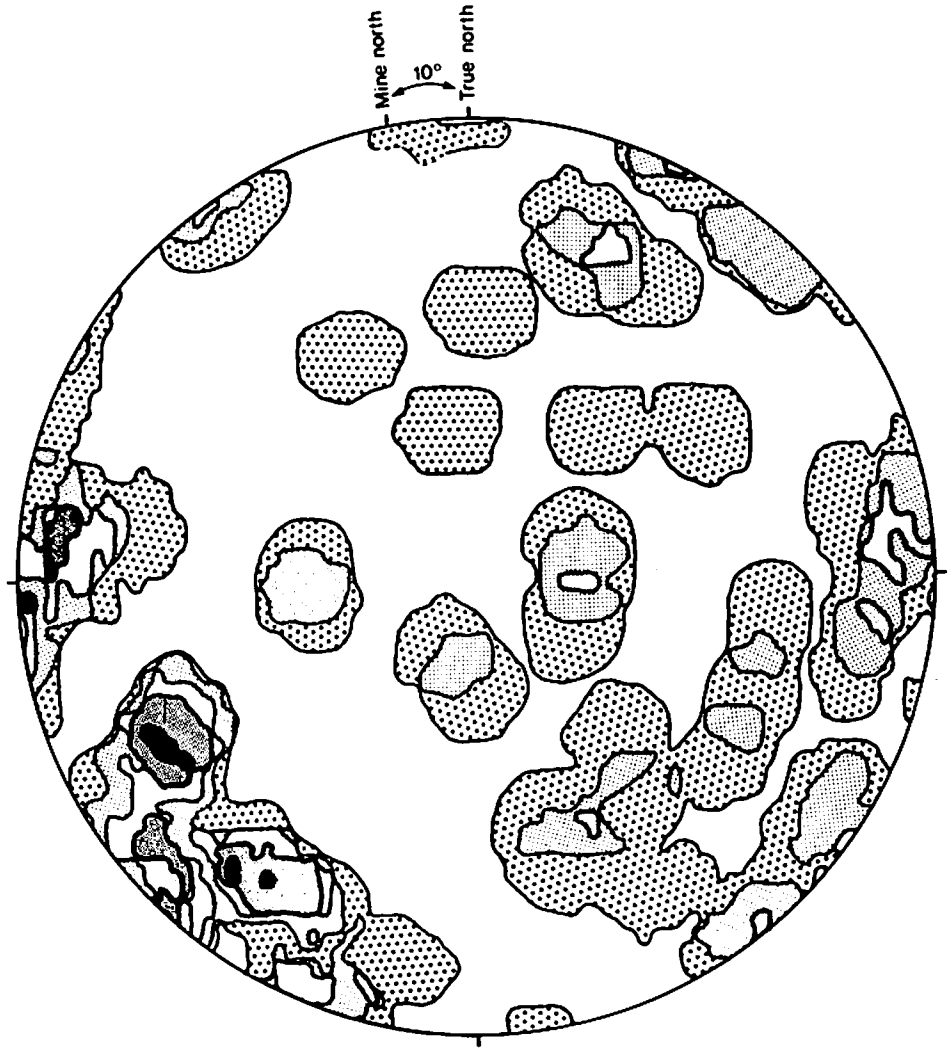

POLES TO PLANES PROJECTED ON LOWER HEMISPHERE OF EQUAL AREA PROJECTION USING SCHMIDT METHOD

Contours of Pole Density (% of total poles)	
0-1	
1-2	
2-4	
4-6	
6-8	
8-9.4	
Total Poles = 64	
Maximum Density = 9.4	

XBL 8111-12176

Fig. 2.4. Stereonet plot of fractures containing calcite logged in boreholes R6 through R10.

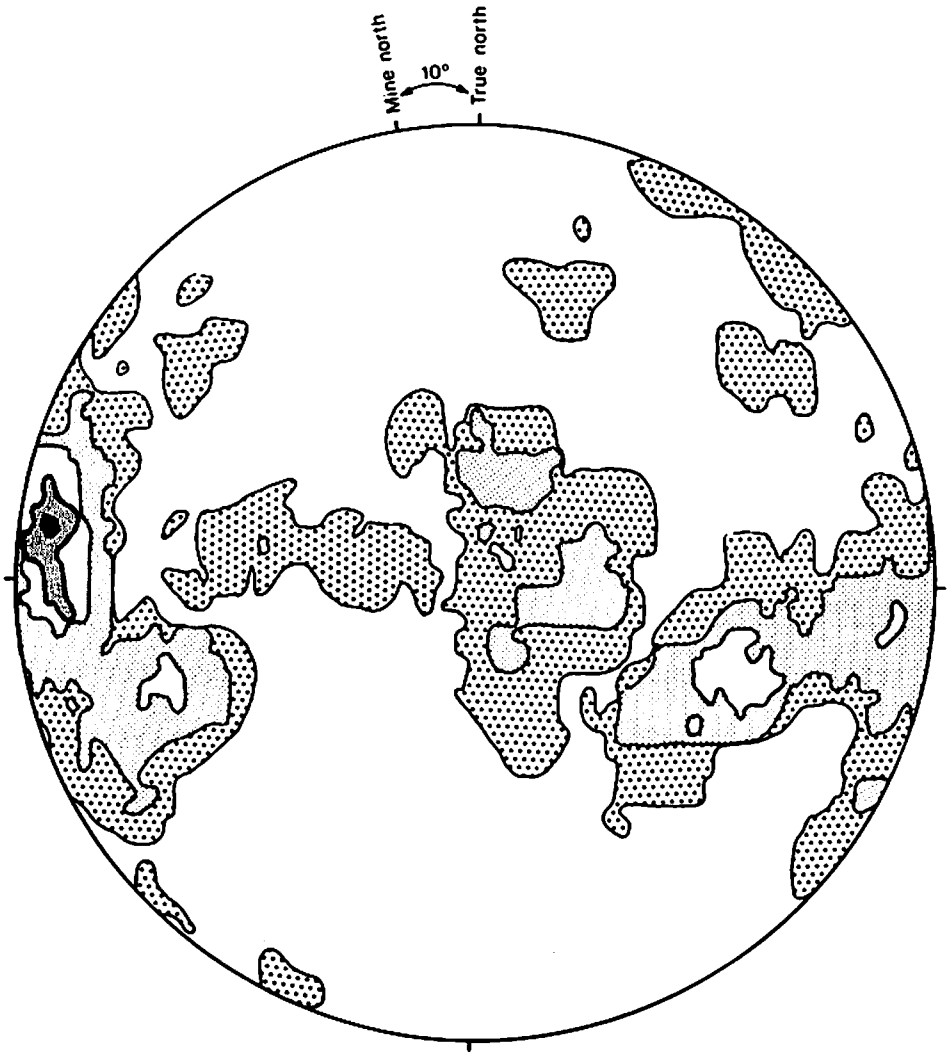

POLES TO PLANES PROJECTED ON LOWER HEMISPHERE OF EQUAL AREA PROJECTION USING SCHMIDT METHOD

Contours of Pole Density (% of total poles)	
0-1	
1-3	
3-6	
6-9	
9-12	
12-12.1	
Total Poles = 132	
Maximum Density = 12.1	

XBL 8111-12177

Fig. 2.5. Stereonet plot of fractures containing epidote logged in boreholes R6 through R10.

3.0 BOREHOLE TESTING

The borehole test program was designed to allow (1) both steady-state injection tests and transient pressure pulse tests in a variety of test intervals, and (2) concurrent monitoring of in-situ groundwater pressures at various positions in the rock mass. The injection and pressure pulse tests were performed in the various test intervals when cavity pressure had reached an approximately steady state. This chapter outlines the procedures taken to prepare and install the test equipment, and the tests themselves.

3.1 Equipment Preparation

Before testing, all equipment components were checked for correct operation and calibrated where necessary. A typical down-hole system is shown in Fig. 3.1. All pipe thread connection ports were pressure-tested (to 2 MPa). Continuous nylon pressure lines, from the surface to the ports, minimized pressure leaks. Details of a pressure/ temperature port are shown in Fig. 3.1; the figure also indicates the nature of the pressure seals. Packer checks were conducted by inflating the packers in steel pipes of the appropriate borehole diameter and monitoring any pressure changes over a 24-hour period. Pressure variations of 0.013 MPa or less over this period were considered adequate. A schematic of the surface equipment is shown in Fig. 3.2.

All pressure gauges, transducers, and flow measurement devices were calibrated throughout the test program, using procedures outlined in Appendix II. During installation, all gauges, lines, and transducers were flushed with water to remove any air in them (de-aired).

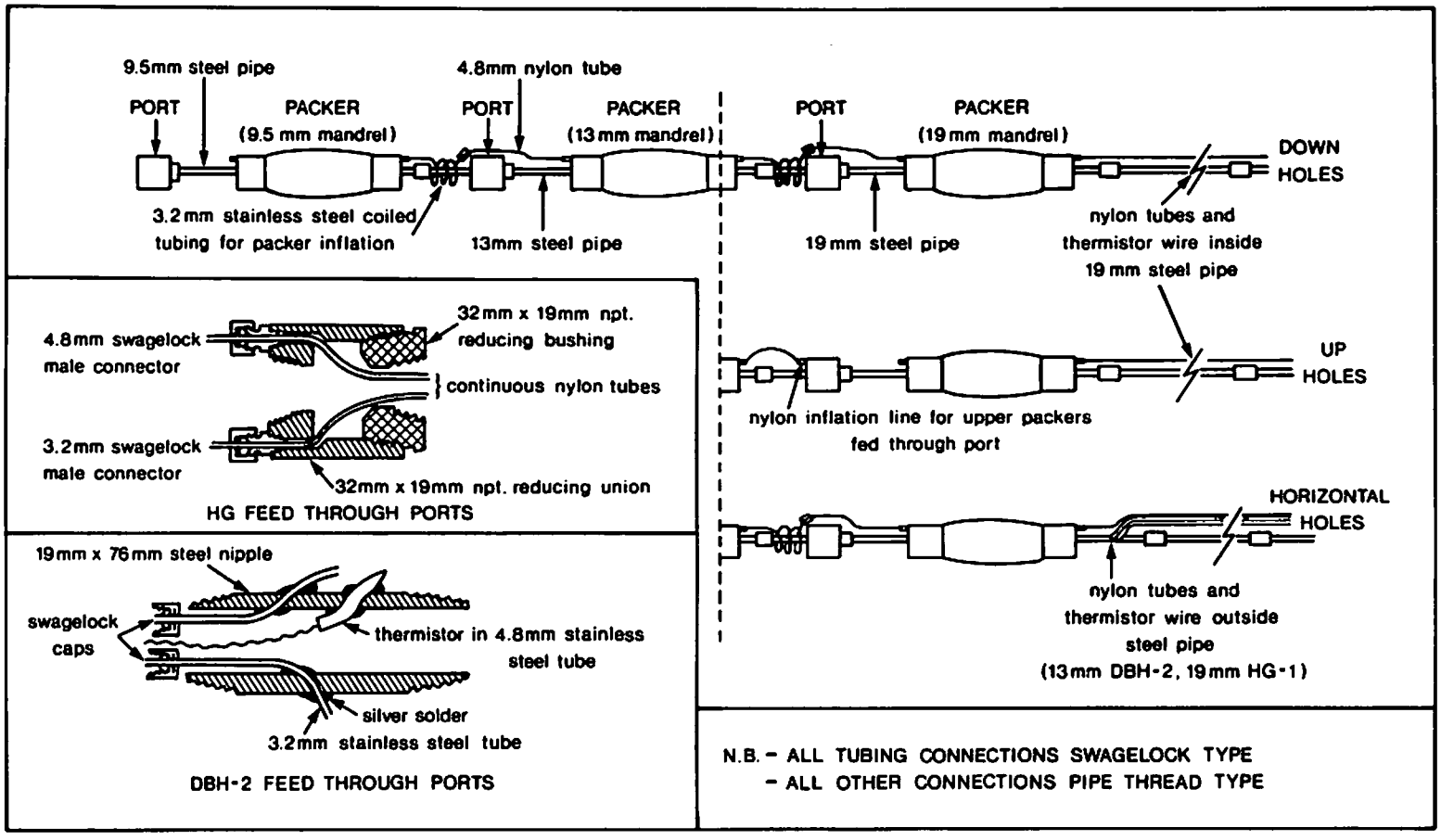

XBL 8111-12178

Fig. 3.1. Schematic of downhole equipment.

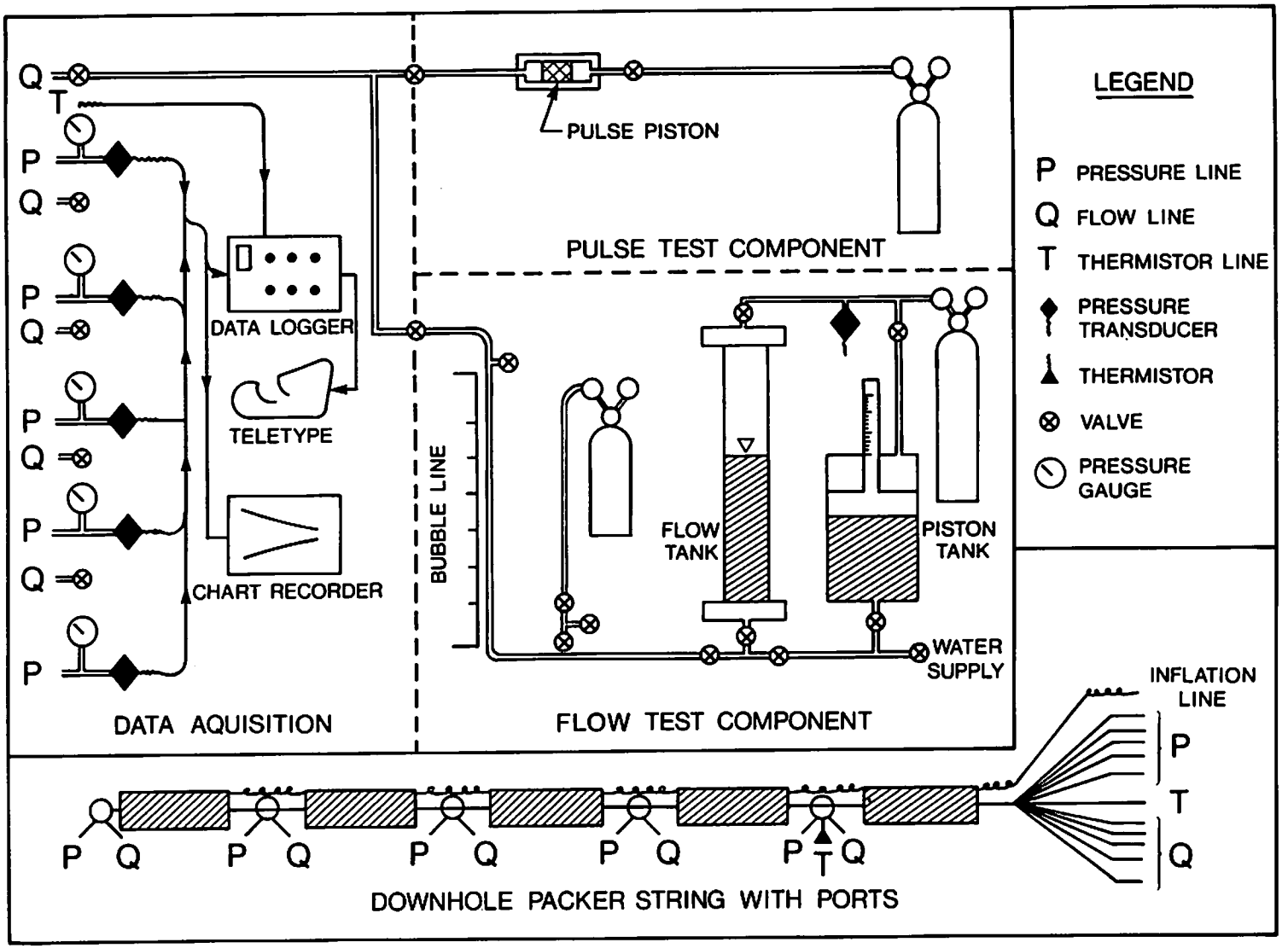

XBL 8111-12179

Fig. 3.2. Schematic of surface equipment with downhole connections.

3.2 Down-Hole Installation

The final borehole installation pattern is shown schematically in Fig. 3.3. Individual borehole installation diagrams may be found in Appendix III. X, Y, Z coordinates of relevant cavity positions are presented in Appendix IV. Down-hole equipment was inserted into the holes by two persons using a 4 strand block and tackle system. To provide manageable equipment lengths, all port connections (but not all pipe thread connections) were completed before installation. Port and packer packer positions were measured for final reference to the borehole collar. As the equipment was inserted into each hole, the remaining pipe thread joints and packer inflations lines were connected (these connections had all been pressure checked prior to assembly). After installation the packers were repeatedly inflated and deflated to check for air leaks and to force air out of the borehole and pressure lines. Finally the pressure lines were connected to the pressure gauge system (Fig. 3.2) and any remaining air was removed from the lines. As each hole was completed, water was cycled through the system to confirm that the lines were open. Packer locations were chosen to provide approximately 7 liters of cavity volume and to intersect a variety of different fracture geometries and spacings. The packer string used in HG1 was set in two different locations (Settings A and B) during the test program; thus, interval HG1 - 4A is not shown in Fig. 3.3. This interval, however, included all of the HG1 intervals. The volumes of intervals HG1 - 4A, HG1 - 4B, and HG3 - 2 were much more than the standard 7 liters (Fig. 3). Although intervals in DBH-2 appear longer than other standard intervals, their volumes were approximately 7 liters because the hole diameter (56 mm) was smaller than the HG hole diameter (76 mm). The minimum distance between cavities in different holes was 0.3 m.

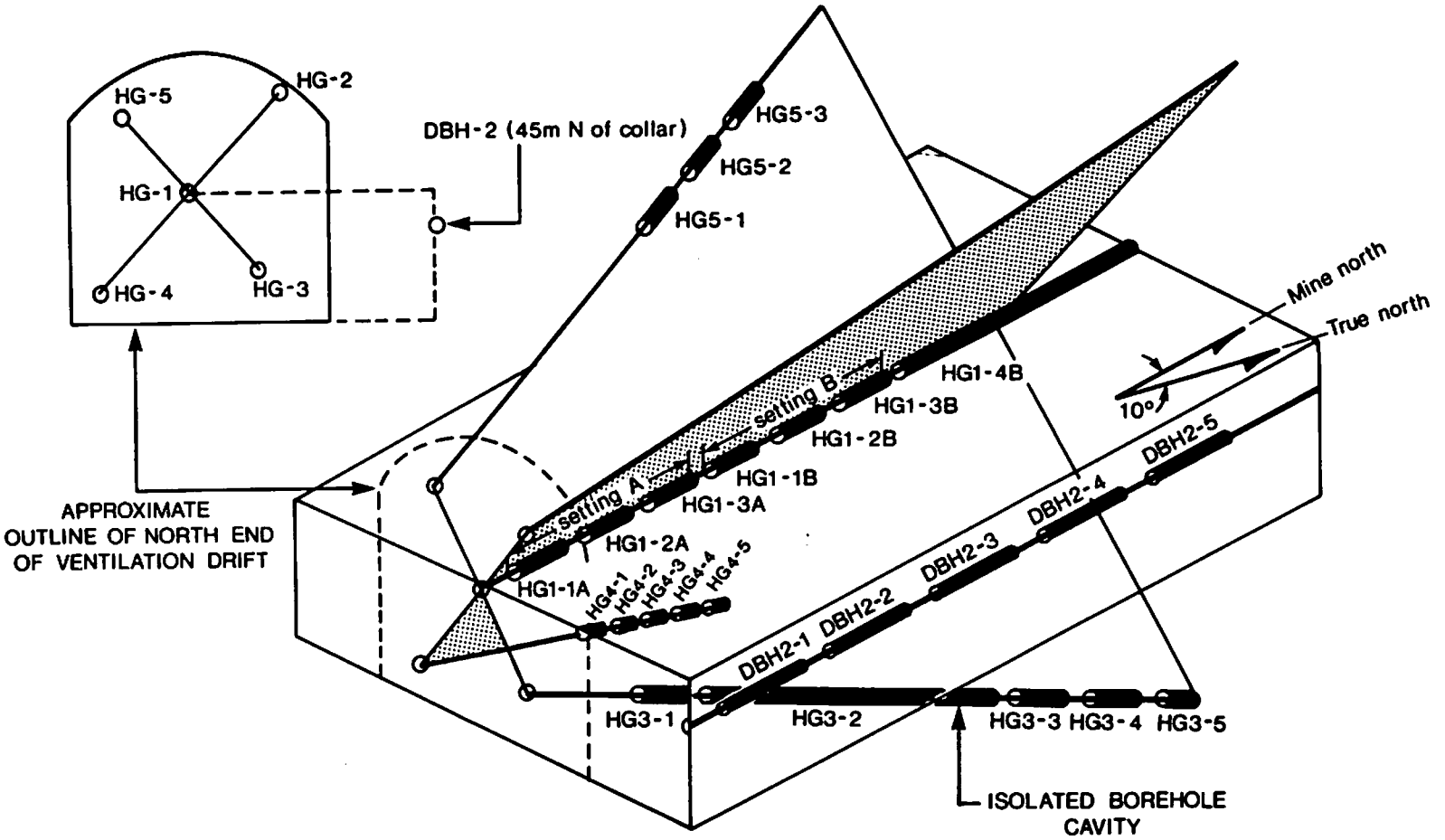

XBL 8111-12180

Fig. 3.3. Schematic perspective of borehole installation pattern.

3.3 Test Procedures

Both injection (steady state) and pressure pulse (transient) permeability tests were conducted in a variety of the test intervals. A detailed log of the testing sequence is contained in Appendix IV.

3.3.1 Injection tests

Injection tests were conducted by measuring the steady state-rate of flow into the test cavity under a steady pressure. Flow rates were measured using the bubble line (short tests) and the flow piston (long-term tests). Water pressures were monitored in the drift by using transducers connected to the test cavity and several of the other intervals. Gauges were used to monitor response in these and the remaining intervals. Temperatures were monitored by downhole thermistors at various positions in the installation. Transducer and thermistor data were recorded using a data logger, teletype, and chart recorder. After steady flow was achieved at a constant injection pressure, the pressure was increased and the flow rate monitored again. At least two, and generally three, pressure increments were conducted in each cavity tested.

3.3.2 Pressure pulse tests

Pressure pulse tests were conducted by displacing a small volume of water (0.9 cm^3 to 4.9 cm^3) in the tube connected to the test cavity and observing the resulting pressure increase and decay. Pressure and temperature were monitored and recorded using the same equipment and procedures as in the steady-state injection tests. Water was displaced by "firing" various-sized pistons in a short tube under 6.8 MPa air pressure (Fig. 3.2). "O" ring seals on the pistons ensured that no air leaked during or after piston firing.

4.0 TEST RESULTS

4.1 Shut-in History

In situ groundwater pressures were monitored in each cavity immediately after it was de-aired and sealed. Zero time corresponds to the shut-in time of the first borehole string (HG-3). Summary plots of the pressure histories for all test cavities are shown in Fig. 4.1. Data plotted in Fig. 4.1 are gauge pressures measured at gauge installation. The plot is arranged to facilitate comparison of the absolute values and time history of the cavity shut-in pressures. Thus all plots have the same X and Y axes. The dotted lines indicate the times of shut-in or release of a particular packer string.

HG5 was shut-in twice. Air was suspected to be in cavity HG5-1, so after the first shut-in, the packers were deflated to release the air then re-inflated for the final shut-in. HG1 was shut-in first at a setting with the first cavity very near the collar, then at a setting somewhat further down the hole (Appendix III). Other variations in shut-in pressure resulted from such factors as: (i) valves opening and closing, (ii) pressure pulse and short-term injection testing, (iii) the "Moebus" experiment and long-term injection testing, and (iv) conductivity characteristics of particular intervals.

Pressure variations caused by the working of valves, pulse testing, and the short-term injection tests are of only minor significance. Variations resulting from the "Moebus" experiment and the long-term injection tests are discussed in section 4.2.

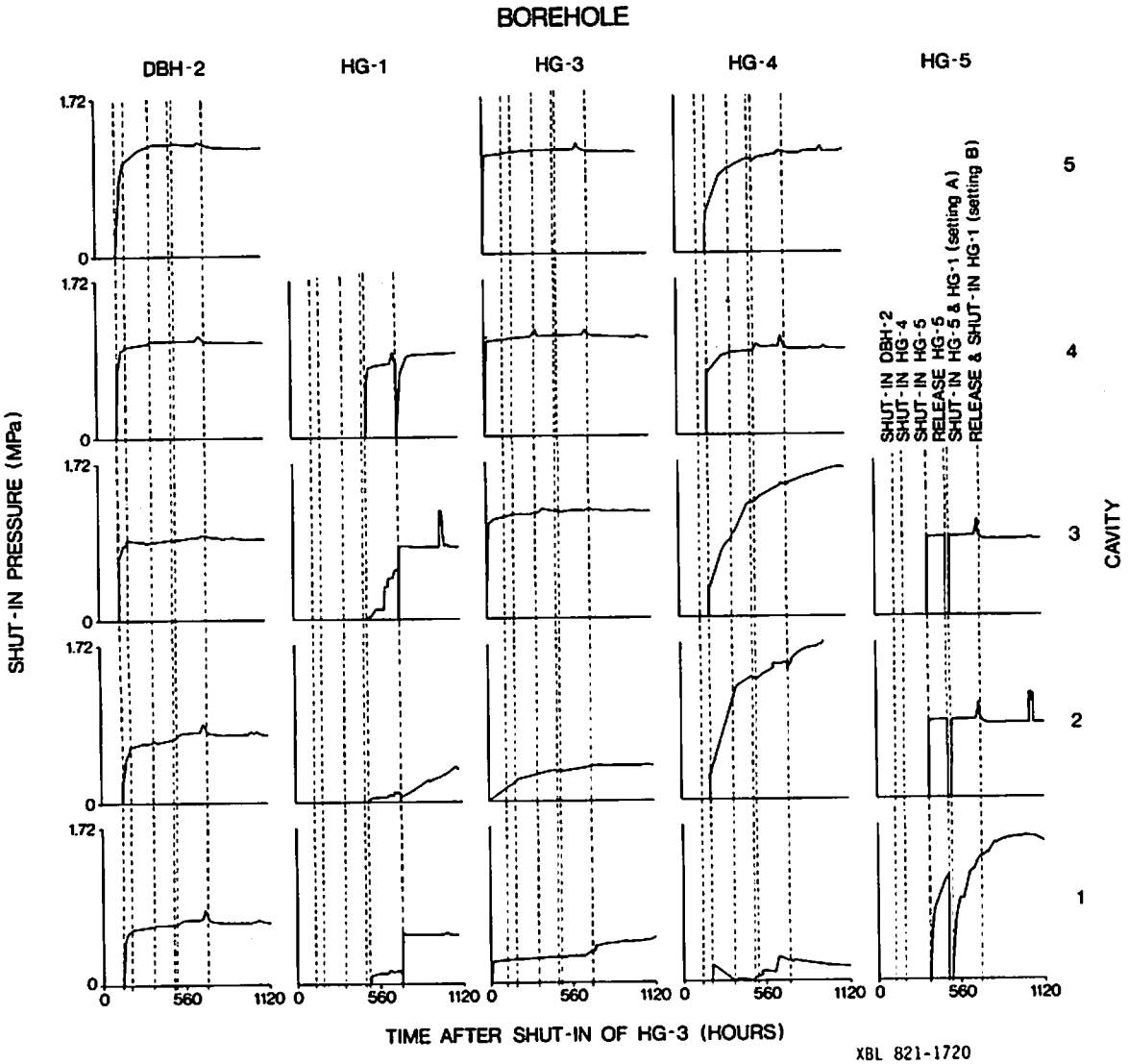

Fig. 4.1. Plots of pressure against time for complete test history.

Several points should be noted about Fig. 4.1. There is a large variation in the time required to reach a stable shut-in pressure (if a stable pressure was indeed reached in the relatively short-term injection experiments). Cavities HG5-2 and HG5-3 stabilized within 10 to 30 minutes; other cavities required several hours to several hundreds of hours to stabilize. All cavities, except HG1-4 and HG3-2, were of approximately the same volume (7 liters). Thus, for cavities with similar volumes, it would be expected that the relative conductivity of each interval could be estimated from the relative times required to reach stable shut-in pressures. It can be seen that the rock surrounding cavities HG5-2 and HG5-3 appears to be the most permeable, while the rock surrounding cavities HG1-2 and HG3-1 is the least permeable. The flow of water into cavities HG1-2 and HG3-1 is apparently so low that the effects of packer compliance and, possibly, air leakage dominate the observed pressure history. The effects of air leaking from the packers into the test zones is evidenced in the steady increase of pressures plotted for HG4-2, HG4-3 and HG5-1 to values well above pressures measured in other intervals. Air leakage and equipment compliance can thus obscure the expected inverse relationship between cavity permeability and the time required to reach a stable shut-in pressure.

Absolute values of pressure measured in each cavity show similarities and variations which are of interest. Table 4.1 shows the stable shut-in values and corresponding hydraulic heads (referenced to the 400-m Z coordinate) reached in each cavity; final shut-in values are shown where stable pressures were not achieved. Stable hydraulic heads range from a low of 76 m in HG1-2A to a high of 184 m in intervals HG3-3 and DBH2-5. The two horizontal holes HG1 and DBH2 give an impression of the pressure gradients existing in the

Table 4.1 Cavity Shut-In Pressures.

Cavity	Shut In Pressure* (MPa)	Hydraulic Head (meters above Z= 400)
DBH2-1	0.70	135.2
-2	0.77	142.3
-3	0.89	154.5
-4	1.06	171.7
-5	1.18	183.9
HG1-1A	0.14	79.6
-2A	0.10	75.5
-3A	0.57**	123.3
-4A	0.79	145.6
HG1-1B	0.55	121.2
-2B	0.34**	99.9
-3B	0.80	146.6
4B	0.92	158.8
HG3-1	0.46	111.6
-2	0.39	104.5
-3	1.18	184.8
-4	1.08	174.6
-5	1.12	178.7
HG4-1	0.15**	80.1
-2	1.74**	241.3
-3	1.62**	229.3
-4	0.94	160.2
-5	1.10	176.4
HG5-1	1.52**	224.6
-2	0.82	149.2
-3	0.83	149.5

* All hydraulic head values are referenced to Z coordinate = 400 m for convenience in comparison.

** Pressure was unstable, but final pressure (at time = 1200 hours) is given.

rock mass under consideration. In DBH2, a steady increase in shut-in pressure occurs as distance from the ventilation drift increases (Fig. 4.2). Data from HG1 show that a similar but steeper increase in shut-in pressure occurs as distance from the ventilation drift increases. Boreholes R1 through R5 and the HG holes are collared at, or near the end of, the drift; thus, there is an increased potential for drainage of water at the drift face as shown by the steeper gradient in HG1. Neglecting the influence of the adjacent mine workings one would expect a maximum shut-in pressure of 3 MPa at 330m below ground. However, shut-in data obtained from SBH1 and R1 (Gale et al., 1980) indicates that drainage of water to the adjacent mine would allow a maximum shut-in pressure of 1.7 MPa. Table 4.1 shows that most pressures fall well below this maximum, indicating a depressurization of the rock mass near the ventilation drift and associated boreholes. In particular, the freely flowing R1 borehole (approximately 0.3 liters/min) acts as a significant local drain, causing a general depression of water pressures at the end of the ventilation drift. Sealing of this borehole during the "Moebus" experiment (just prior to the repositioning of HG1 packers) caused a significant increase in many cavity pressures (Fig. 4.1); this confirmed that R1 acts as a local drain.

Interborehole pressure effects were also caused by sealing and releasing various packer strings. Particularly good examples of this occur in DBH2 where pressure increases occur in most cavities in response to sealing boreholes HG4 and HG5. In addition, many cavities show a general decrease in pressure in response to changing HG1 from setting A to setting B. In the change of setting, the packers are reset 10 m deeper in the hole, allowing 10 extra meters of drainage into the drift which tends to depressurize

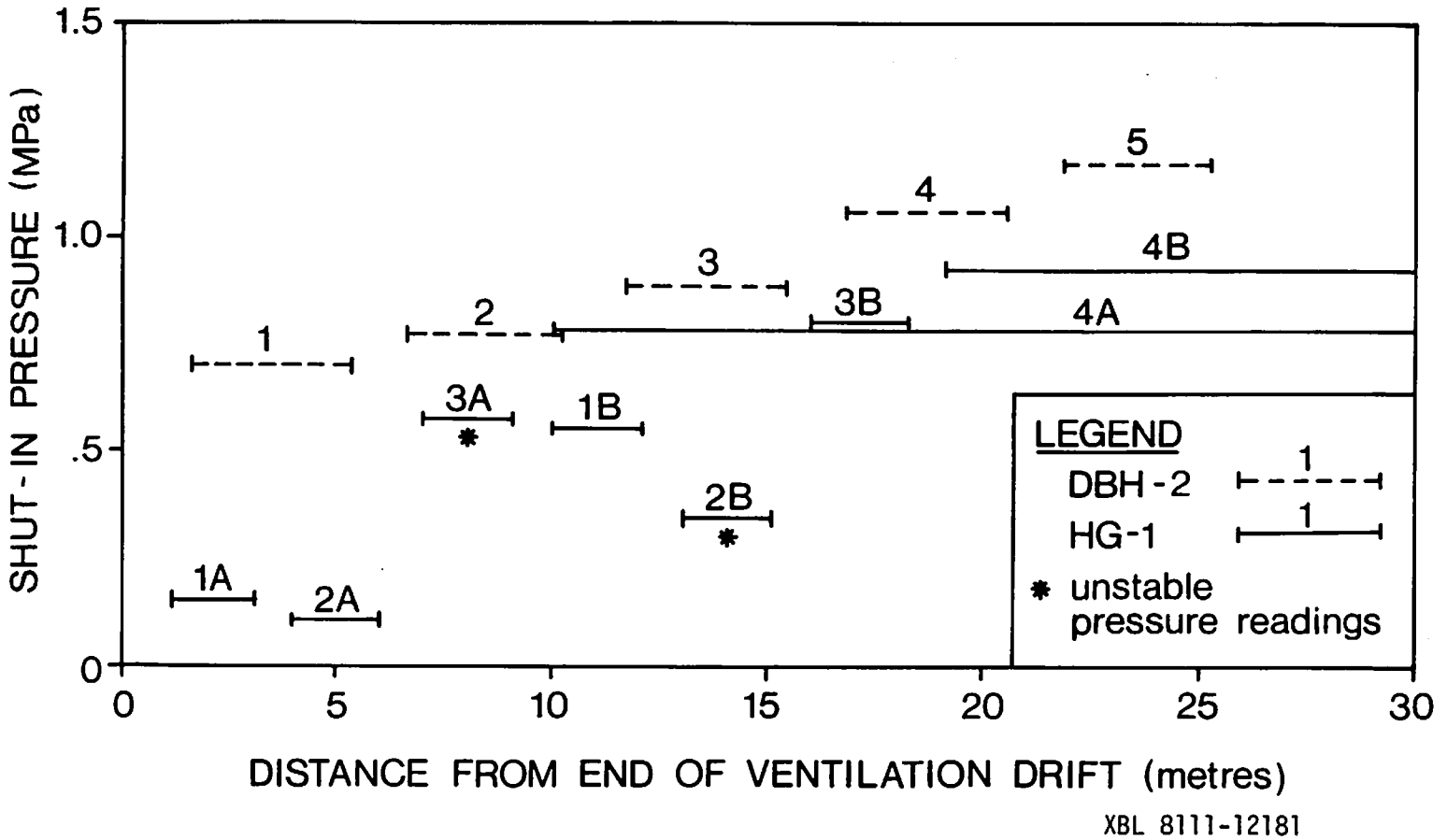

Fig. 4.2. Variation of shut-in pressure as a function of distance from end of the ventilation drift in horizontal boreholes HG1 and DBH2.

more of the rock mass. Thus, it is evident that the fracture system is reasonably well interconnected, but in a fairly complex manner. It also appears that the pressure distribution observed in the HG holes is determined primarily by the drainage from the R1 holes, the HG holes, and the drift faces (in order of importance) and secondly by the influence of the adjacent mine workings.

4.2 Injection Test Results

4.2.1 Short-term tests

Routine injection tests of less than 2 hours were run throughout the test program. Results are shown in Table 4.2. Injection tests yield values of flow rate Q at specified pressure for several pressure increments ΔP. These flow-rate values are used to calculate a steady-state conductivity value under standard assumptions of ideal porous media flow. It was assumed that the tests were performed in a homogeneous and isotropic porous medium with only radial flow from the cavity. These assumptions are obviously not correct in a fractured granite system. However, a preliminary assessment of the relative conductivities of each interval may be obtained for comparison to the pressure pulse test results. Calculated conductivity values range from less than 10^{-11} cm/sec to 2×10^{-7} cm/sec. Injection rates of 0.007 cm^3/min to 0.826 cm^3/min were used. Thus, the total volume of of water pumped into the rock during a single two-hour test was on the order of 1 to 100 cm^3. Minimum flow rates (minimum conductivities) are dictated by the sensitivity of the flow-rate measurement equipment (Appendix II). In situ pressures (used in the calculations made for each test) were considered to be the cavity pressure values immediately before the test, but only after a reasonably stable short-term (1 hour or more) pressure history. During the short-term tests, no significant pressure response was noted in any of the observation cavities.

Table 4.2. Results of short-term injection tests.

Cavity	Test	Q_3 (cm /min)	$P_{in-situ}$ (MPa)	ΔP (MPa)	K_{ss}* x 10^9 (cm/sec)	Mean Interval K_{ss} x 10^9 (cm/sec)
HG1-1	A	0.0073		0.017	1.3	
	B	0.015		0.038	1.2	
	AA	0.0068	0.534	0.017	1.2	1.2
	BB	0.014		0.038	1.1	
	CC	<0.0024**		0.073	-	
HG1-2	-	-	-	-	-	-
HG1-3	A	0.137		0.041	9.9	
	B	0.323	0.797	0.092	10.0	10
	C	0.469		0.127	12.0	
HG3-1	-	-	-	-	-	-
HG3-2	-	-	-	-	-	-
HG3-3	A	0.0117		0.084	0.39	
	B	0.0137	1.170	0.116	0.33	0.35
	C	0.0205		0.168	0.34	
HG3-4	A	0.0108		0.023	1.3	
	B	0.0391	1.092	0.074	1.5	1.5
	C	0.0782		0.123	1.8	
HG3-5	A	0.440		0.037	45	
	B	1.017	1.104	0.084	45	45
	C	1.526		0.126	45	
HG4-1	-	-	-	-	-	-
HG4-2	-	-	-	-	-	-
HG4-3	-	-	-	-	-	-
HG4-4	A	0.0068		0.034	0.65	
	B	0.0081	0.936	0.049	0.42	0.46
	C	0.0108		0.109	0.32	
HG4-5	A	<0.0016**	1.110	0.052	<0.14	<0.14
	B	<0.0023**		0.074	<0.14	
HG5-1	A	<0.0024**	1.572	0.038	<0.28	<0.04
	B	<0.0008**		0.071	<0.037	
HG5-2	A	2.62		0.049	180	
	B	4.34	0.704	0.083	180	180
	C	5.95		0.111	180	

Table 4.2, continued

Cavity	Test	Q_3 (cm /min)	$P_{in\text{-}situ}$ (MPa)	ΔP (MPa)	K_{ss}* x 10^9 (cm/sec)	Mean Interval K_{ss} x 10^9 (cm/sec)
HG5-3	B	2.19		0.047	152	
	C	3.52	0.826	0.074	152	152
	D	6.55		0.135	152	

$$* \quad K_{ss} = \frac{Q}{2\pi L \Delta h} \ln \frac{r_e}{r_o}$$

where Q = flow rate (cm^3/sec)

Δh = head drop (cm)

L = interval length (cm)

r_e = radius of influence

r_o = radius of well = 76 mm

$\frac{r_e}{r_o} = 10$

** Minimum flow measurement = 0.0488 cm^3.
Thus zero flow over specified time yields maximum possible flow rate.

4.2.2. Long-term tests

Some injection tests were performed over a period of tens of hours. This category includes the inadvertent "Moebus" experiment. Injection testing of the adjacent R holes was being carried out concurrently with the pressure pulse field experiment. The concurrent injection testing resulted in the shutting in of a high-outflow zone (approximately 0.3 liters/min) in borehole R1 (Fig. 1.4) for approximately 14.5 hours. This shutting in of the high-flow cavity in R1 produced significant pressure changes in a number of the test cavities and is referred to as the "Moebus" experiment (after M. Moebus, who assisted with the field program). This experiment inadvertently demonstrated that much of the fracture system in the rock mass around the ventilation drift is well interconnected and that a pressure perturbation in a small borehole cavity can influence the pore pressures in a very large volume of fractured rock.

Pressure responses were also observed in a number of observation cavities as a result of the routine injection tests. Figures 4.3 and 4.4 show the pressure history during long-term injection tests and during the "Moebus" experiment, respectively. Note that the shut-in pressure on the y axes of the plots represents a base pressure that differs between individual intervals in order to provide a visual comparison of individual pressure-time plots.

Figure 4.3 shows the pressure variation in all cavities during the 150-hour period from 970 to 1120 hours. (Zero time refers to the time at which the cavities were shut-in). During this 150-hour period, two long injection tests were performed. The first test was performed in HG1-3 (at 989 hours) and the second in HG5-2 (at 1021 hours). The dotted and dashed lines on the

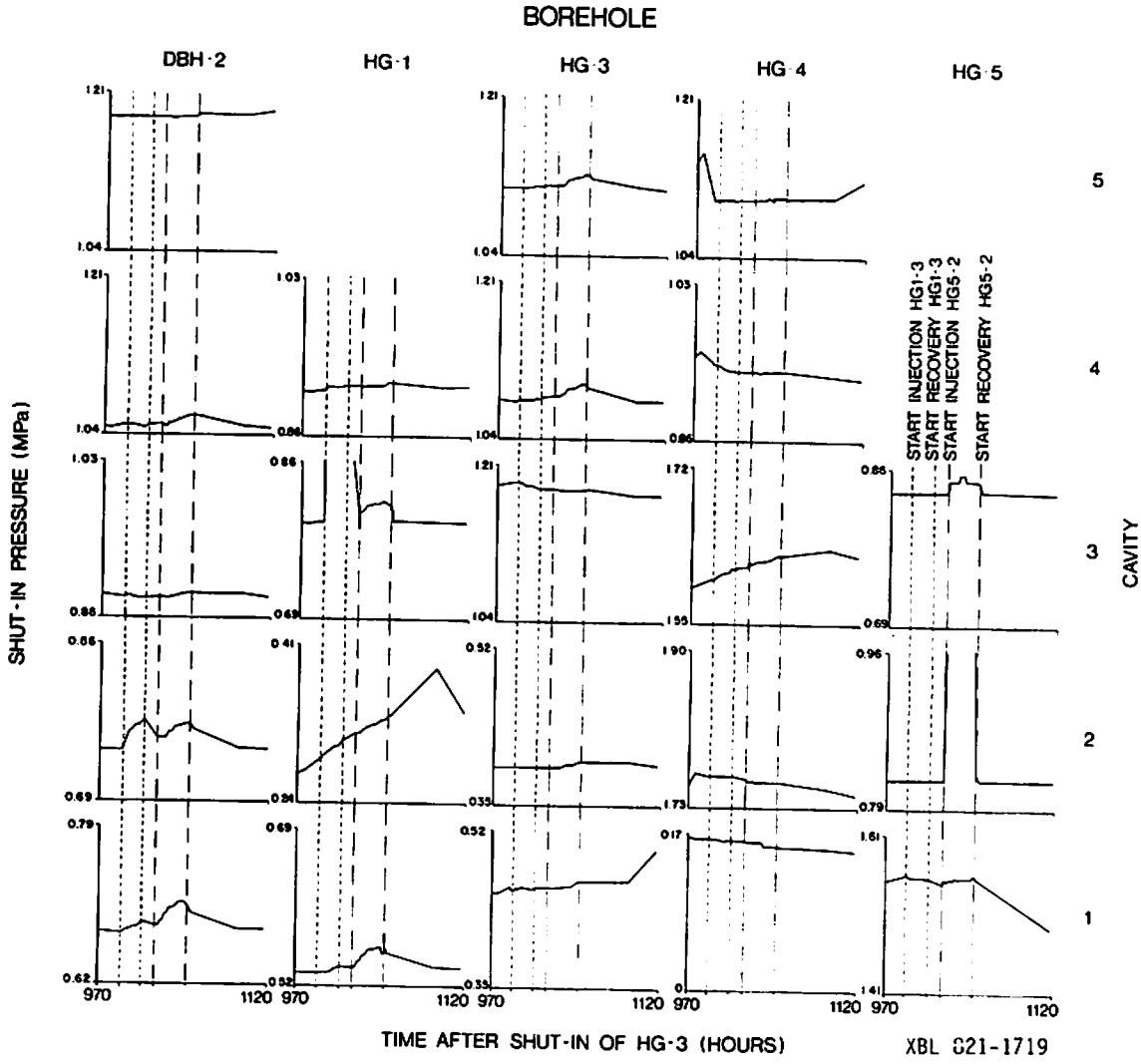

Fig. 4.3. Plots of pressure against time during long-term injection tests.

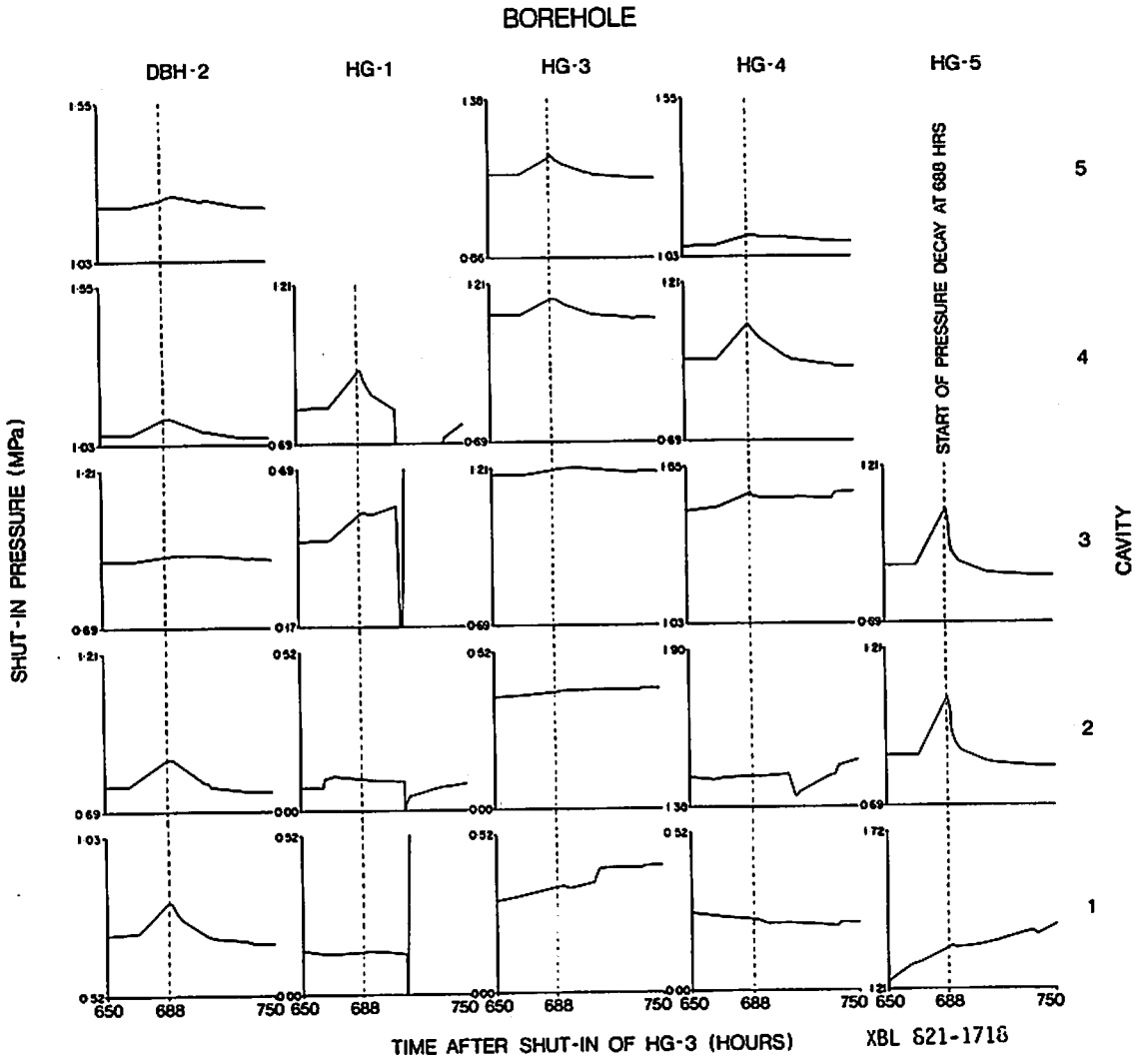

Fig. 4.4. Plots of pressure against time during "Moebus" experiment.

plot show the times for start of injection and start of recovery for each test. Table 4.3 shows the flow rate (Q), injection pressures (ΔP), total volume injected (Q net), gauge shut-in pressure (P in-situ) and the resultant hydraulic conductivities (K_{ss}).

Table 4.3. Results of long term injection.

Test Cavity	3^{Q} (cm3/min)	Test Time (hours)	Q net (litres)	P in-situ (MPA)	ΔP (MPa)	$^{*}K_{ss} \times 10^{-9}$ (cm/sec)
HG1-3	0.94	19.5	1	0.797	0.393	7
HG5-2	12	27	19	0.704	0.310	130

K values from long-term tests calculated using same assumptions (including radius of influence) as values from short-term tests.

Since similar injection pressures of 0.39 and 0.31 MPa above ambient were used, the difference in flow rates--approximately one order of magnitude --reflects the difference in cavity conductivities.

Calculated conductivities are similar to values obtained by short-term injection testing of the same intervals (Table 4.2). The short-term tests are thus expected to provide an adequate measure of conductivities for comparison with pressure-pulse results, although they appear to overestimate conductivity when compared with long-term injection tests; this is assumed to result from an increased radius of influence in the long-term tests.

For selected borehole cavities, detailed plots of pressure variations during long-term injection tests are shown in Figs. 4.5 and 4.6. Straight-line distances between the injection cavity and a specified observation cavity are included on the plots.

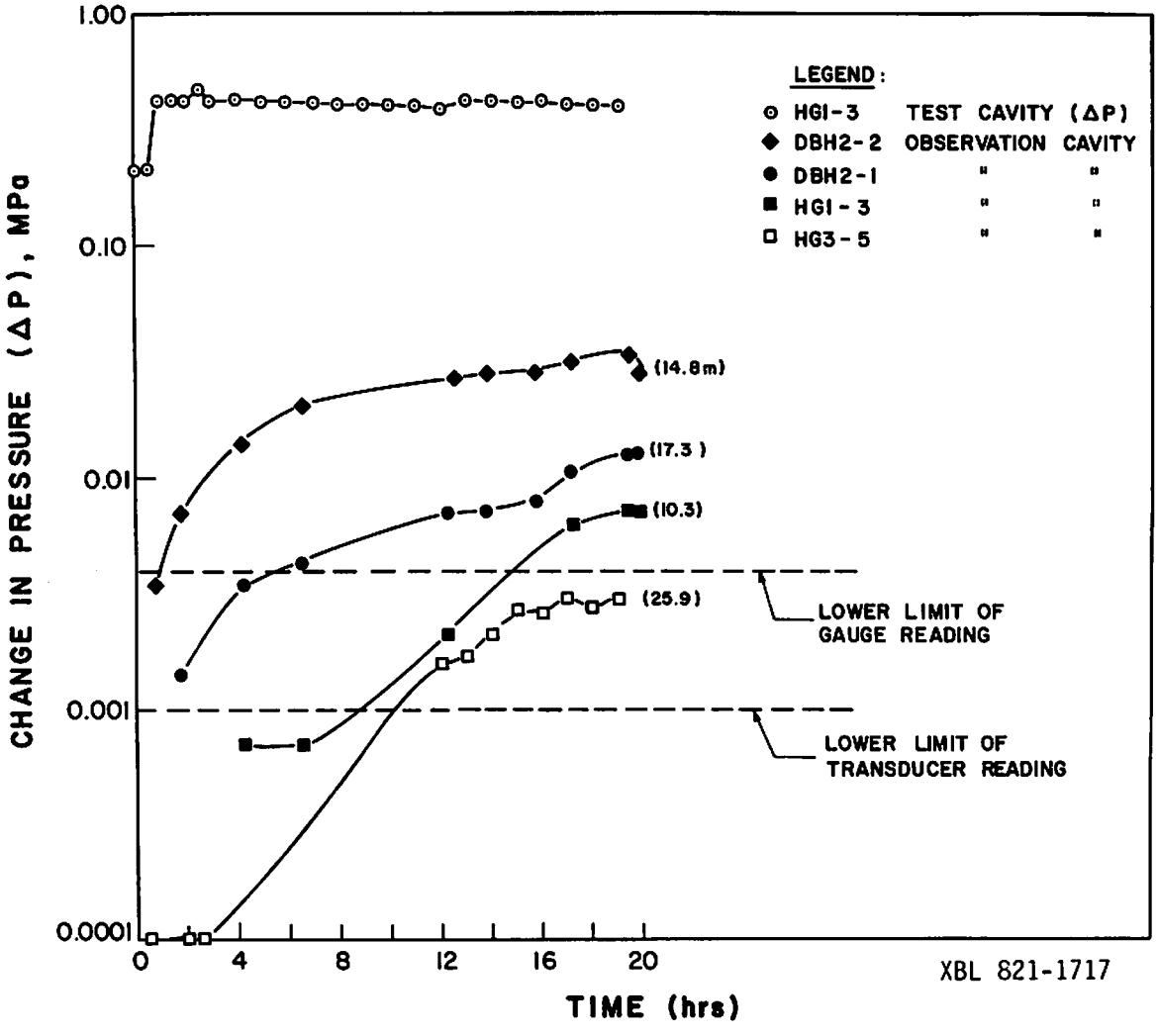

Fig. 4.5. Pressure responses to long term injection tests in HG1-3.

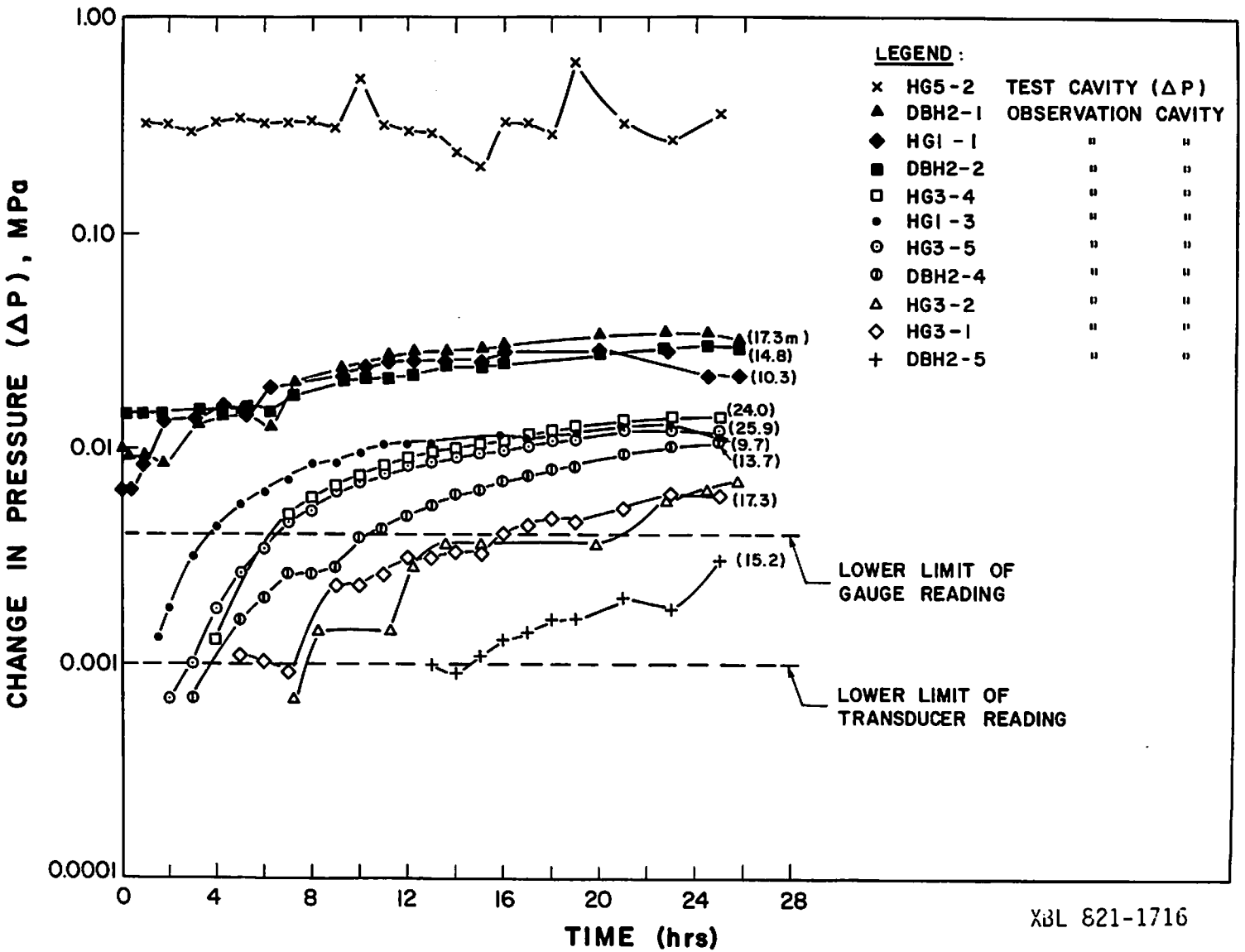

Fig. 4.6. Pressure responses to long term injection tests in HG5-2.

The ability to determine whether a pressure response occurred in a particular cavity depends on the sensitivity of the monitoring equipment. In this case, transducer data is believed to be reliable at pressure differences in excess of 0.001 MPa. Table 4.4 shows the cavities where a pressure response was noted and the equipment which measured the response. Some cavities had not fully recovered from testing of HG1-3 (Fig. 4.3), so their early pressures were affected, to varying degrees, by this residual pressure; however, the final P values are presumed to reflect the response to the HG5-2 test rather than the HG1-3 test.

Table 4.4 shows that a pressure response was observed in 38% of the observation cavities during HG1-3 testing and in 67% during HG5-2 testing. This difference is attributed to the difference in total injected volumes of water (HG1-3 received 1 liter; HG5-2, 19 liters). The greater the volume of water injected, the greater the volume of rock affected by the test. In general, the magnitude of the pressure response resulting from the HG5-2 test is greater than that from the HG1-3 test. Results from both tests indicate a variation in the magnitude of the pressure response and the time required to create a significant response. This variation is not directly related to the straight-line distance between pressure test and observation cavities. However, for both tests the maximum observed pressure response was approximately 0.03 MPa, or 10%, of the applied injection pressures in HG1-3 (0.4 MPa) and HG5-2 (0.3 MPa). Both tests in DBH2-1, DBH2-2, and HG1-1 produced maximum pressure responses. Also, many of the observation cavity pressures reached a quasi-steady state during testing of HG5-2, while only one cavity attained such a condition during testing of HG1-3. The lack of correlation between straight-line distance and pressure response (magnitude and time

Table 4.4. Response to long-term injection tests.

Cavity	Monitor		Response to:	
	Gauge	Transducer	HG1-3	HG5-2
DBH2-1	*		*	*
2	*		*	*
3	*		#	*
4	*	*	*	*
5	*	*	#	*
HG1- 1	*		*	*
2	*		#	#
3	*	*	-	*
4	*		*	*
HG3- 1	*	*	#	*
2	*		#	*
3	*	*	#	#
4	*	*	*	*
5	*	*	#	*
HG4- 1	*		#	#
2	*		#	#
3	*		*	*
4	*	*	#	#
5	*	*	#	#
HG5- 1	*		#	#
2	*	*	*	-
3	*		#	*

* Response noted.
# No response noted.

to reach steady state) is attributed to the fact that effective radius of influence in a fractured rock mass is a tortuous path of interconnected fractures with a length which cannot be compared to a straight-line distance.

Figure 4.4 shows the pressure variations in all cavities during the 100-hour period from 650 to 750 hours ("Moebus" experiment). Durings this period, a high outflow zone in borehole R2 (Fig. 1.4) was shut-in, creating pressure increases in almost all cavities (Table 4.5). Pressures were not monitored overnight during the shut-in; however, upon the packer release at 688 hours, cavity pressures were monitored on a regular basis. If the total outflow of R1 was redirected into the local rock mass then approximately 2,600 liters of water were injected over the 155-hour shut-in period. The resulting pressure responses range from 0 to 0.18 MPa and are shown in Fig. 4.4 and tabulated in Table 4.5. Trends in pressure response were similar to pressure responses caused by the long-term injection tests (in that the same cavities were affected), except that greater magnitudes were created by the "Moebus" experiment.

It appears that the large volume of water redirected by this test affected the rock mass much as the long-term tests did. However, the increase in the "injected" volume caused a corresponding increase in the magnitude of the pressure response.

4.3 Pressure Pulse Tests

4.3.1 Pressure pulse test results

The operational log for the pressure pulse tests is given in Appendix V. Results of selected pressure pulse tests are tabulated in Appendix VI

Table 4.5. Pressure increase during "Moebus" experiment.

Cavity	Pressure Prior to Test (MPa)	ΔPressure (MPa)
DBH2-1	0.72	0.10
2	0.77	0.09
3	0.91	0.02
4	1.07	0.05
5	1.21	0.02
HG1- 1	0.13	0.01
2	0.10	*
3	0.46	0.09
4	0.81	0.13
HG3- 1	0.32	*
2	0.37	0.01
3	1.18	0.02
4	1.10	0.05
5	1.13	0.07
HG4- 1	0.24	*
2	1.47**	0.01
3	1.42**	0.05
4	0.95	0.12
5	1.07	0.03
HG5- 1	1.30	0.06
2	0.86	0.15
3	0.88	0.18

* No significant pressure increase observed.

**High pressure attributed to packer leakage.

and presented in the normalized pressure versus log time plots of Figs. 4.7, 4.8, 4.9 and 4.10. Test conditions for all pulse tests are tabulated in Appendix VII. Steady-state conductivity values corresponding to each pulse tested interval are also shown on the plots for comparison with the rate of pulse decay. Fractures mapped during core logging are also shown in Figs. 4.7, 4.8 and 4.10. These logs are included to provide an impression of the fracture frequency encountered in each test interval.

4.3.2 Comparison of Pressure Pulse Decay and Steady-State Tests

If the tests shown in Figs. 4.7 through 4.10 were performed in an ideal porous medium, one would expect the pulse tests with the longest decay times to correspond to the lowest steady-state conductivities and those with the shortest decay times to the highest steady state conductivities. Data presented in Figs. 4.9 and 4.10 show that this trend occurs in general, but they also show several tests in Fig. 4.9 that deviate from this trend. These deviations are attributed to one or more of the following:

(i) effects of fracture geometry;

(ii) compliance effects;

(iii) differences in the effective radii of influence of by each test type.

4.3.2.1 Effects of Fracture Geometry. Some insight into the effects of fracture geometry and fracture interconnection can be gained from the work of Wang et al. (1977). Using a semi-analytical model, Wang was able to show that the characteristic pulse decay curve for a single fracture with specified aperture could also represent a set of fractures with a different total

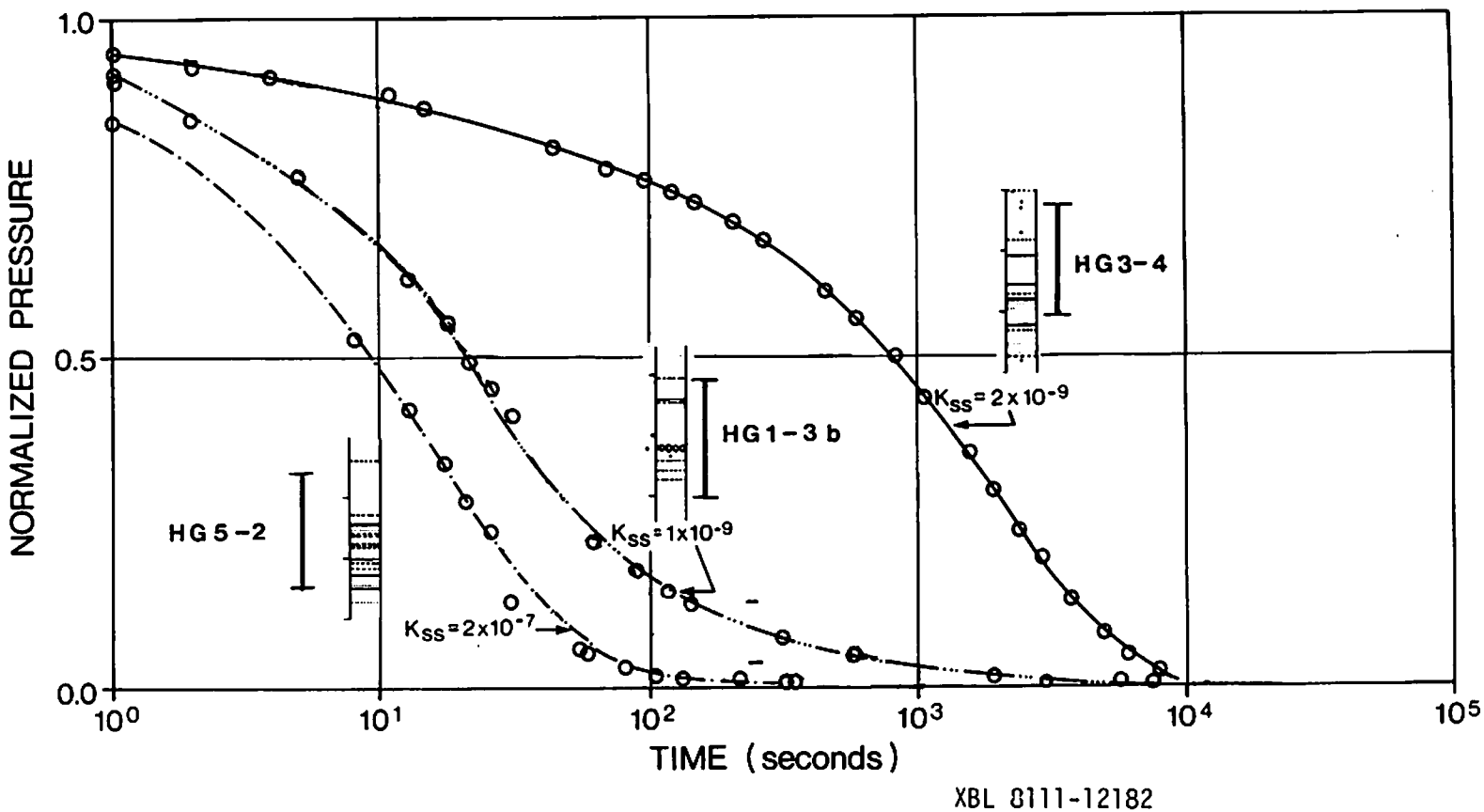

Fig. 4.7. Plots of normalized pressure against log time for pressure pulse tests in intervals HG5-2, HG1-30 and HG3-4.

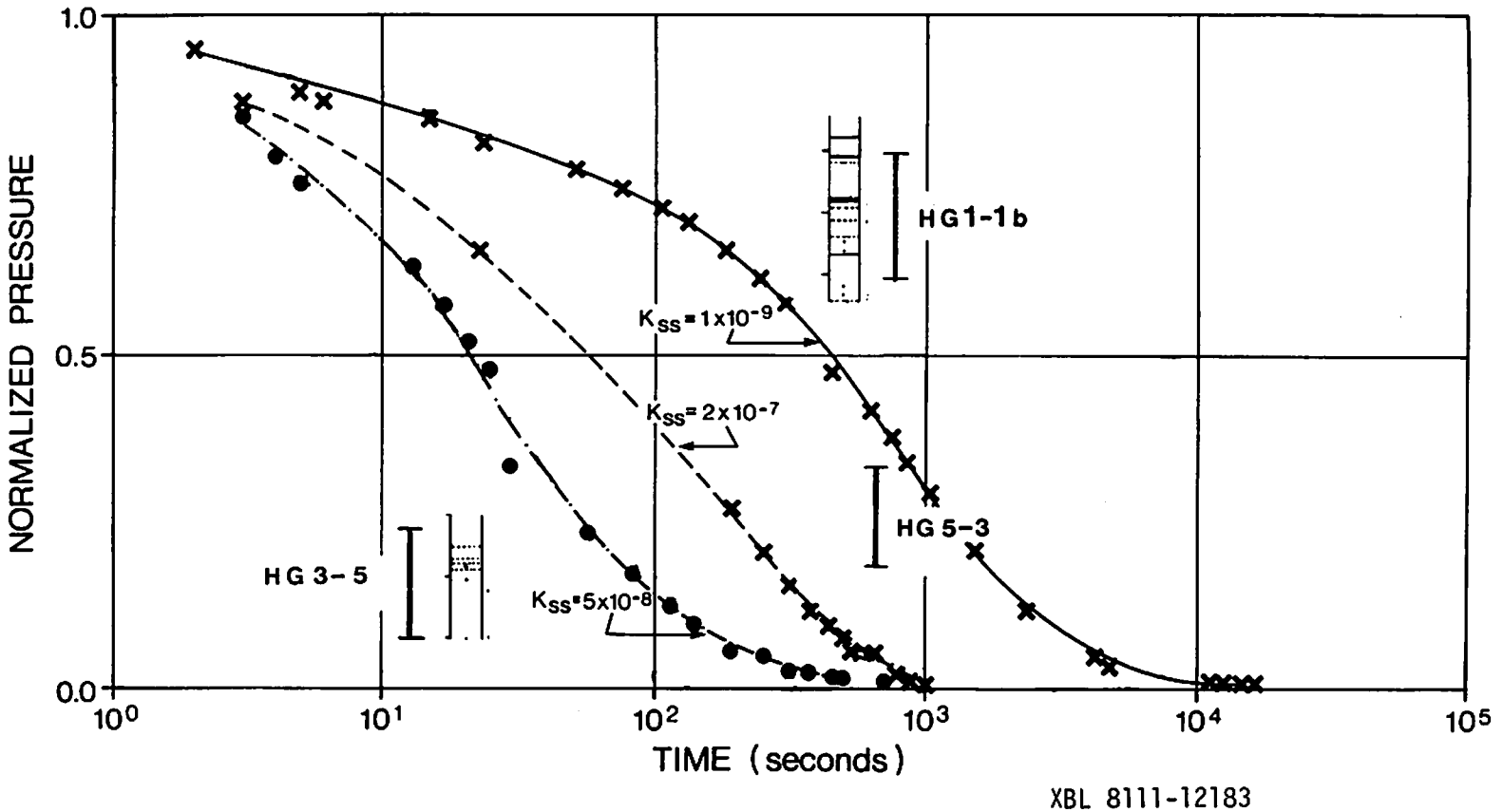

Fig. 4.8. Plot of normalized pressure against log time for pressure pulse tests in intervals HG-2, HG5-3, and HG2-1b.

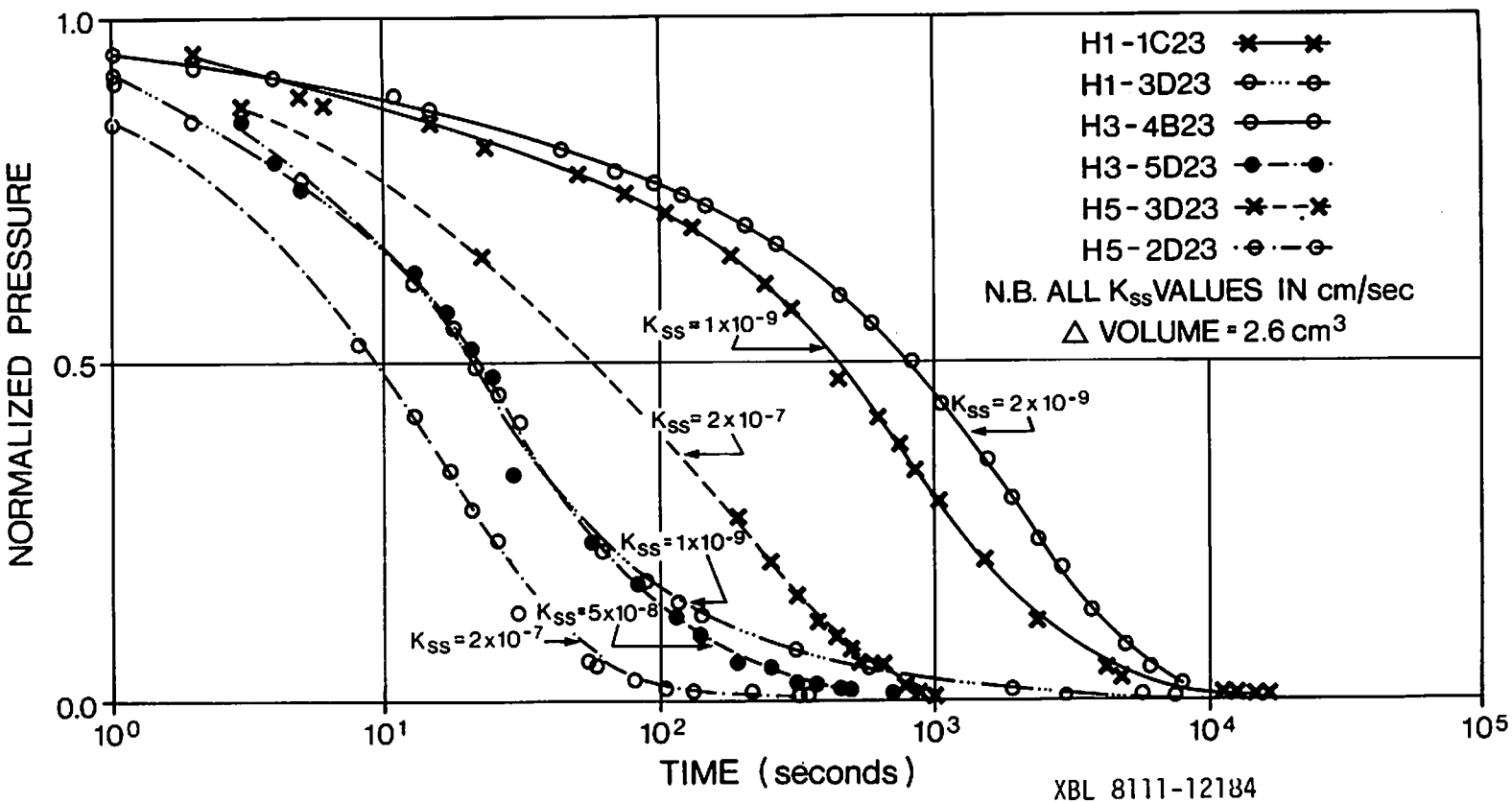

Fig. 4.9. Summary plot of normalized pressure against log time. Curves from Figs. 4.5 and 4.6.

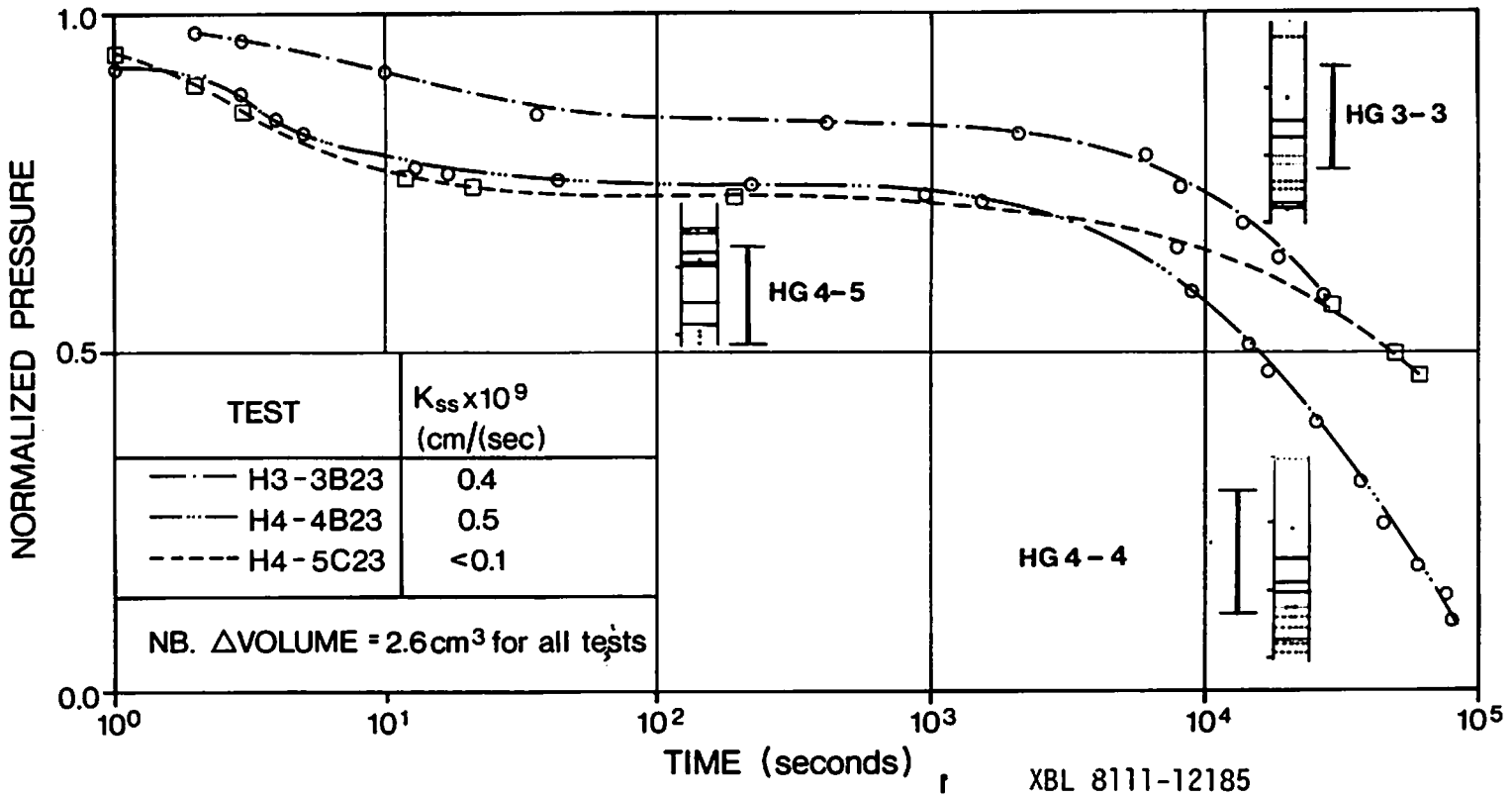

Fig. 4.10. Plot of normalized pressure against lot time for selected pulse tests with extended decay characteristics.

aperture. Fracture logs shown in Figs. 4.7 and 4.8 show that there is quite a variation in number of fractures tested, and presumably there is also a variation in fracture apertures.

Variation in the correlation between steady-state conductivity and pulse decay rate may reflect the difficulties associates in comparing results from test cavities which intersect different numbers and types of fractures. Figure 4.11 shows how two fractures, either in series or parallel, with different aperture and extent, tend to extend the pulse decay curve in a manner similar to the results shown in Fig. 4.10. This effect may also be caused by air in the test cavities, as discussed in the following section on compliance effects.

4.3.2.2 Compliance Effects. The effects of packer compliance, air in test intervals (packer leakage), and temperature variations can also be expected to contribute to the character of the pulse decay curve. The volume-pressure relationships for a sealed, incompressible water-filled container (with volumes of 6, 7, and 8 liters) are shown in Fig. 4.12. These curves were calculated using the compressibility of water β_W obtained from this relationship:

$$\beta_W = \frac{1}{V} \frac{\partial V}{\partial P} \quad , \tag{4.1}$$

where β_W is a function of the container volume V, the change in volume ΔV and the corresponding change in pressure ΔP. Thus, for the ideal field situation of zero permeability and zero compliance effects, these lines would also represent the relationship between volume change caused by piston firing and the resulting pressure pulse. However, with an increase in permeability the slope of the ΔP versus ΔV curve would decrease, reflecting

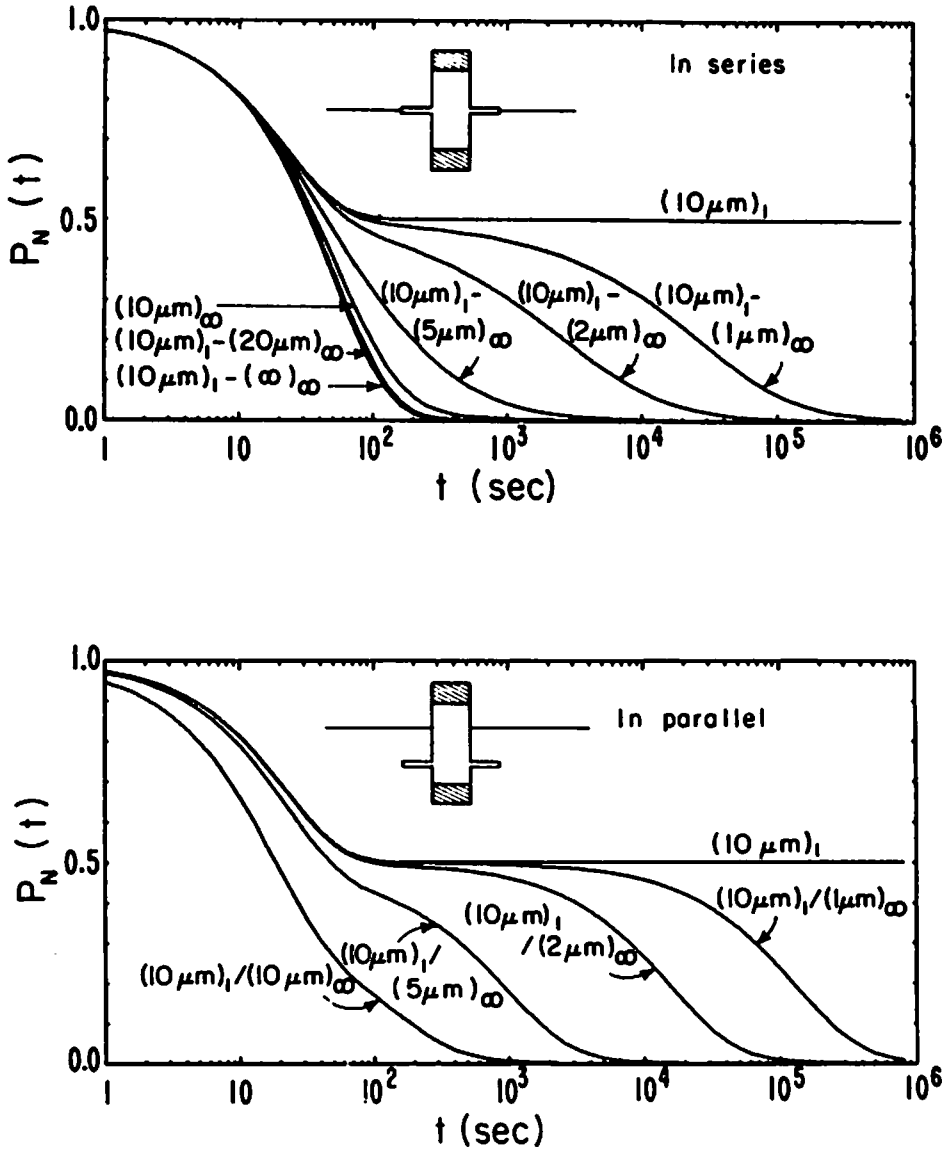

XBL 8111-12186

Fig. 4.11. Normalized pressure decay at a wellbore intersected by a 10 μm fracture with finite volume $V_F/V_W = 1$ in series (a), or in parallel (b) with an aperture 2b fracture with infinite volume. (After Wang et al., 1977).

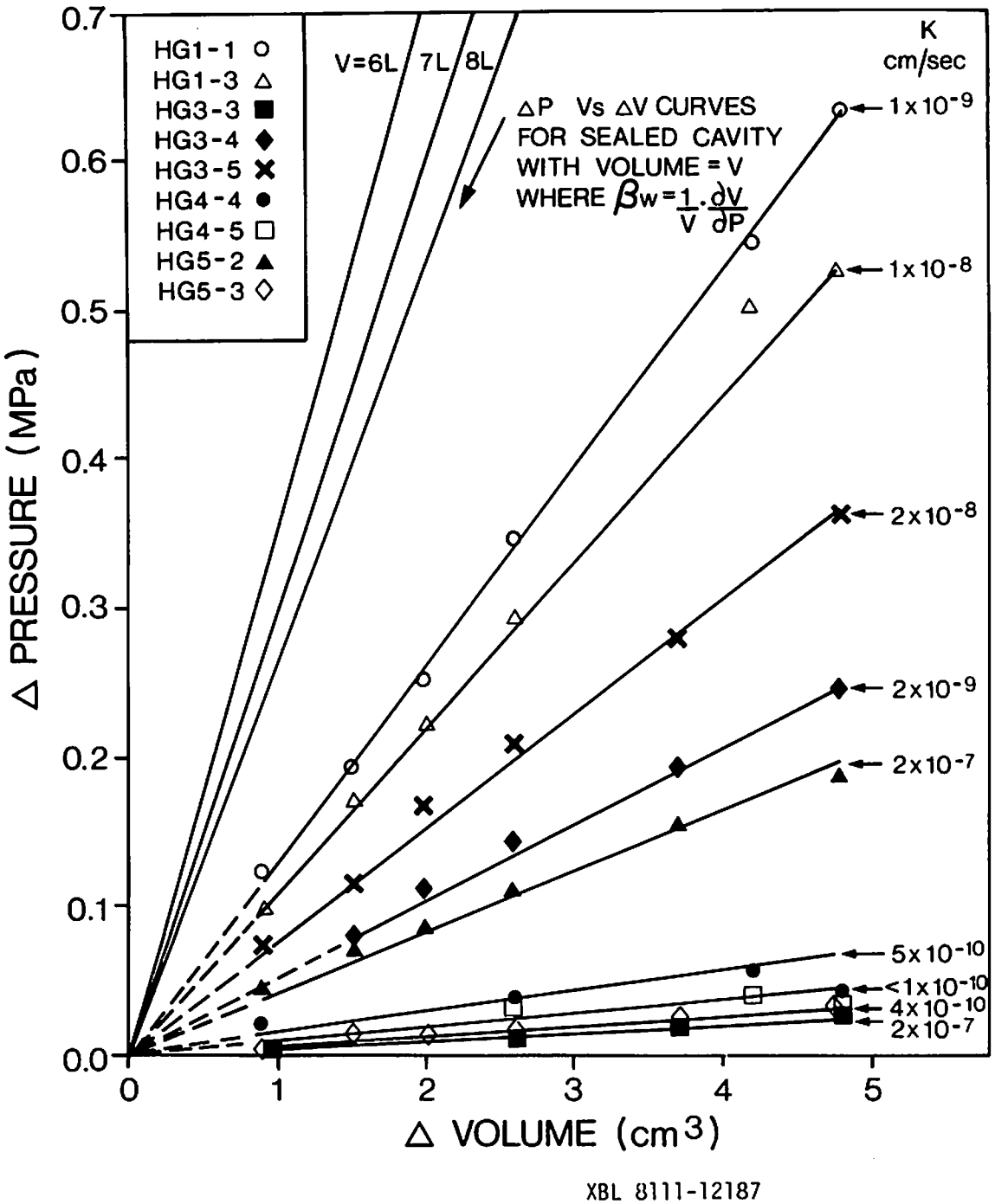

Fig. 4.12. Pulse pressure (ΔP) resulting from imposed displacement volume (ΔV)

an effective increase in the cavity volume. In addition nonlinearities could be introduced in Eq. (4.1) and the resulting ΔP-ΔV curve by the nonlinear effects of packer compliance, temperature fluctions, and air included in the cavity. Cavity air could also provide an effective increase in cavity volume, causing a decrease in the slope of the ΔP-ΔV curve.

Figure 4.12 shows, as expected, that all field ΔP versus ΔV data plot below the ideal curves. However, the expected decrease in the ΔP versus ΔV slope with increasing steady-state permeability is not strictly obeyed. This is similar to the lack of correlation between pulse decay rate and steady-state conductivity. Thus the extended decay curves of Fig. 4.10 correspond to the low conductivity, low slope, and non-linear ΔP versus ΔV curves of Fig. 4.12.

Tests performed by Gale and Raven (1979) indicate that air in a cavity will extend the decay curve in a manner similar to the test results shown in Fig. 4.10. Tests by Forster and Gale (1980) and Gale and Raven (1979) show that packer compliance also tends to increase the decay time and that temperature variations in excess of 0.01°C can either increase or decrease the decay time, depending on the temperature gradient. Temperature fluctuations monitored during testing of HG1-1B and HG3-4 were found to vary up to ± 0.009°C from the initial temperature, with most variation falling near ± 0.005°C (Appendix VI). Temperature effects are thus not believed to cause the extended decay curves of Fig. 4.10. Air was found in some of the HG4 and HG3 cavities at the end of testing and is suspected to have entered to a lesser degree in other cavities. This air is considered the most likely reason for the extended decay characteristics of tests HG3-3, HG4-4 and HG4-5

(Fig. 4.10). Calibration of the field test equipment in the laboratory would help to isolate the effects of packer compliance, including air and temperature variation, on the field test results and to verify that these effects caused only minor variations in the decay curves.

Figure 4.13 is a schematic diagram of the two types of pressure-time curves observed during the test program. As discussed earlier, variations in cavity pressures are a function of several variables, including interval conductivity, fracture geometry, equipment compliance, and air in the cavity. Type A pressure-time histories (Fig. 4.13) show sharp increases in pressure in response to piston firing, then damped pressure oscillations and decay. The pressure oscillations appear to result from transmission of the pulse down the long tubes (3 to 30 m) and back to the pressure transducer. During transmission, the equipment expands and contracts and water flows into the rock surrounding the test interval, resulting in the pressure fluctuations. Thus, the maximum pressure achieved was generally considered to be not the effective pulse pressure but a somewhat lower value chosen by extending the non-oscillating portion of the curve back to t_0 with reference to the degree of pressure oscillation and the number of oscillations in the early portion of the curve. Type B pressure-time histories (Fig. 4.13) show slow increases in pressure to a maximum and then a very gentle decay. Tests performed in DBH2 characteristically produced pressure-time curves of this form. It is suspected that very long tubes (50-80 m) and smaller and more elastic packers used in this installation (rather than the presence of included air) caused the extended decay-time and slow pulse increase.

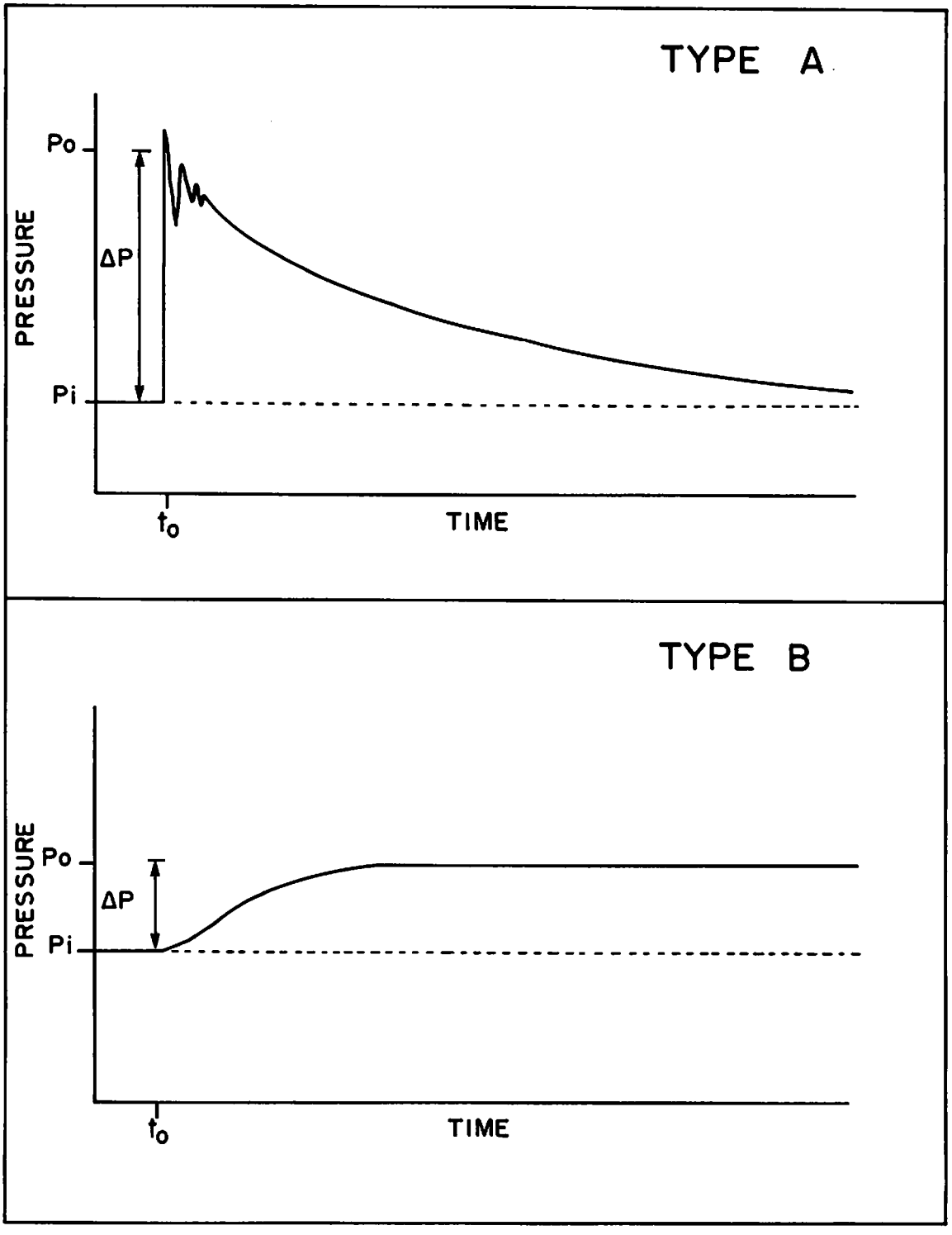

XBL 8111-12188

Fig. 4.13. Schematic diagram of typical field pressure against time decay curves.

4.2.3.3 Radius of Influence. Neither pressure pulse nor short-term injection tests were able to produce an observable pressure response in any observation cavity. Thus, there is no means of estimating the radius of influence of either test. The distance between test cavities ranges from 0.3 m to 25 m but interference effects noted during the long-term injection tests suggest that the effective radius of influence may be unrelated to the straight-line radius of influence. Therefore, the relative spatial position of two cavities cannot be used to predict the presence or absence of a pressure response. Instead, the total volumes of water displaced by the various test techniques must be compared to assess the relative regions of influence of each kind of test.

Table 4.6 indicates that with displacement volume as the criterion, the pulse test has the minimum region of influence. However, it can be seen that for some short-term injection tests (total displacement 1 to 100 cm^3), the region of influence would exceed that of the pulse test. Thus, comparison of steady-state injection tests and pulse decay data may be complicated by differing radius of influence of a particular test type as well as by the fracture geometry near the borehole. A tight fracture that intersects many well-connected and reasonably open fractures close to the borehole, will have a low steady-state conductivity with a large pressure pulse and long decay time. A large open fracture near the borehole, connected only to tight fractures, might have both a small pulse, relatively short decay time and low steady-state conductivity.

Table 4.6. Test Displacement Volumes.

Test type	Increase in Region of influence		
Pulse	1	to	5 cm^3
Short-term injection	1	to	100 cm^3
Long-term injection	1000	to	1900 cm^3
"Moebus" experiment			2000 cm^3

5.0 CONCLUSIONS

The purpose of this study was to (i) assist in determining the radius of influence of a pressure pulse test in fractured rock, (ii) compare steady-state and transient conductivity tests in fractured rock, and (iii) assess the practical difficulties of performing pressure pulse tests in the field. This study has addressed these questions, but further work is required before they can be fully answered.

Radius-of-influence effects were not observed in any borehole cavity in response to either pressure pulse or short-term injection tests. The long-term injection tests and the "Moebus" experiment did create significant pressure responses, indicating that the system is interconnected. The lack of pressure response in the peripheral intervals suggests that the boreholes are separated by distances greater than the effective radius of influence of the pressure pulse tests (minimum distance between cavities is 0.3 m). Other factors, however, may preclude observation of a pressure response even if the boreholes are within the effective radius of influence. Volume displacements of 0.9 to 4.8 cm^3 created pressure pulses up to 0.63 MPa in the test cavities. Thus, to create a significant pressure response (greater than 0.001 MPa) in an observation cavity, water volumes of 0.002 to 0.008 cm^3 must be transmitted from the test cavity to the observation cavity. But even if a low fracture porosity is assumed (say 0.005), then a 5 cm^3 pulse displacement might affect a volume of rock of approximately 100 cm^3 with an effective radius of 0.03 m for a 2-m borehole length or a radius of 62m for a single 10μm fracture. Larger pulse displacements and smaller observation cavities must be used to create a pressure response. Injected volumes of 1 to 19 liters were required during long-term injection tests to

create pressure responses up to 0.03 MPa. The small volume displaced in the pulse test is likely to have quickly dissipated around the borehole in the highly fractured rock of the test location. Also, air in the observation cavities and packer compliance effects would tend to reduce the magnitude of the observed pressure response.

Steady-state conductivity tests were compared to pressure pulse test results, but no discernable trends were observed. A better comparison may be achieved when (i) the 3-dimensional fracture system is better characterized, (ii) type curve solutions are developed for the pulse test results, (iii) effects of air leakage and packer compliance are isolated by equipment calibration, and (iv) the effective radius of influence of the pulse test is more clearly defined for comparison with the effective radius of steady-state tests.

Except for packer inflation, the testing equipment performed satisfactorily. The potential for air leaking into the test and observation cavities could be eliminated by using a mechanically sealing packer. Such packers would also assist in removing some of the packer compliance effects.

Results obtained from the test program are useful in evaluating the hydrological character of the rock around of the ventilation drift. Conductivities of 2-meter intervals, intersecting a variety of fractures, range from 10^{-11} to 10^{-7} cm/sec. Water drainage into the drift borehole R-1 is expected to be a major factor determining groundwater pressure in the north end of the ventilation drift. Long-term injection tests and the "Moebus" experiment indicate that the fracture system is well-connected.

Correlation of dominant fracture trends to this hydraulic interconnection was not attempted.

It appears that understanding and analyzing results of pressure pulse tests performed in fractured rock is a complex problem. This study has served to identify some of those problems in the field. Recommendations for further work are made in the following chapter.

6.0 RECOMMENDATIONS

Future work on the data from this field experiment should include (1) an evaluation of the effects of packer compliance and air leakage on the test results, (2) characterization of the three-dimensional fracture system, and (3) an attempt to generate type curves for analysis of the pressure pulse tests, with the real characteristics of the fracture taken into account. This would lead to a more meaningful correlation of steady-state and transient test results.

In any similar experiment to further evaluate the pressure pulse technique, the following modifications should be made:

(1) The boreholes should be drilled parallel and closer to each other (perhaps 1 meter separation) to better identify interconnected fractures.

(2) The boreholes should not be allowed to drain prior to testing and should be sealed soon after drilling, to maintain shallow groundwater pressure gradients along the boreholes.

(3) There should be smaller and more numerous test cavities to increase the possibility of observing small pressure responses in peripheral boreholes.

(4) To remove the problem of air leakage, mechanically sealing packers should be used.

(5) The monitoring system should be upgraded to provide simultaneous monitoring of all cavity pressures with pressure transducers and chart records.

6) Long shut-in times should be allowed in order to properly set up the experiment and to let all cavity pressures stabilize before testing.

7) A longer test period should be used to allow greater separation of pulse tests. If long response times exist, they can thus be observed during the time between tests.

ACKNOWLEDGMENTS

This study was supported by funds from the Lawrence Berkeley Laboratory, under subcontract No. 4500410, provided through the Waterloo Research Institute. Special thanks are extended to M. Moebus for assistance provided in the field and to J. Baleshta for assistance in report preparation.

The Stripa project is supported by the Assistant Secretary for Nuclear Energy, Office of Waste Isolation of the U.S. Department of Energy under contract DE-AC0376SF00098. Funding for the project is administered by the Office of Nuclear Waste Isolation at Battelle Memorial Institute.

REFERENCES

Brace, W.F., J.B. Walsh, and W.T. Frangos, 1968. "Permeability of Granite Under High Pressure." J. Geophysics Res., Vol. 73, No. 6, pp. 2225-2236.

Forster, C.B. and J.E. Gale, 1980. A Laboratory Assessment of the Use of Borehole Pressure Transients to Measure Permeability of Fractured Rock Masses. Lawrence Berkeley Laboratory report 8674, SAC-28, Berkeley, California.

Gale, J.E., O. Quinn, C. Wilson, C. Forster, P.A. Witherspoon, and L. Jacobson, 1980. "Hydrogeologic Characteristics of Fractured Rocks for Waste Isolation - the Stripa Experience." Symposium on Scientific Basis for Nuclear Waste Management. Materials Research Society Annual Meeting (1979). Cambridge, Massachusetts, 10 pp.

Gale, J.E. and R.K. Raven, 1979. An Assessment and Evaluation of Compliance Effects of Borehole Transient Test Equipment. University of Waterloo, Waterloo, Ontario, Canada.

Gale, J.E. and P.A. Witherspoon, 1979. An Approach to the Fracture Hydrology at Stripa: Preliminary Results. Lawrence Berkeley Laboratory report LBL-8280, SAC-16, Berkeley, California.

Lin, W., 1977. Compressible Fluid Flow Through Rocks of Variable Permeability, Lawrence Livermore Laboratory report UCRL 52304, Livermore, California.

Lin, W., 1979. Measuring the Permeability of Eleana Argillite from Area 17, Nevada Test Site, Using the Transient Method. Lawrence Livermore Laboratory report UCRL 52604, Livermore, California.

Olkiewicz, A., J.E. Gale, R. Thorpe, and B. Paulsson, 1979. Geology and Fracture System at Stripa. Lawrence Berkeley Laboratory report LBL-8907, SAC-21, Berkeley, California.

Wang, J.S.Y., J.H. Narasimhan, C.F. Tsang, and P.A. Witherspoon, 1977. "Transient Flow in Tight Fractures," in Proceedings of Invitational Well-Testing Symposium, October 1977, Berkeley, California.

APPENDIX I

STEREONET PLOTS OF FRACTURE ORIENTATIONS

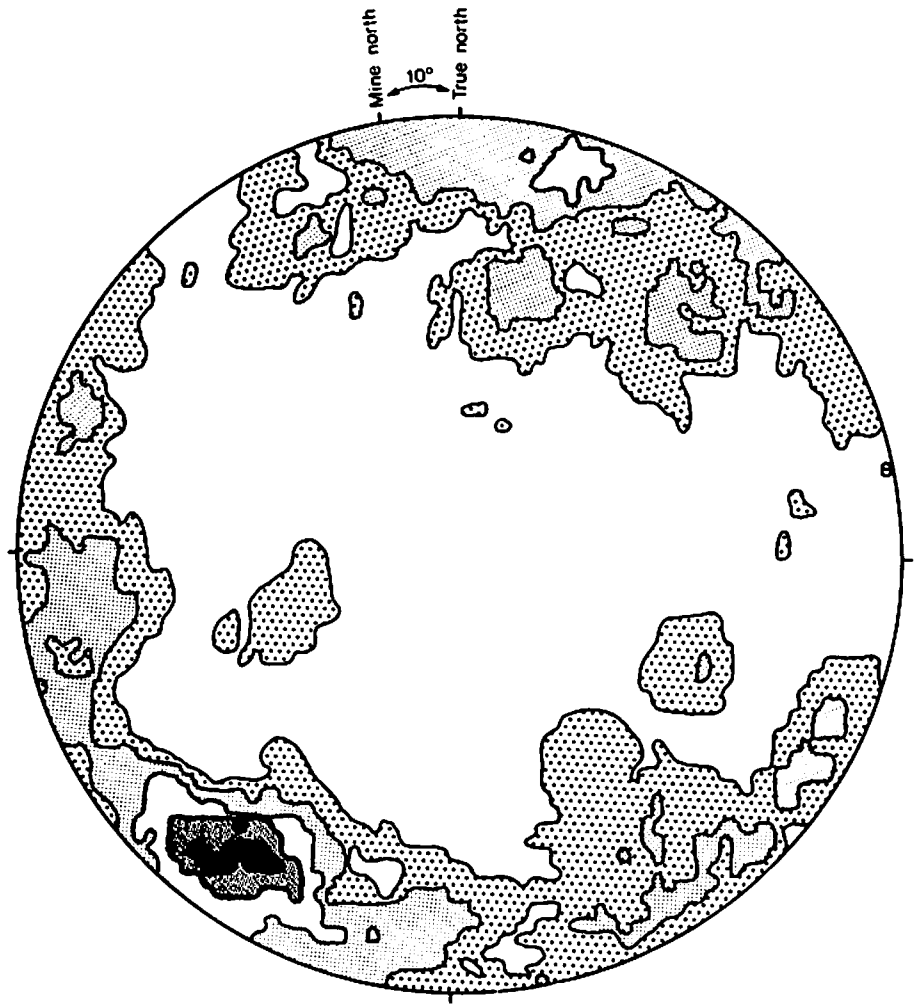

POLES TO PLANES PROJECTED ON LOWER HEMISPHERE OF EQUAL AREA PROJECTION USING SCHMIDT METHOD

Contours of Pole Density (% of total poles)	
0-1	
1-2	
2-4	
4-6	
6-8	
8-9.3	
Total Poles = 318	
Maximum Density = 9.3	

XBL 8111-12189

Fig. I.1. Stereonet plot of fracture logged in boreholes HG1 through HG5.

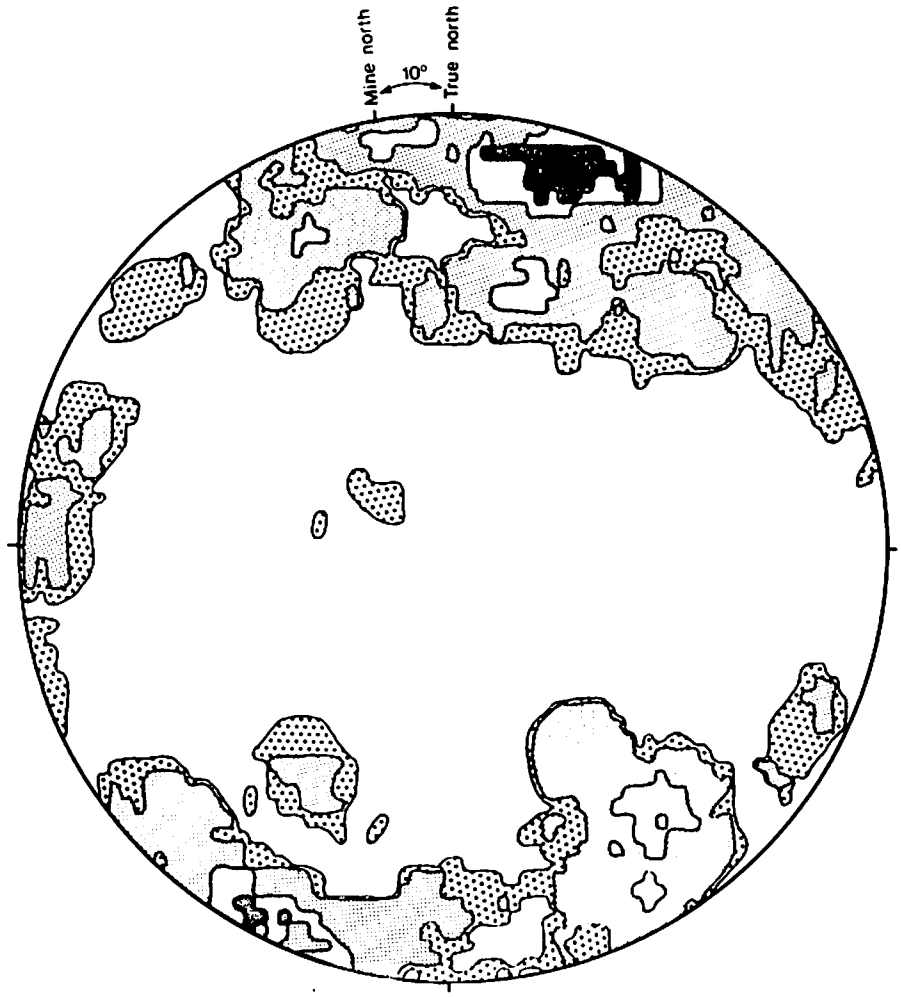

POLES TO PLANES PROJECTED ON LOWER HEMISPHERE OF EQUAL AREA PROJECTION USING SCHMIDT METHOD

Contours of Pole Density (% of total poles)	
0-1	
1-2	
2-4	
4-6	
6-8	
8-8.4	
Total Poles = 131	
Maximum Density = 8.4	

XBL 8111-12190

Fig. I.2. Stereonet plot of fractures containing calcite logged in boreholes HG1 through HG5.

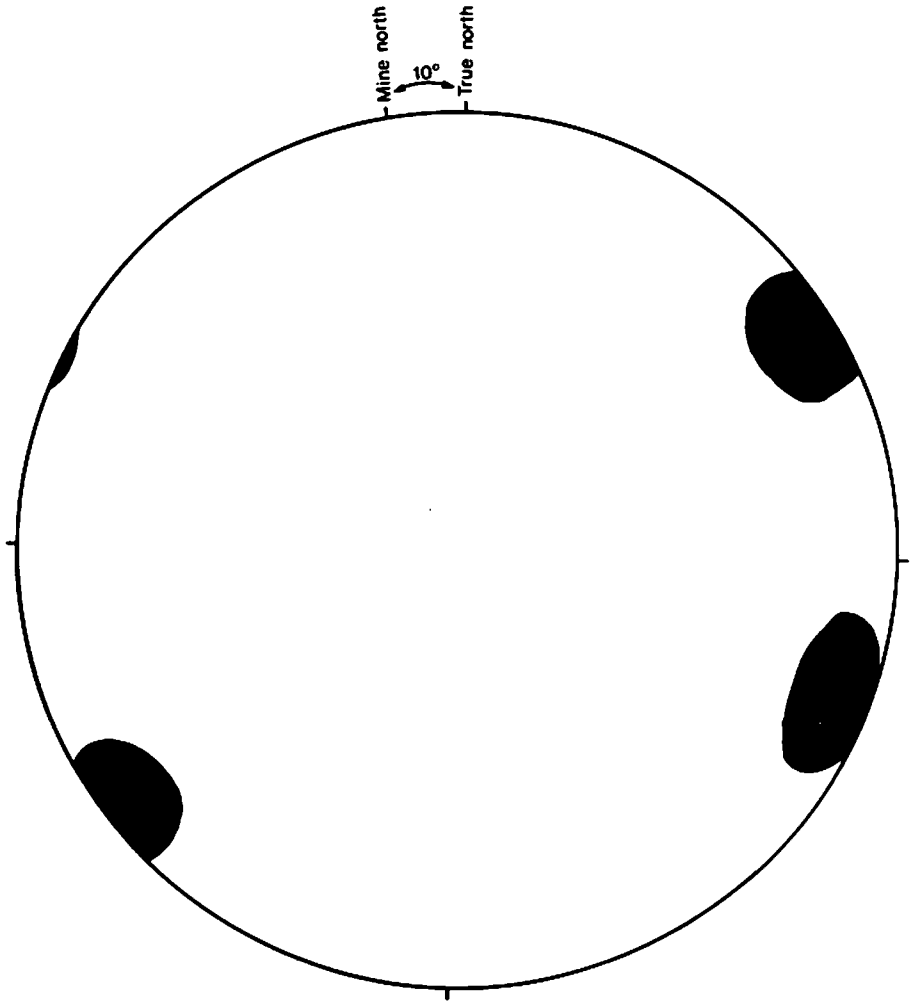

POLES TO PLANES PROJECTED ON LOWER HEMISPHERE OF EQUAL AREA PROJECTION USING SCHMIDT METHOD

Contours of Pole Density (% of total poles)	
0 - 1	
1 - 5	
5 - 10	
10 - 15	
15 - 20	
20 - 50	
Total Poles = 4	
Maximum Density = 50	

XBL 8111-12191

Fig. I.3. Stereonet plot of fractures containing chlorite logged in boreholes HG1 through HG5.

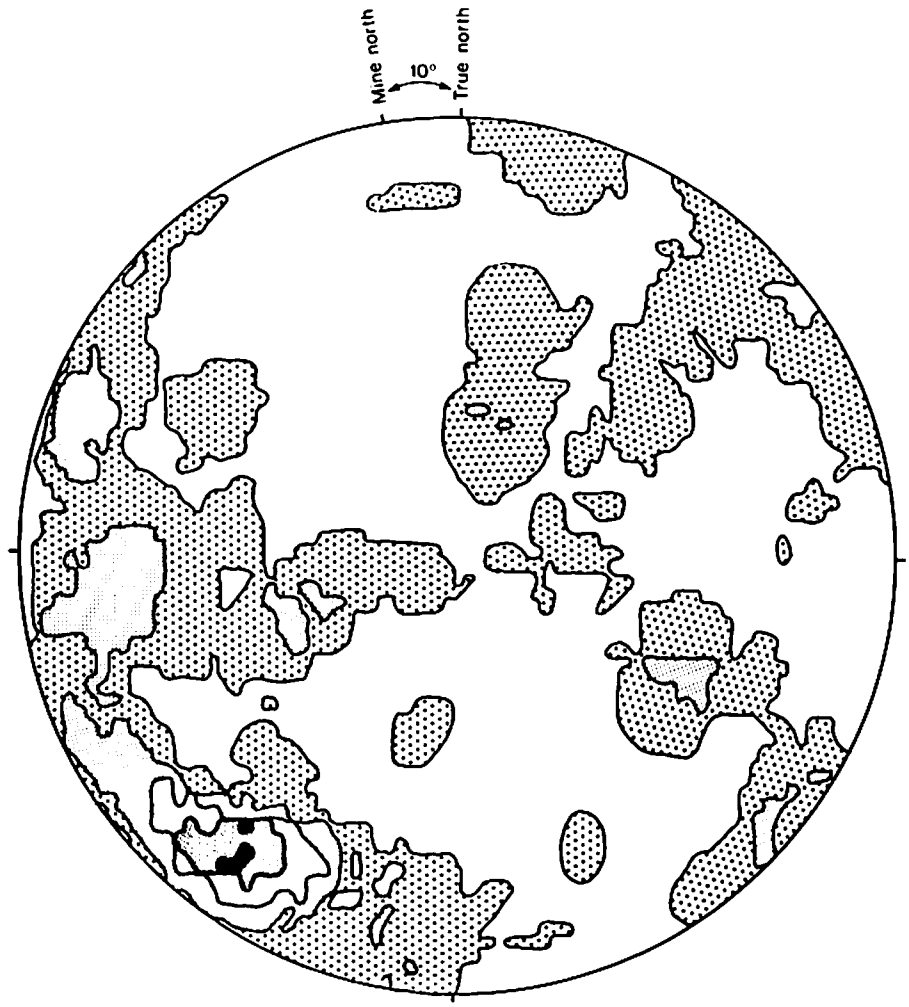

POLES TO PLANES PROJECTED ON LOWER HEMISPHERE OF EQUAL AREA PROJECTION USING SCHMIDT METHOD

Contours of Pole Density (% of total poles)	
0-1	
1-3	
3-6	
6-9	
9-12	
12-12.8	
Total Poles = 179	
Maximum Density = 12.8	

XBL 8111-12192

Fig. I.4. Stereonet plot of fractures containing epidote logged in boreholes HG1 through HG5.

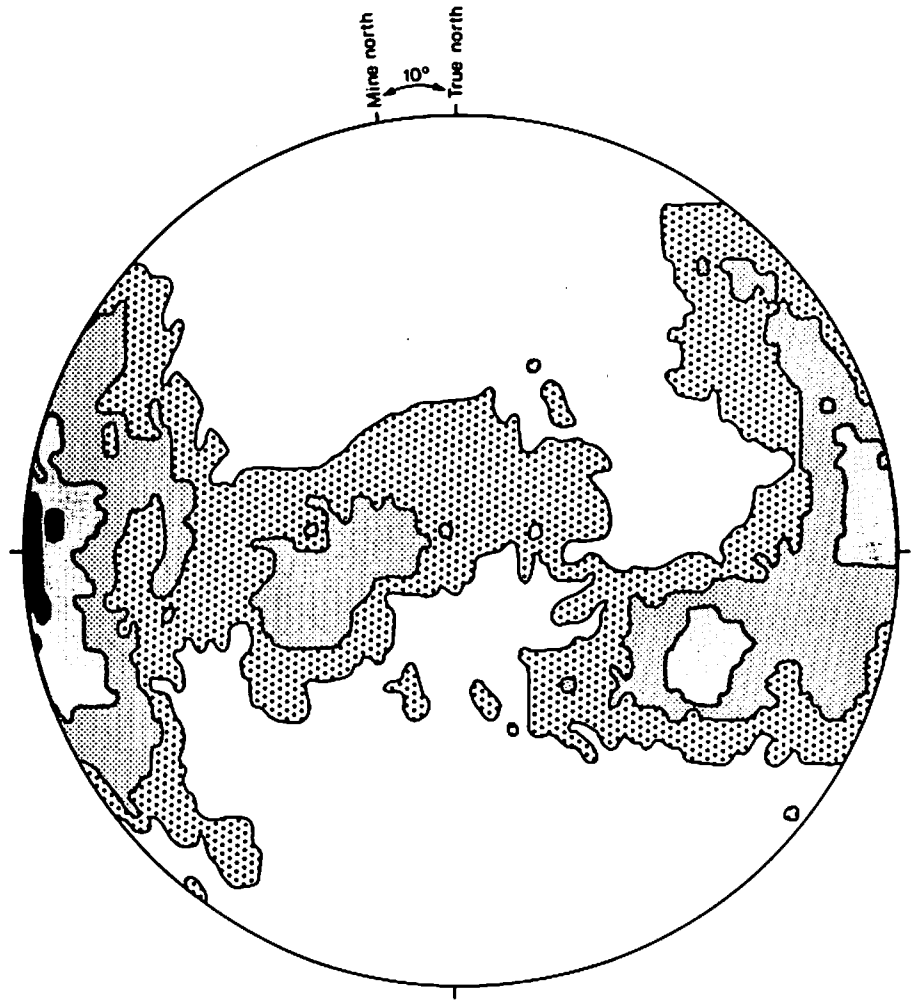

POLES TO PLANES PROJECTED ON LOWER HEMISPHERE OF EQUAL AREA PROJECTION USING SCHMIDT METHOD

Contours of Pole Density (% of total poles)	
0-1	
1-2	
2-4	
4-6	
6-7.5	
Total Poles = 680	
Maximum Density = 7.5	

XBL 8111-12193

Fig. I.5. Stereonet plot of fractures logged in boreholes R1 through R5.

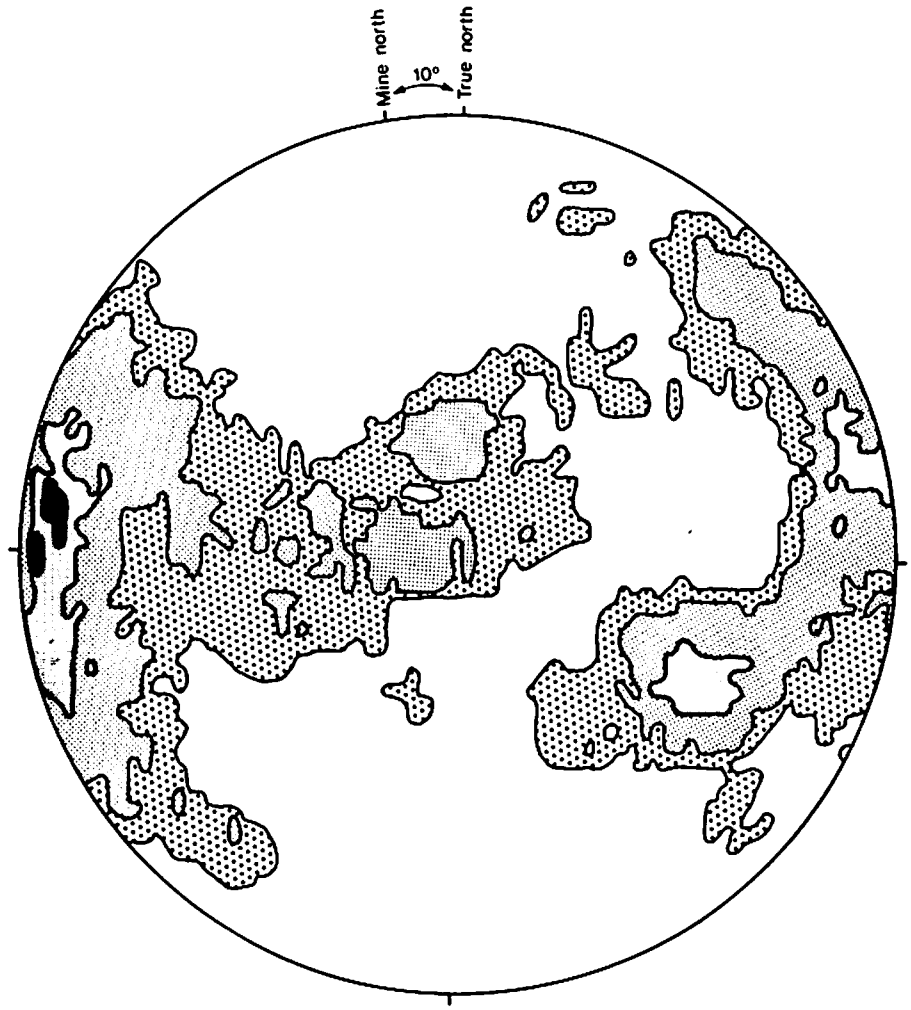

POLES TO PLANES PROJECTED ON LOWER HEMISPHERE OF EQUAL AREA PROJECTION USING SCHMIDT METHOD

Contours of Pole Density (% of total poles)	
0-1	
1-2	
2-4	
4-6	
6-7.9	
Total Poles = 444	
Maximum Density = 7.9	

XBL 8111-12194

Fig. I.6. Stereonet plot of fractures containing chlorite logged in boreholes R1 through R5.

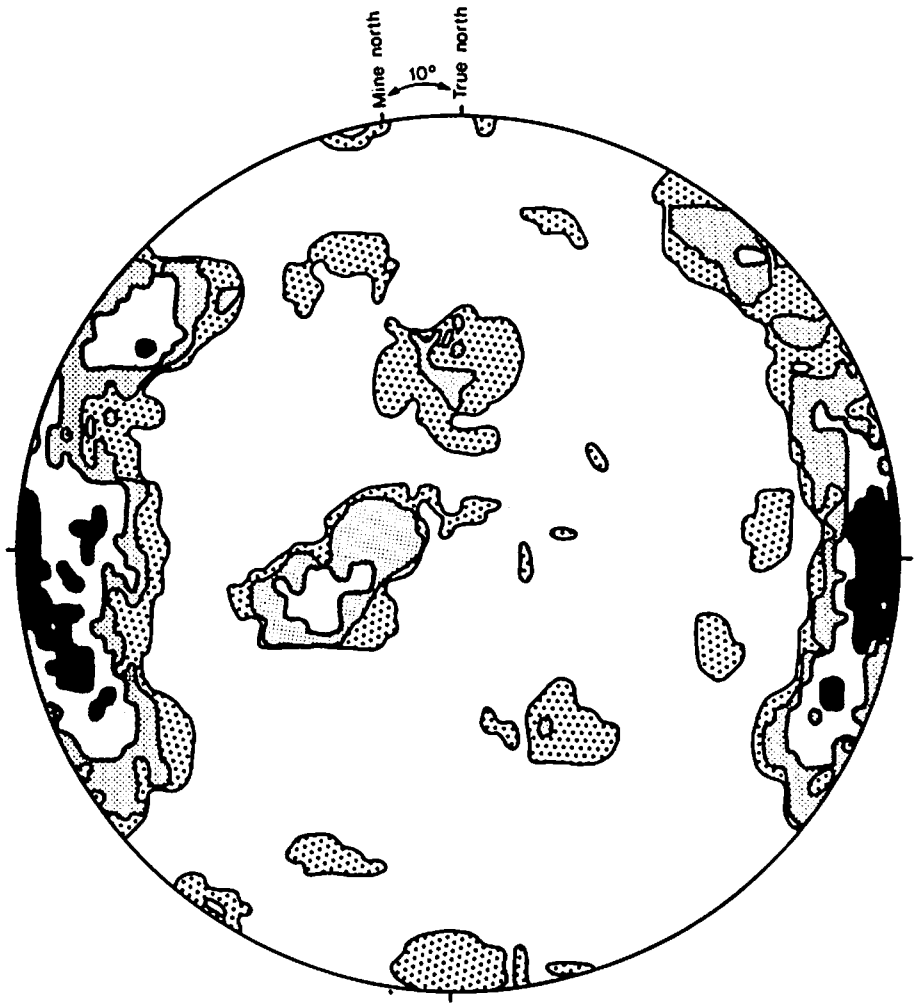

POLES TO PLANES PROJECTED ON LOWER HEMISPHERE OF EQUAL AREA PROJECTION USING SCHMIDT METHOD

Contours of Pole Density (% of total poles)	
0-1	
1-2	
2-4	
4-6	
6-8	
8-9.8	
Total Poles = 122	
Maximum Density = 9.8	

XBL 8111-12195

Fig. I.7. Stereonet plot of fractures containing calcite logged in boreholes R1 through R5.

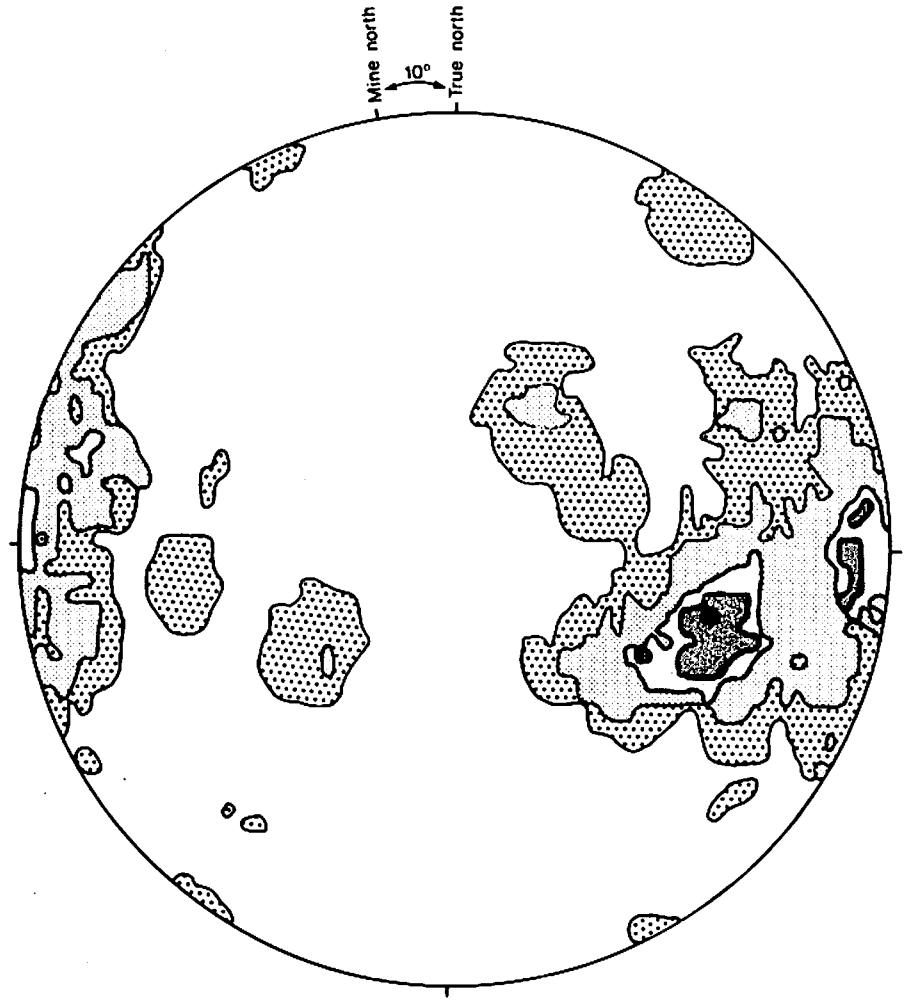

POLES TO PLANES PROJECTED ON LOWER HEMISPHERE OF EQUAL AREA PROJECTION USING SCHMIDT METHOD

Contours of Pole Density (% of total poles)	
0-1	
1-3	
3-6	
6-9	
9-12	
12.0-12.5	
Total Poles = 120	
Maximum Density = 12.5	

XBL 8111-12196

Fig. I.8. Stereonet plot of fractures containing epidote logged in boreholes R1 through R5.

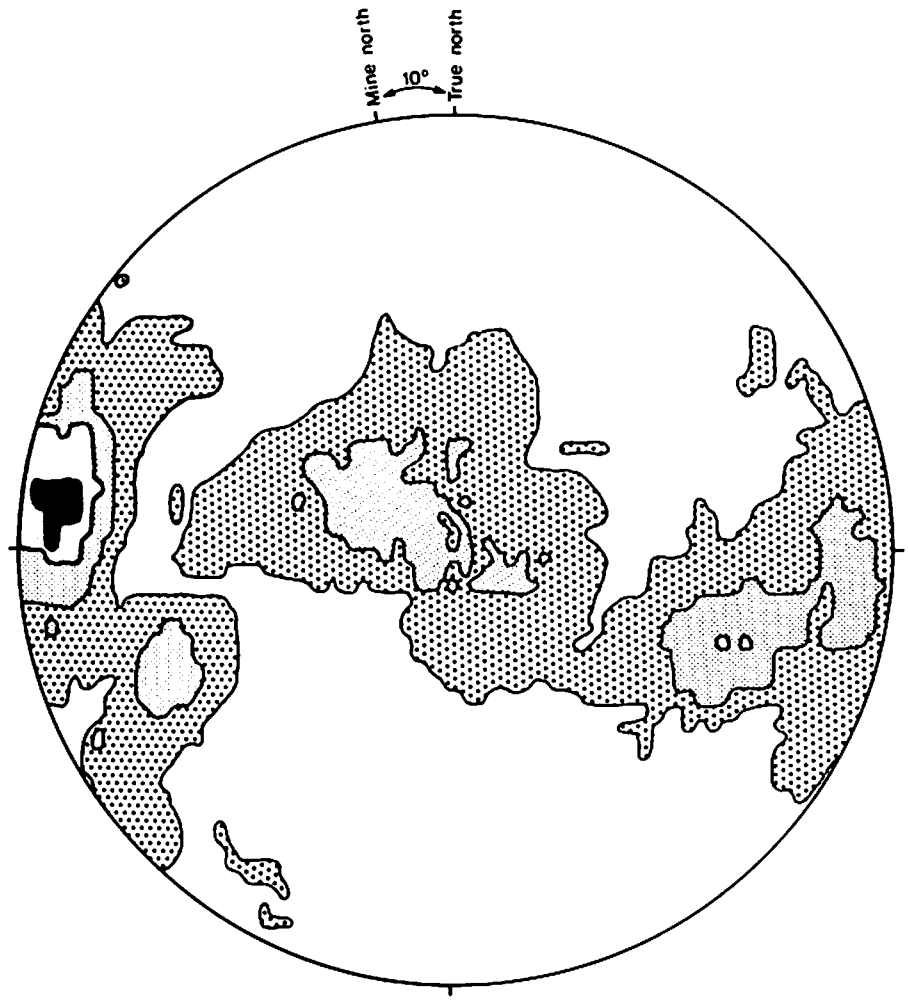

POLES TO PLANES PROJECTED ON LOWER HEMISPHERE OF EQUAL AREA PROJECTION USING SCHMIDT METHOD

Contours of Pole Density (% of total poles)	
0-1	
1-3	
3-6	
6-9	
9-11.2	
Total Poles = 649	
Maximum Density = 11.2	

XBL 8111-12197

Fig. I.9. Stereonet plot of fractures logged in boreholes R6 through R10.

APPENDIX II

EQUIPMENT CALIBRATION

APPENDIX II: EQUIPMENT CALIBRATION

Pressures were measured during the test program, using the Bourdon gauges and pressure transducers listed in Table II.1

Table II.1 Pressure-measuring equipment.

Equipment	Number of Units	Range	Gauge Divisions or Full-scale Output	Range
5	Gauge	0-4 MPa	0.034 MPa	Packer Pressure
22	Gauge	0-2 MPa	0.0035 MPa	Cavity Pressure
1	Shaevitz Transducer	0-3.5 MPa	5 volts	
10	C.J. Enterprise Transducer	0-7 MPa	5 volts	
1	Shaevitz Transducer	0-7 MPa	5 volts	

Each piece of equipment was calibrated against a 0-7 MPa Heise test gauge with 0.007 MPa divisions. Before calibration, the pressure was cycled up and down several times to remove any stiffness, then 5 to 10 calibrations were carried out on the final up-and-down cycle. These calibrations were carried out before and after the test program and occasionally during it.

Flow rates were measured using either a bubble line or flow piston. The bubble line is calibrated by measuring the outflow from the tube during the time required for a specified distance of bubble travel. The accuracy of the flow measurement depends on the accuracy of the measurement of bubble

travel (assuming negligible temperature and flow variations during the measurement period). Bubble travel of 0.5 cm is the mimimum accurately measureable distance; thus, a 1/4-inch nylon tube yields a minimum measureable distance volume of 0.0488 cm^3. The minimum accurately measureable flow rate is therefore 0.0488 cm^3/min for a 1-hour test. The flow piston is calibrated in a similar manner, except that distance of piston travel is measured rather than distance of bubble travel. Again, the minimum accurately measureable distance is 0.5 cm, which yields 0.92 cm^3. Thus the minimum accurately measureable flow rate for the flow piston is 0.014 cm^3/min for a 1-hour test. Calibrations were carried out before and after the test program.

APPENDIX III

BOREHOLE INSTALLATION DIAGRAMS

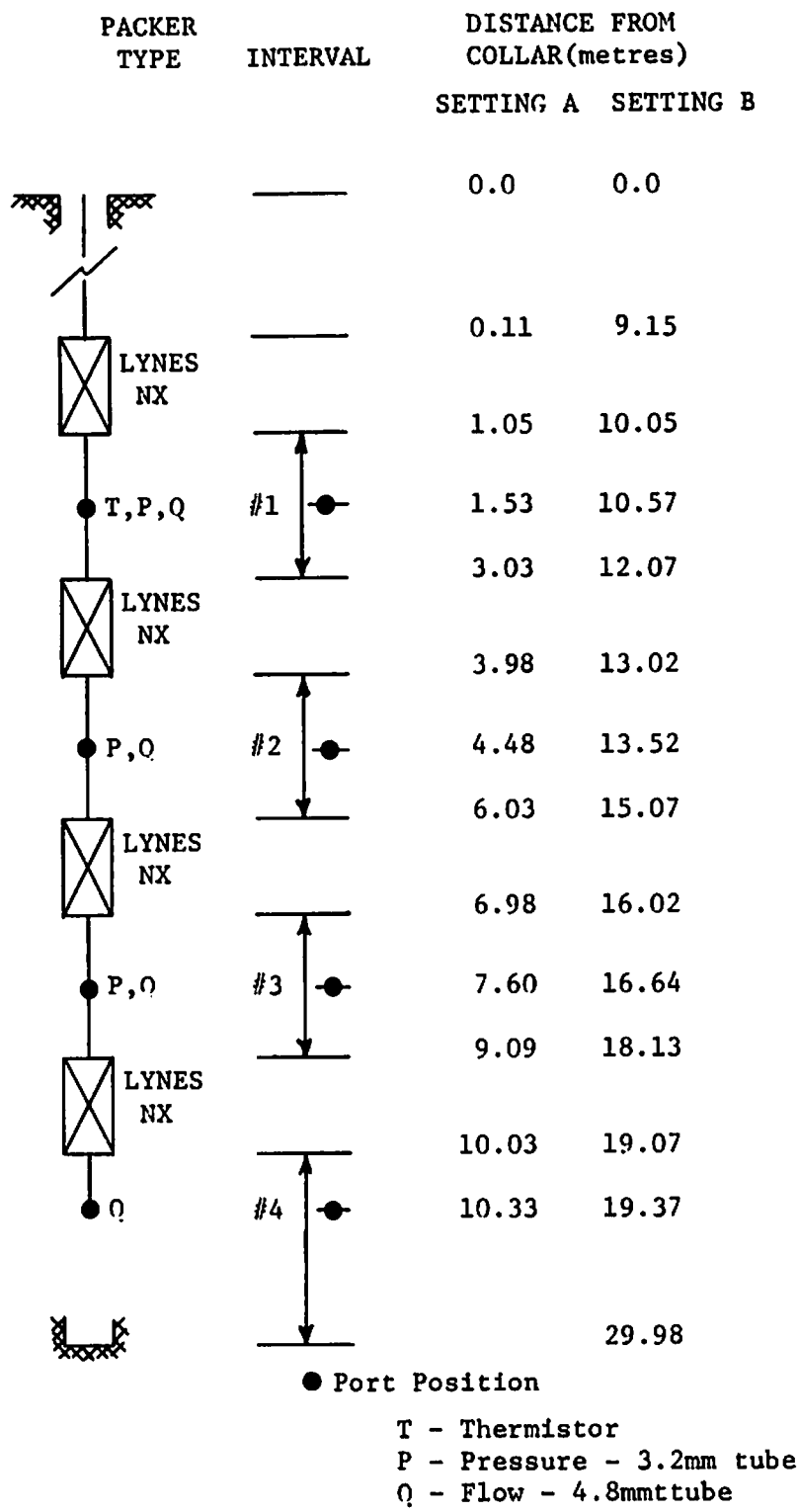

Fig. III.1. HG1 installation diagram.

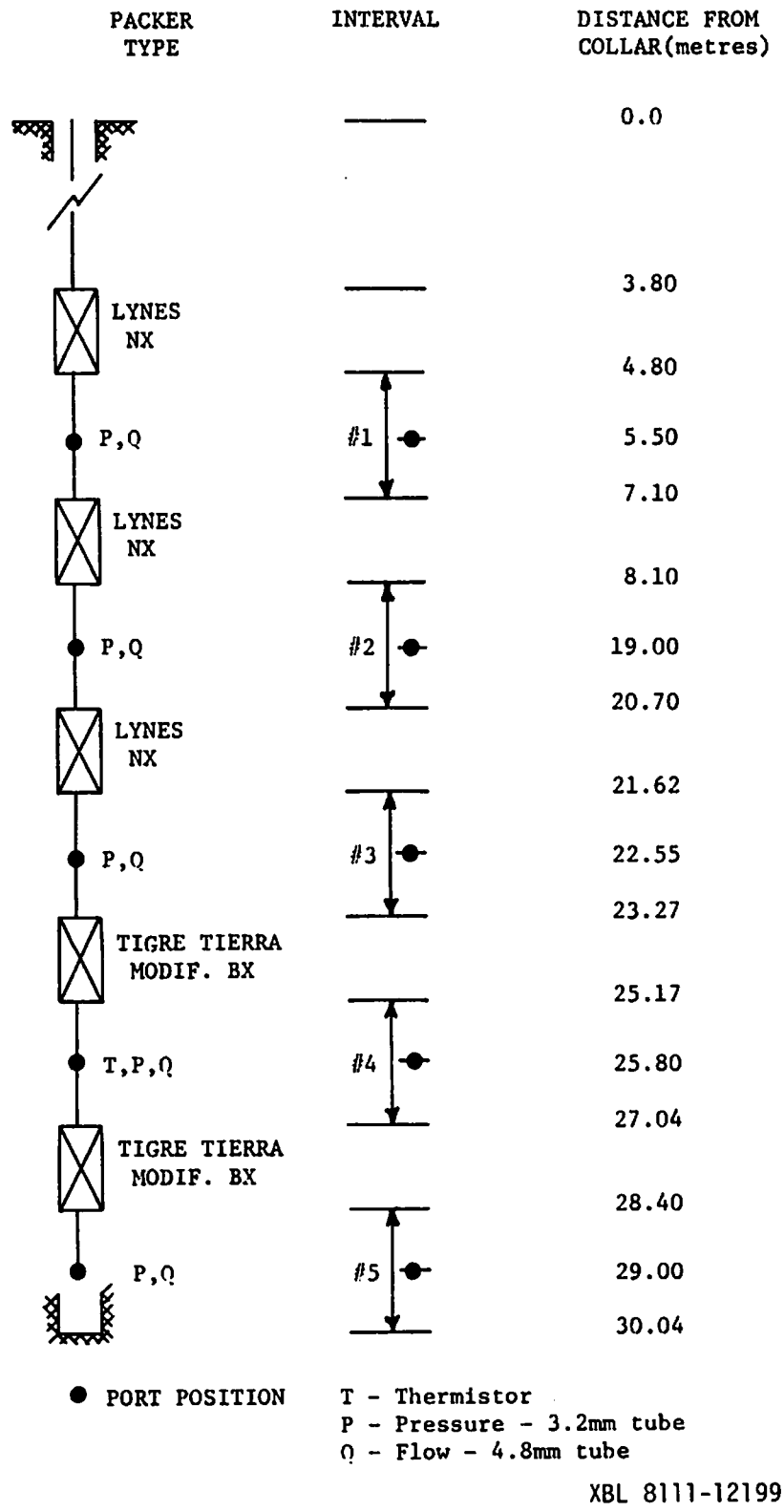

Fig. III.2. HG3 installation diagram.

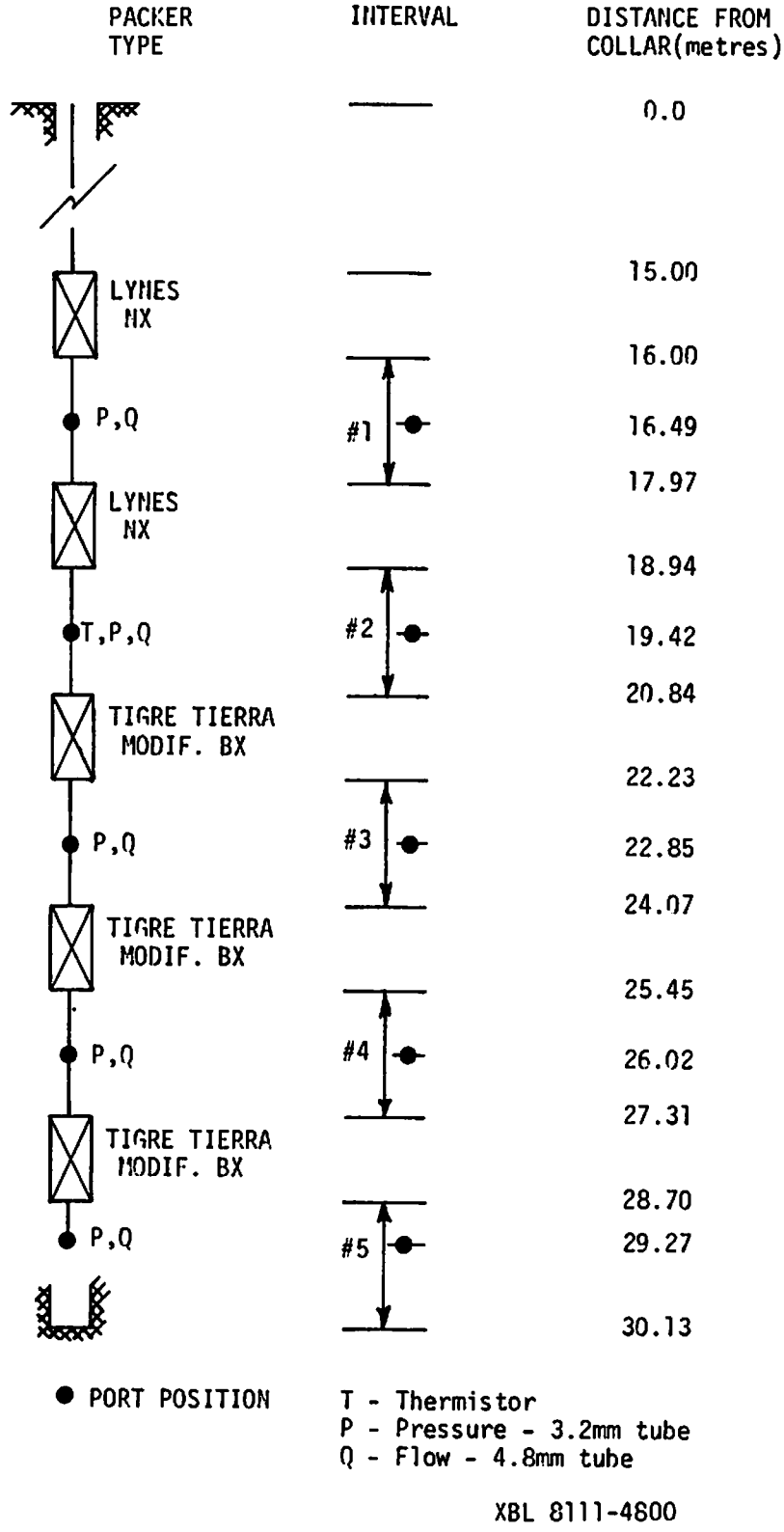

Fig. III.3. HG4 installation diagram.

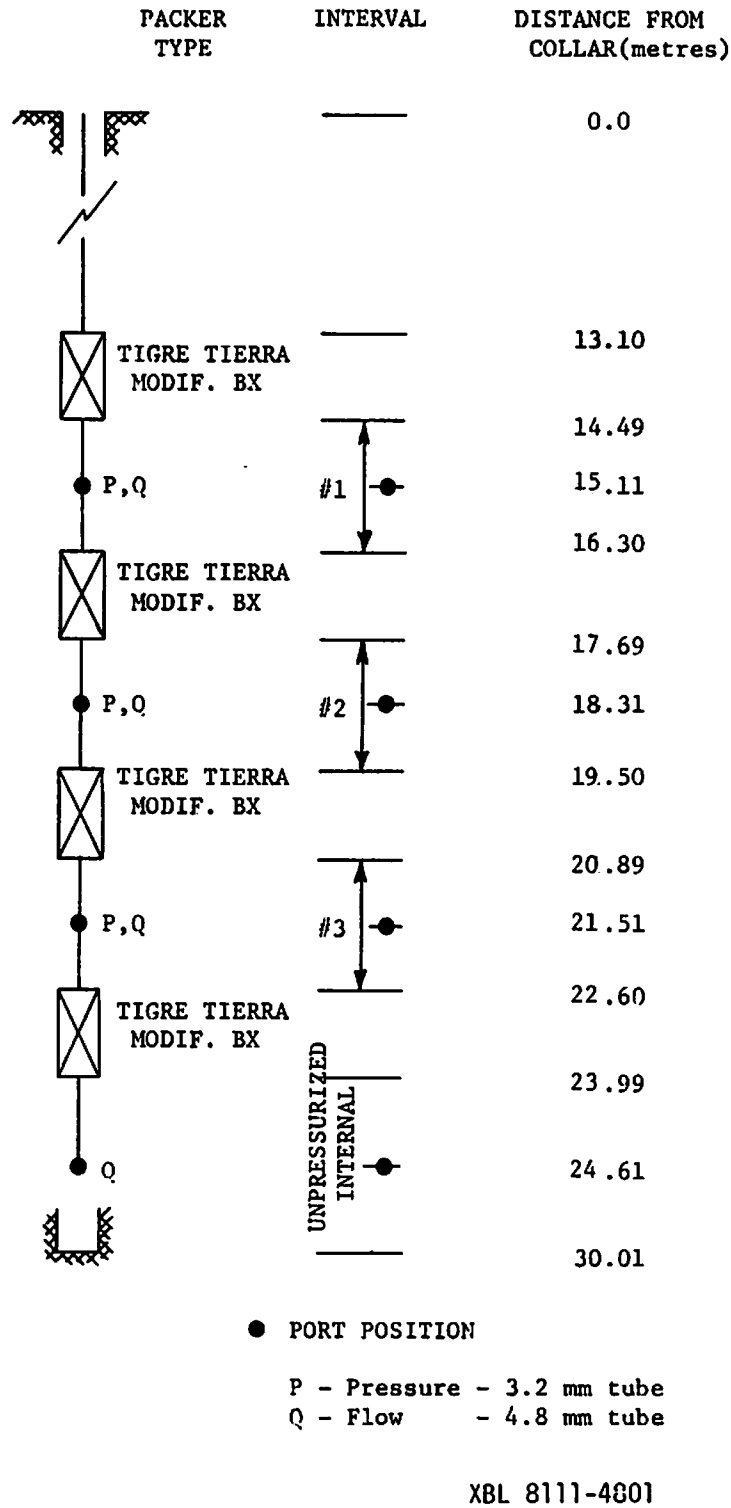

Fig. III.4. HG5 installation diagram.

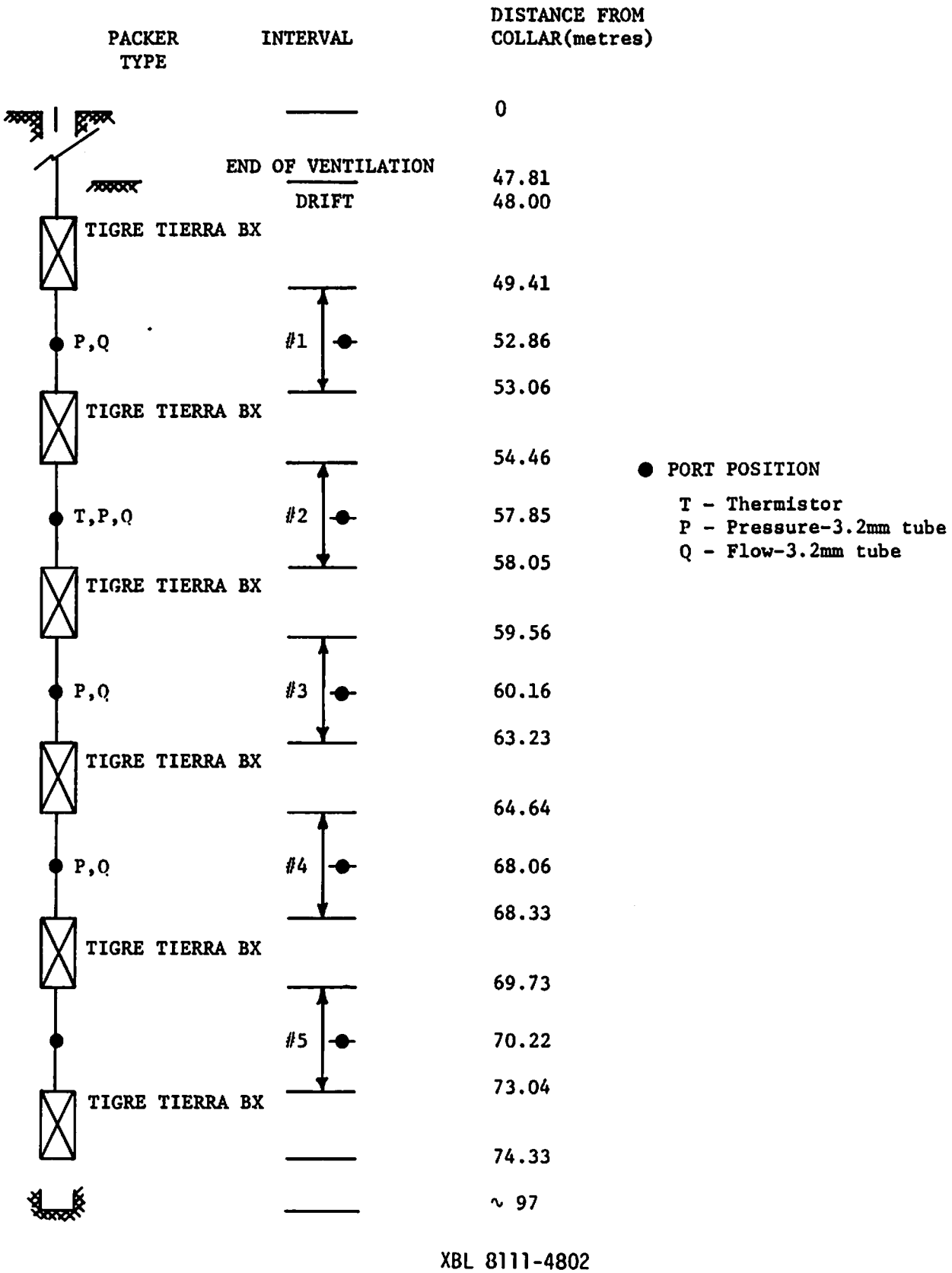

Fig. III.5. DBH-2 installation diagram.

APPENDIX IV

X, Y, Z COORDINATES OF TEST CAVITIES

APPENDIX IV X, Y, Z COORDINATES OF TEST CAVITIES

Explanation of abbreviations:

PT = Beginning of cavity and end of packer seal, referenced to the collar of the borehole.

Port = Location of end of open plastic tube, measuring pore pressures in a cavity

PB = End of cavity and beginning of packer seal, referenced to the collar of the borehole.

MP = Midpoint of cavity interval.

INTERVAL COORDINATES DBH-2

INTERVAL/REFERENCE POINT		x (m)	y (m)	z (m)
	Collar	338.32	980.3	336.0
#1	PT	387.71	980.3*	336.0*
	Port	391.16	980.3	336.0
	PB	391.36	980.3	336.0
	MP	389.54	980.3	336.0
#2	PT	392.76	980.3	336.0
	Port	396.12	980.3	336.0
	PB	396.35	980.3	336.0
	MP	394.56	980.3	336.0
#3	PT	397.86	980.3	336.0
	Port	399.46	980.3	336.0
	PB	401.53	980.3	336.0
	MP	399.70	980.3	336.0
#4	PT	402.94	980.3	336.0
	Port	406.36	980.3	336.0
	PB	406.63	980.3	336.0
	MP	404.79	980.3	336.0
#5	PT	408.03	980.3	336.0
	Port	408.52	980.3	336.0
	PB	411.34	980.3	336.0
	MP	409.69	980.3	336.0

*Hole is assumed to be horizontal and parallel to x coordinate.

INTERVAL COORDINATES HG-1 (A-setting)

INTERVAL/REFERENCE POINT		x (m)	y (m)	z (m)
	Collar	386.220	976.593	334.376
#1	PT	387.27	976.60	334.38
	Port	387.75	976.60	334.38
	PB	389.25	976.60	334.38
	MP	388.26	976.60	334.38
#2	PT	390.2	976.60	334.38
	Port	390.7	976.60	334.38
	PB	392.25	976.60	334.38
	MP	391.23	976.60	334.38
#3	PT	393.2	976.60	334.38
	Port	393.82	976.60	334.38
	PB	395.31	976.60	334.38
	MP	394.26	976.60	334.38
#4	PT	396.25	976.60	334.38
	Port	396.55	976.60	334.38
	PB	416.204	976.629	334.383
	MP	406.23	976.60	334.38

INTERVAL COORDINATES HG-1 (B-setting)

INTERVAL/REFERENCE POINT		x (m)	y (m)	z (m)
	Collar			
#1	PT	-396.27	976.60	334.38
	Port	396.79	976.60	334.38
	PB	-398.29	976.60	334.38
	MP	397.28	976.60	334.38
#2	PT	399.24	976.60	334.38
	Port	399.74	976.60	334.38
	PB	401.29	976.60	334.38
	MP	400.27	976.60	334.38
#3	PT	402.24	976.60	334.38
	Port	402.86	976.60	334.38
	PB	404.35	976.60	334.38
	MP	403.30	976.60	334.38
#4	PT	405.29	976.60	334.38
	Port	405.59	976.60	334.38
	PB	416.20	976.60	334.38
	MP	410.75	976.60	334.38

INTERVAL COORDINATES HG-3

INTERVAL/REFERENCE POINT		x (m)	y (m)	z (m)
	Collar	386.867	978.239	335.211
#1	PT	391.026	980.079	336.25
	Port	391.633	980.347	336.38
	PB	393.019	980.96	336.69
	MP	392.023	980.52	336.47
#2	PT	393.885	981.34	336.90
	Port	404.677	985.52	339.16
	PB	404.80	986.17	339.53
	MP	404.34	983.76	338.22
#3	PT	405.60	986.53	339.72
	Port	406.41	986.89	339.92
	PB	407.030	987.16	340.07
	MP	406.315	986.85	339.90
#4	PT	408.68	981.89	340.46
	Port	409.23	988.13	340.59
	PB	410.30	988.60	340.85
	MP	409.49	988.25	340.66
#5	PT	411.47	989.12	341.14
	Port	411.99	989.35	341.20
	PB	412.893	989.751	341.480
	MP	412.182	989.436	341.31

INTERVAL COORDINATES HG-1 (B-setting)

INTERVAL/REFERENCE POINT		x (m)	y (m)	z (m)
	Collar			
#1	PT	-396.27	976.60	334.38
	Port	396.79	976.60	334.38
	PB	-398.29	976.60	334.38
	MP	397.28	976.60	334.38
#2	PT	399.24	976.60	334.38
	Port	399.74	976.60	334.38
	PB	401.29	976.60	334.38
	MP	400.27	976.60	334.38
#3	PT	402.24	976.60	334.38
	Port	402.86	976.60	334.38
	PB	404.35	976.60	334.38
	MP	403.30	976.60	334.38
#4	PT	405.29	976.60	334.38
	Port	405.59	976.60	334.38
	PB	416.20	976.60	334.38
	MP	410.75	976.60	334.38

INTERVAL COORDINATES HG-4

INTERVAL/REFERENCE POINT		x (m)	y (m)	z (m)
	Collar	386.003	974.888	333.518
#1	PT	399.02	969.64	329.91
	Port	399.57	969.41	329.75
	PB	400.64	968.99	329.45
	MP	399.83	969.32	329.68
#2	PT	401.89	968.49	329.11
	Port	402.45	968.26	328.95
	PB	403.52	967.83	328.66
	MP	402.71	968.16	328.88
#3	PT	404.77	967.33	328.31
	Port	405.32	967.11	328.16
	PB	406.30	966.71	327.88
	MP	405.54	967.02	328.10
#4	PT	407.55	966.21	327.53
	Port	408.11	965.99	327.38
	PB	412.95	964.02	326.04
	MP	410.25	965.12	326.79

APPENDIX V

TEST LOG FOR PRESSURE PULSE TESTS

APPENDIX V TEST LOG FOR PRESSURE PULSE TESTS

(i) All testing was carried out in boreholes in the ventilation drift. For locations, refer to Figs. 1.4 - 1.6, Chapter 1.0.

(ii) Reference code for borehole testing:

Example: "Pulse Test HG5-3-A (22) ch. 8"

Explanation:

HG - Borehole set designation

5 - Borehole number

3 - Packer interval

A - Test order

(22) - Pulse piston classification (corresponding to displacement volume (V) for each piston classification listed in Table VII.1

ch.8 - Channel of data logger monitoring this test

(iii) Temperature measurements:

Example: "Ch.0 @ 550" refers to channel zero of the data logger, which is monitoring a thermistor with a zero'd potential balance reading of 550.

(iv) Reference code for transducers

Example: "s/n 461 C.J.0-1000"

Explanation:

s/n 461 - serial number 461

C.J. - transducer type (see Table II.1)

0-1000 - 0 to 1000 psi pressure measurement capability

DATE	TIME	ACTIVITY
7/9/79	07:30:00	Background Data
		Temp HG1-1 ch. 0 @ 550
		Temp HG3-4 ch. 1 @ 524
		Temp HG4-2 ch. 3 @ 521
		Temp DBH2-2 Defunct

Transducer	Channel	Interval
	6	DBH2-3
	7	HG1-2
	8	HG5-3
	9	DBH2-1
	10	HG3-3
	11	HG3-4
	12	HG5-2
	13	HG4-4
	14	HG1-3
	15	HG1-1

	09:05:34	Pulse Test HG5-3-A(22) ch.8
	10:13:55	Pulse Test HG5-2-A(21) ch.12
	10:37:28	Pulse Test HG5-3 B(22) ch.8
	11:16:20	Pulse Test HG5-2 B(21) ch.12
	11:37:26	Start Last Test Over
	11:54:51	Remove Piston 21 from HG5-2 ch. 12
		Remove Piston 22 from HG5-3 ch. 8
		Install Piston 21 on HG5-3 ch. 8
		Install Piston 22 on HG5-2 ch. 12
	12:30:06	Pulse Test HG5-2-C(22) ch. 12
	12:49:52	Pulse Test HG5-3-C(21) ch. 8
	12:53:34	Open Valve HG5-2 ch. 12
	13:07:11	Open Valve HG3-3 ch. 10
	13:11:57	Open Valve HG4-4 ch. 13
	13:24:08	Pulse Test HG3-4-A(24) ch. 11
	14:19:39	Pulse Test DBH2-3-C-(23) ch. 6
	14:30:10	Remove Piston 23 DBH2-3 ch. 6
	14:30:20	Install Piston 23 DBH2-1 ch. 9
	16:29:22	Pulse Test DBH2-1-C(23) ch. 9

DATE	TIME	ACTIVITY
7/9/79	17:18:21	Open valve HG5-2 ch. 12
	17:35:51	Pulse test HG5-2-O(23) ch. 12
	17:46:58	Remove Piston 23 ch. 12
		Install Pistonn 23 HG5-3 ch. 8
	17:56:04	Pulse test HG5-3-O(23) ch. 8
	18:00:59	Close valve HG3-4 ch. 11
	18:01:59	Open valve HG5-2 ch. 12 (for piston 24)
	18:16:49	Pulse test HG3-3-A(22) ch. 10
	18:22:37	Remove Piston HG-3 ch. 8
		Install Piston 23 HG3-4 ch. 11
	18:34:11	Pulse test HG4-4-A (22) ch. 13
	18:40:55	Remove piston HG5-2 ch. 12
		Install piston 24 HG 5-3 ch. 8
7/10/79	07:54:08	Remove Piston HG3-3 ch. 10
		Install Piston 22 HG1-3 ch. 14
	08:18:24	Pulse test HG3-4-B(23) ch. 11
	09:25:59	Install ch. 16 s/n 461 C.J.O-1000 HG3-5
		Trans. Zero = 0.0245 ch. 16
	09:39:47	Pulse test HG5-3-E(24) ch. 8
	10:04:15	Pulse test HG1-3-A(22) ch. 14
	10:14:03	Remove Piston HG5-3 ch. 8
		Install Piston 24 HG5-2 ch. 12
	10:32:17	Pulse Test HG5-2-E(24) ch. 12
	10:40:28	Remove Piston HG5-2 ch. 12
		Install Piston 24 HG1-1 ch. 15
	10:44.24	Remove Piston HG1-3 ch. 14
		Install Piston 22 HG3-5 ch. 16
	11:44:24	Close valve HG4-4 ch. 13
		Close valve HG3-4 ch. 11
		Install Piston 21 HG3-4 ch. 11
		Install Piston 23 HG4-4 ch. 13
	11.59:24	Install transd. ch. 7 on HG4-5
		Transd. Zero = 0.1534 ch. 7
	12:11:44	Pulse test HG3-5-A(22) ch. 16
	12:37:32	Pulse Test HG1-A(24) ch. 15

DATE	TIME	ACTIVITY
7/10/79	13:39:49	Remove Piston ch. 16 HG3-5
		Install Piston
	13:41:57	Pulse test HG4-4-B(23) ch. 13
	13:58:09	Pulse test HG3-4-C(21) ch. 11
	16:25:09	Pulse test HG4-5-A(22) ch. 7
	16:28:12	Close valve HG4-5 ch. 7
		Close valve HG1-1 ch. 15
		Close valve HG3-4 ch. 11
		Close valve HG4-4 ch. 13
	17:03:55	Install Piston 22 HG1-1 ch. 15
		Install Piston 21 HG1-3 ch. 14
		Install Piston 23 HG3-3 ch. 10
	17:18:55	Install Piston 24 HG3-5 ch. 16
	17:35:17	Flow test HG5-2 ch. 12
	18:18:37	Pulse test HG1-1-B(22) ch. 15
7/11/79	08:06:39	Remove Piston HG1-1 ch. 15
		Install Piston 22 HG4-4 ch. 13
	08:33:13	Pulse test HG1-3-B(21) ch. 14
	08:55:22	Pulse test HG3-5-B(24) ch. 16
	09:20:34	Pulse test HG3-3-B(23) ch. 10
	09:30:08	Remove Piston HG3-5 ch. 16
		Install Piston 24 HG4-5 ch. 7
	09:40:08	Remove Piston HG4-4 ch. 13 (no test)
	09:55:08	Install Piston 25 DBH2-1 ch. 9
	10:05:26	Pulse test DBH2-1-D(25) ch. 9 (aborted)
	10:24:13	Install Piston 25 DHB2-3 ch. 6
	10:54:07	Pulse test DBH2-3-D(25) ch. 6
	11:10:36	Install Piston 25 HG5-3 ch. 8
	11:15:36	Close valve HG3-3 ch. 10
		Close valve HG1-1 ch. 14
	11:25:36	Install Piston 23 HG1-1 ch. 15
		Install Piston 21 HG3-5 ch. 16
	11:33:48	Pulse test HG5-3-F(25) ch. 8
	12:12:33	Pulse test HG4-5-B(24) ch. 7 (aborted)
	12:25:08	Pulse test HG3-5-C(21) ch. 16

DATE	TIME	ACTIVITY
7/11/79	12:50:54	Install Piston 25 HG5-2 ch. 12
	13:14:02	Pulse test HG1-1-C(23) ch. 15
	13:27:34	Pulse test HG5-2-F(25) ch. 12
	13:54:47	Close valve HG4-5 ch. 7
		Close valve HG1-1 ch. 15
	14:09:47	Install Piston 25 HG3-4 ch. 11
	14:25:44	Pulse test HG3-5-O(23) ch. 16
	14:37:18	Close valve HG3-5 ch. 16
	16:27:46	Remove ch. 9. Zero = 0.0283
	16:31:46	Install ch. 9 on DBH2-2
	16:42:32	Pulse test HG1-3-C(24) ch. 14
	17:34:36	Pulse test HG3-4-E(25) ch. 11
	17:50:06	Install Piston 21 HG1-1 ch. 15
	17:57:21	Install Piston 24 DBH2-2 ch. 9
	18:03:21	Install Piston 23 HG4-5 ch. 7
	18:07:21	Pulse test HG4-5-C (23) ch. 7
7/12/79	09:45	Install 23 on HG1-3 ch. 14
		25 on HG3-5 ch. 16
	10:25	Pulse test HG1-1-D(21) ch. 15
	10:49	Pulse test DBH2-2-A(24) ch. 9
	11:11	Remove Piston ch. 16
	11:29	Install 25 HG3-3 ch. 10
	11:36	Install 27 HG4-5 ch. 7
		Remove 21 HG1-1 ch. 15
	11:45	Install 27 HG4-4 ch. 13
	11:51	Pulse test HG2-3-D(23) ch. 14
	12:04	Pulse test HG3-3-C(25) ch. 10
	12:09	Remove Piston ch. 10
	12:11	Remove Piston ch. 14
	12:37	Pulse test HG4-4-C(27) ch. 13
	12:44	Remove Piston ch. 13
	12:51	Install 26 HG5-2 ch. 12
		Install 26 HG5-3 ch. 8
	13:01	Pulse test HG5-2-G(26) ch. 12

DATE	TIME	ACTIVITY
7/12/79	13:23	Pulse test HG5-3-G(26) ch. 8
	13:32	Remove Piston ch. 12
	13:38	Install 26 HG3-5 ch. 16
	14:03	Pulse test HG3-5-F(26) ch. 16
	14:26	Pulse test HG3-4-F(26) ch. 11
7/13/79	07:34	Drop Press ch. 7
	08:00	Install 26 HG1-1 ch. 15
		Install 26 HG1-3 ch. 14
		Install 27 DBH2-2 ch. 9
		Install 27 DBH2-3 ch. 6
	08:09	Remove 27 from DBH2-3 ch. 6
		Install 27 HG4-5 ch. 7
	08:27	Pulse test HG1-3-E(26) ch. 14
	08:47	Pulse test HG1-1-E(26) ch. 15
	11:02	Pulse test DBH2-2-B(27) ch. 9
	13:18	Install 26 DBH2-3 ch. 6
	13:28	Pulse test HG4-5-D(27) ch. 7
	13:52	Pulse test DBH2-3-E(26) ch. 6
	14:03	Install 27 HG1-1 ch. 15
		Install 27 HG1-3 ch. 14
		Remove 24 HG4-5 ch. 7
	16:17	Pulse test HG1-1-E(27) ch. 15
	16:37	Pulse test HG1-3-E(27) ch. 14
	17:12	Close valves and adj. chs. 14, 15
	17:29	Flow test HG5-3 ch. 8
7/14/79	08:22	Ch. 10 failure-discontinued
		Install ch. 8 HG3-3 (from HG5-3)
		Trans. Z = 0.0563 ch. 8
		Install 26 HG3-3 ch. 8
	09.07	Flow-test HG1-3 ch. 14
	11:37	Open valve ch. 14
	11:45	Flow test HG1-1 ch. 15

DATE	TIME	ACTIVITY
7/14/79	09:11	Flow test HG1-1 ch. 15 (repeat)
	11:16	Flow test HG3-5 ch. 16
	12:31	Flow test HG3-4 ch. 11
7/16/81	07:48	Remove ch. 6 from DBH2-3
		Install ch. 6 on DBH2-4
		Trans. Z = 0.0806 ch. 6
		Install 26 DBH2-2 ch. 9
		Install 26 DBH2-4 ch. 6
	08:19	Flow test HG4-4 ch. 13
	11:05	Pulse test HG3-3D(26) ch. 8
	11:15	Pulse test DBH2-4-A(27) ch. 6
	11:29	Pulse test DBH2-2-C(26) ch. 9
	11:43	Remove ch. 12 from HG5-2
		Install ch. 12 HG5-1
		Install 26 HG5-1 ch. 12
		Trans. Z = 0.0600 ch. 12
	12:12	Flow test HG4-5 ch. 7
	13:41	Pulse test HG5-2 ch. 12
	16:04	Install ch. 15 HG3-1
		Install 22 HG3-1 ch. 15
		Trans Z = 0.0125 ch. 15
		Install ch. 14 HG4-2
		Trans. Z = 0.0357 ch. 14
	16:57	Pulse test HG-3-1-C(26) ch. 15
	17:22	Pulse test HG4-2 ch. 14
7/17/79	08:40	Install ch. 9 DBH2-5
		Install 26 DBH2-5 ch. 9
		Install 26 DBH2-4 ch. 6
	09:11	Pulse test HG3-1-(26) ch. 15 (aborted)
	09:26	Flow test HG5-1 ch. 12
	11:02	Calibration ch. 17 s/n 2616 C.5.0-1000
		Trans. Z = 0.0430 ch. 17
	11:18	Install ch. 17 HG1-3

DATE	TIME	ACTIVITY
7/17/79	11:39	Pulse test DBH2-4-B(26) ch. 6
	11:48	Pulse test DBH2-5-A(26) ch. 9
	12:33	Flow test HG3-3 ch. 8
	19:18	Trans. ch. 12 to HG1-1
		Rel. Press. HG5-1 no transd.
		Rel. Press HG4-5 ch. 7
	19:33	Rel. Press. HG3-3 ch. 8
		Prep flow test
		Install ch. 14 HG5-2
	22.34	Long flow test HG1-3 ch. 17
7/18/79	18:27	Recovery
7/19/79	06:59	Long flow test HG5-2 ch. 14
7/20/79	10:43	Recovery
7/21/79	06:58	Ch. 12 Defunct for past 3 days (valve closed)
		Install 26 DBH2-1
		Install ch. 6 DBH2-1
		Install ch. 14 HG5-1
		Install ch. 12 HG1-2
		Install ch 11 HG4-1
		Install ch. 17 HG4-2
		Install ch 16 HG4-3
		Install 26 HG4-1
		Install 22 HG1-2
7/22/79	07:35	Pulse test HG1-2 ch. 12
	07:46	Install 22 ch 17 HG4-2
	07:53	Pulse test HG4-2-C(22) ch. 17
	08:00	Install 22 ch. 16 HG4-3
	08:09	Pulse test DBH2-1-E(26) ch. 6

DATE	TIME	ACTIVITY
7/22/79	08:30	Remove 26 ch. 6 DBH2-1
		Install 26 ch. 13 HG4-4
	08:26	Pulse test GH4-3-A(22) ch. 16
	08:41	Pulse test HG4-1-C(26) ch. 11
	08.53	Install 22 HG5-1 ch. 14
	09:02	Pulse test HG5-1-C(22) ch. 14
	09:37	Install 26 ch. 9 DBH2-5
	10:49	Install 26 ch. 7 HG4-5
	10:56	Pulse test HG4-4-D(26) ch. 13
	11:06	Pulse test HG4-5-E(26) ch. 7
	11:13	Pulse test DBH2-5-B(27) ch. 9
	11:29	Remove Piston HG4-5 ch. 7
	11:30	Abort test HG4-4 ch. 13 (Opened valve)
	11:43	Flow test HG3-1 ch. 15
7/23/79	07:25	Power Failure
	07:33-11:30	Volume - Pressure Release, All cavities

APPENDIX VI

SELECTED PRESSURE PULSE TEST DATA

TEST: HG1-1B C(23)

SHUT-IN PRESSURE (P in-situ) = 0.531 MPa

DISPLACEMENT VOLUME (ΔVol) = 2.6 cm^3

PRESSURE PULSE (ΔP) = 0.344 MPa

TIME after PULSE seconds)	NORMALIZED PRESSURE	TEMPERATURE VARIATION ΔT (°C) FORM Te-time t=0
2	.9487	
4	.9037	
5	.8884	
6	.8797	
8	.8734	
15	.8529	
19	.8422	
24	.8071	+.001
51	.7728	+.001
78	.7428	<.001
106	.7168	+.001
133	.6919	+.001
187	.6489	<.001
243	.6107	<.001
303	.5728	<.001
452	.4671	+.001
632	.4174	+.002
752	.3759	+.003
872	.3385	+.002
1052	.2915	+.003
1546	.2004	+.001
2343	.1195	+.003
4200	.0438	-.006
4767	.0343	-.004
11522	.0071	-.005

Time Pulse	Normalized Pressure	Temperature Variation
12408	.0039	-.005
14809	.0012	+.002
15912	.0016	-.003

TEST: HG1-3B D23

SHUT-IN PRESSURE (P in-situ) = 0.796 MPa

DISPLACEMENT VOLUME (ΔVol) = 2.6 cm^3

PRESSURE PULSE (ΔP) = 0.292 MPa

TIME after PULSE (seconds)	NORMALIZED PRESSURE
1	.9057
2	.8507
4	.8049
5	.7639
13	.6066
18	.5422
22	.4904
26	.4456
31	.4083
35	.2977
62	.2142
90	.1717
117	.1437
144	.1260
171	.1106
313	.0737
583	.0457
993	.0275
1938	.0145
3097	.0070
5828	.0037
7793	.0009
9606	.0009

TEST: HG3-3 B23

SHUT-IN PRESSURE (P in-situ) = 1.160 MPa

DISPLACEMENT VOLUME (ΔVol) = 2.6 cm^3

PRESSURE PULSE (ΔP) = 0.0136 MPa

TIME after PULSE (seconds)	NORMALIZED PRESSURE
0	1.0000
2	.9700
3	.9600
10	.9100
36	.8500
422	.8400
2101	.8200
6138	.7900
8159	.7400
14070	.6900
18485	.6400
27230	.5800
29578	.5600

TEST: HG3-4 B(23)

SHUT-IN PRESSURE (P in-situ) = 1.096 MPa

DISPLACEMENT VOLUME (ΔVol) = 2.6 cm^3

PRESSURE PULSE (ΔP) = 0.142 MPa

TIME after PULSE (seconds)	NORMALIZED PRESSURE	TEMPERATURE VARIATION T (^oC) from Te time=0
1	.9480	
2	.9275	
4	.9157	
11	.8833	
15	.8686	
20	.8373	
45	.8039	
71	.7775	<.001
97	.7588	+.001
123	.7422	+.002
150	.7258	-.002
210	.6841	-.001
270	.6676	+.006
450	.5951	+.009
601	.5471	+.005
804	.4931	+.004
1044	.4353	-.004
1524	.3422	+.005
1884	.2882	+.008
2364	.2314	+.007
2855	.1833	-.001
3682	.1284	-.001
4748	.0804	+.001
6075	.0441	+.001
7834	.0216	+.004
11687	.0029	+.001

TEST: HG3-5 D23

SHUT-IN PRESSURE (P in-situ) = 1.108 MPa

DISPLACEMENT VOLUME (ΔVol) = 2.6 cm^3

PRESSURE PULSE (ΔP) = 0.208 MPa

TIME after PULSE (seconds)	NORMALIZED PRESSURE
1	.9147
3	.8488
4	.7975
5	.7562
13	.6276
17	.5656
21	.5157
25	.4724
30	.3278
57	.2265
84	.1632
112	.1219
139	.0933
193	.0506
252	.0420
312	.0233
372	.0180
460	.0127
494	.0093
621	.0073

TEST: HG3-5 D23

SHUT-IN PRESSURE (P in-situ) = 1.108 MPa

DISPLACEMENT VOLUME (ΔVol) = 2.6 cm^3

PRESSURE PULSE (ΔP) = 0.208 MPa

TIME after PULSE (seconds)	NORMALIZED PRESSURE
1	.9147
3	.8488
4	.7975
5	.7562
13	.6276
17	.5656
21	.5157
25	.4724
30	.3278
57	.2265
84	.1632
112	.1219
139	.0933
193	.0506
252	.0420
312	.0233
372	.0180
460	.0127
494	.0093
621	.0073

TEST: HG4-4 B23

SHUT-IN PRESSURE (P in-situ) = 0.932 MPa

DISPLACEMENT VOLUME (ΔVol) = 2.6 cm^3

PRESSURE PULSE (ΔP) = 0.037 MPa

TIME after PULSE (seconds)	NORMALIZED PRESSURE
1	.9196
3	.8785
4	.8430
5	.8206
13	.7757
17	.7645
43	.7570
213	.7495
952	.7346
1518	.7215
7820	.6523
8915	.5851
14405	.5159
17041	.4766
25539	.3963
37239	.3047
45339	.2449
58839	.1832
66083	.1514
69193	.1009

TEST: HG4-5 C23

SHUT-IN PRESSURE (P in-situ) = 1.099 MPa

DISPLACEMENT VOLUME (ΔVol) = 2.6 cm^3

PRESSURE PULSE (ΔP) =

TIME after PULSE (seconds)	NORMALIZED PRESSURE
1	.9381
2	.8905
3	.8524
12	.7571
21	.7429
193	.7333
8208	.6571
28908	.5714
49608	.5000
58712	.4667
62719	.4667

TEST: HG5-2 D23

SHUT-IN PRESSURE (P in-situ) = .829 MPa

DISPLACEMENT VOLUME (ΔVol) = 2.6 cm^3

PRESSURE PULSE (ΔP) = 0.1142 MPa

TIME after PULSE (seconds)	NORMALIZED PRESSURE
1	.9286
8	.5190
13	.4155
17	.3369
21	.2774
26	.2310
30	.1250
56	.0560
82	.0274
107	.0167
133	.0107
159	.0119
219	.0071
279	.0048
339	.0024

TEST: HG5-3 D23

SHUT-IN PRESSURE (P in-situ) = 0.829 MPa

DISPLACEMENT VOLUME (ΔVol) = 2.6 cm^3

PRESSURE PULSE (ΔP) = 0.1089 MPa

TIME after PULSE (seconds)	NORMALIZED PRESSURE
1	.9286
3	.8714
10	.7429
23	.6500
194	.2643
254	.2071
314	.1571
374	.1143
434	.0929
494	.0786
522	.0500
642	.0500
762	.0214
882	.0143
1002	0.0
1388	0.0

APPENDIX VII

TABULATED TEST CONDITIONS FOR ALL PRESSURE PULSE TESTS

APPENDIX VII NOTES:

(i) For location of boreholes refer to Chapter 1, Figs. 1.4 - 1.6.

(ii) Reference code for borehole tests are explained in Appendix IV.

(iii) For borehole HG1 there is an additional classification with the cavity designation, i.e., "A" or "B":

A - preliminary position of the packer assembly

B - final setting of packer assembly and test position.

(iv) In reference to Table VII:

P in situ - Shut-in pressure

ΔVol - displacement volume

ΔP - pressure pulse.

Table VII. Pressure pulse test.

Cavity	Test	$P_{in\text{-}situ}$	ΔVOL (cm^3)	ΔP MPa
HG1-1b	A(24)	0.533	2.0	0.252
	B(22)	0.5333	0.9	0.123
	C(23)	0.531	2.6	0.344
	D(21)	0.533	1.5	0.192
	E(26)	0.534	4.8	0.634
	F(27)	0.533	4.2	0.543
HG1-2b	A(22)	0.351	0.9	0.00155
HG1-3b	A(22)	0.796	0.9	0.098
	B(21)	0.796	1.5	0.170
	C(24)	0.794	2.0	0.221
	D(23)	0.796	2.6	0.292
	E(26)	0.796	4.8	0.522
	F(27)	0.796	4.2	0.510
HG3-1	-	-	-	-
HG3-2	-	-	-	-
HG3-3	A(22)	1.164	0.9	0.0053
	B(23)	1.160	2.6	0.0136
	C(25)	1.163	3.7	0.0206
	D(26)	1.163	4.8	0.0230
HG3-4	A(24)	1.096	2.0	0.110
	B(23)	1.096	2.6	0.142
	C(21)	1.093	1.5	0.081
	D(22)	-	0.9	-
	E(25)	1.094	3.7	0.195
	F(26)	1.094	4.8	0.245

Cavity	Test	P in-situ	ΔVOL (cm^3)	ΔP MPa
HG5-2	A(21)	0.828	1.5	0.0772
	B(21)	0.828	1.5	0.0691
	C(22)	0.828	0.9	0.0434
	D(23)	0.829	2.6	0.1142
	E(24)	0.828	2.0	0.0835
	F(25)	0.828	3.7	0.156
	G(26)	0.829	4.8	0.186
HG5-3	A(22)	0.825	0.9	0.00622
	B(22)	0.825	0.9	0.0070
	C(21)	0.825	1.5	0.145
	D(23)	0.826	2.6	0.189
	E(24)	0.825	2.0	0.145
	F(25)	0.825	3.7	0.256
	G(26)	0.825	4.8	0.0299
DBH2-1	A	-	-	-
	B	-	-	-
	C(23)	0.663	2.6	0.0138
	D	-	-	-
	E(26)	0.662	4.8	0.019
DBH2-2	A(24)	0.738	2.0	0.0058
	B(27)	0.742	4.2	0.0108
	C(26)	0.742	4.8	0.0107
DBH2-3	A	-	-	-
	B	-	-	-
	C(23)	0.884	2.6	0.0157
	D(25)	0.880	3.7	0.0229
	E(26)	0.881	4.8	0.030
DBH2-4	A(27)	1.025	4.2	0.0111
	B(26)	1.026	4.8	0.0124
DBH2-5	A(26)	1.166	4.8	0.0049
	B(27)	1.166	4.2	0.0045

Cavity	Test	P in-situ	ΔVOL (cm^3)	ΔP MPa
HG3-5	A(22)	1.107	0.9	0.072
	B(24)	1.107	2.0	0.167
	C(26)	1.106	1.5	0.117
	D(23)	1.108	2.6	0.208
	E(25)	1.106	3.7	0.279
	F(26)	1.106	4.8	0.361
HG4-1	A	-	-	-
	B	-	-	-
	C(26)	.142	4.8	0.634
HG4-2	A	-	-	-
	B(26)	1.693	4.8	0.111
	C(22)	1.749	0.9	0.0053
HG4-3	A(22)	-	0.9	-
HG4-4	A(22)	0.938	0.9	0.021
	B(23)	0.932	2.6	0.037
	C(27)	0.929	4.2	0.054
	D(26)	0.931	4.8	0.040
HG4-5	A(22)	-	0.9	-
	B(24)	-	2.0	-
	C(23)	1.099	2.6	-
	D(27)	1.094	4.2	-
	E(26)	1.109	4.8	-
HG5-1	A	-	-	-
	B	-	-	-
	C(22)	-	0.9	-